

Imię i nazwisko autora rozprawy: Frank Fernando Llovera Trujillo
Dyscyplina naukowa: Matematyka

ROZPRAWA DOKTORSKA

Tytuł rozprawy w języku polskim: Dyskretny model neuronu z punktu widzenia teorii układów dynamicznych

Tytuł rozprawy w języku angielskim: Discrete neuron models from the point of view of dynamical system theory

Promotor
<i>podpis</i>
dr hab. Piotr Bartłomiejczyk
Promotor pomocniczy
<i>podpis</i>
dr inż. Justyna Signerska-Rynkowska

Gdańsk, 2025



The author of the doctoral dissertation: Frank Fernando Llovera Trujillo
Scientific discipline: Mathematics

DOCTORAL DISSERTATION

Title of doctoral dissertation: Discrete neuron models from the point of view of dynamical system theory

Title of doctoral dissertation (in Polish): Dyskretne modele neuronu z punktu widzenia teorii układów dynamicznych

Supervisor
<i>signature</i>
dr hab. Piotr Bartłomiejczyk
Auxiliary supervisor
<i>signature</i>
dr inż. Justyna Signerska-Rynkowska

OŚWIADCZENIE

Autor rozprawy doktorskiej: Frank Fernando Llovera Trujillo

Ja, niżej podpisany(a), oświadczam, iż jestem świadomy(a), że zgodnie z przepisem art. 27 ust. 1 i 2 ustawy z dnia 4 lutego 1994 r. o prawie autorskim i prawach pokrewnych (t.j. Dz.U. z 2021 poz. 1062), uczelnia może korzystać z mojej rozprawy doktorskiej zatytułowanej:

Dyskretne modele neuronu z punktu widzenia teorii układów dynamicznych
do prowadzenia badań naukowych lub w celach dydaktycznych.¹

Świadomy(a) odpowiedzialności karnej z tytułu naruszenia przepisów ustawy z dnia 4 lutego 1994 r. o prawie autorskim i prawach pokrewnych i konsekwencji dyscyplinarnych określonych w ustawie Prawo o szkolnictwie wyższym i nauce (Dz.U.2021.478 t.j.), a także odpowiedzialności cywilno-prawnej oświadczam, że przedkładana rozprawa doktorska została napisana przeze mnie samodzielnie.

Oświadczam, że treść rozprawy opracowana została na podstawie wyników badań prowadzonych pod kierunkiem i w ścisłej współpracy z promotorem dr hab. Piotrem Bartłomiejczykiem, promotorem pomocniczym dr inż. Justyną Signerską-Rynkowską.

Niniejsza rozprawa doktorska nie była wcześniej podstawą żadnej innej urzędowej procedury związanej z nadaniem stopnia doktora.

Wszystkie informacje umieszczone w ww. rozprawie uzyskane ze źródeł pisanych i elektronicznych, zostały udokumentowane w wykazie literatury odpowiednimi odnośnikami zgodnie z przepisem art. 34 ustawy o prawie autorskim i prawach pokrewnych.

Potwierdzam zgodność niniejszej wersji pracy doktorskiej z załączoną wersją elektroniczną.

Gdańsk, dnia

.....
podpis doktoranta

Ja, niżej podpisany(a), wyrażam zgodę na umieszczenie ww. rozprawy doktorskiej w wersji elektronicznej w otwartym, cyfrowym repozytorium instytucjonalnym Politechniki Gdańskiej.

Gdańsk, dnia

.....
podpis doktoranta

¹Art. 27. 1. Instytucje oświatowe oraz podmioty, o których mowa w art. 7 ust. 1 pkt 1, 2 i 4–8 ustawy z dnia 20 lipca 2018 r. – Prawo o szkolnictwie wyższym i nauce, mogą na potrzeby zilustrowania treści przekazywanych w celach dydaktycznych lub w celu prowadzenia działalności naukowej korzystać z rozpowszechnionych utworów w oryginale i w tłumaczeniu oraz zwielokrotniać w tym celu rozpowszechnione drobne utwory lub fragmenty większych utworów.

2. W przypadku publicznego udostępniania utworów w taki sposób, aby każdy mógł mieć do nich dostęp w miejscu i czasie przez siebie wybranym korzystanie, o którym mowa w ust. 1, jest dozwolone wyłącznie dla ograniczonego kręgu osób uczących się, nauczających lub prowadzących badania naukowe, zidentyfikowanych przez podmioty wymienione w ust. 1.



STATEMENT

The author of the doctoral dissertation: Frank Fernando Llovera Trujillo

I, the undersigned, declare that I am aware that in accordance with the provisions of Art. 27 (1) and (2) of the Act of 4th February 1994 on Copyright and Related Rights (Journal of Laws of 2021, item 1062), the university may use my doctoral dissertation entitled:

Discrete neuron models from the point of view of dynamical system theory

for scientific or didactic purposes.¹

Gdańsk,

.....
signature of the PhD student

Aware of criminal liability for violations of the Act of 4th February 1994 on Copyright and Related Rights and disciplinary actions set out in the Law on Higher Education and Science (Journal of Laws 2021, item 478), as well as civil liability, I declare, that the submitted doctoral dissertation is my own work.

I declare, that the submitted doctoral dissertation is my own work performed under and in cooperation with the supervision of dr hab. Piotr Bartłomiejczyk, the auxiliary supervision of dr inż. Justyna Signerska-Rynkowska.

This submitted doctoral dissertation has never before been the basis of an official procedure associated with the awarding of a PhD degree.

All the information contained in the above thesis which is derived from written and electronic sources is documented in a list of relevant literature in accordance with Art. 34 of the Copyright and Related Rights Act.

I confirm that this doctoral dissertation is identical to the attached electronic version.

Gdańsk,

.....
signature of the PhD student

I, the undersigned, agree to include an electronic version of the above doctoral dissertation in the open, institutional, digital repository of Gdańsk University of Technology.

Gdańsk,

.....
signature of the PhD student

¹ Art 27. 1. Educational institutions and entities referred to in art. 7 sec. 1 points 1, 2 and 4–8 of the Act of 20 July 2018 – Law on Higher Education and Science, may use the disseminated works in the original and in translation for the purposes of illustrating the content provided for didactic purposes or in order to conduct research activities, and to reproduce for this purpose disseminated minor works or fragments of larger works.

2. If the works are made available to the public in such a way that everyone can have access to them at the place and time selected by them, as referred to in para. 1, is allowed only for a limited group of people learning, teaching or conducting research, identified by the entities listed in paragraph 1.

Streszczenie

Modele neuronowe oparte na iterowaniu odwzorowania są ważnym narzędziem w modelowaniu dynamiki neuronów i mogą być traktowane jako istotna alternatywa dla zwykle bardziej kosztownych obliczeniowo modeli ciągłych lub hybrydowych. Jednak ze względu na ich dyskretną naturę, ich ścisła analiza matematyczna może być trudna. W naszej pracy koncentrujemy się na badaniu dwóch dobrze znanych modeli opartych na odwzorowaniach zarówno od strony teoretycznej jak i numerycznej oraz dostarczamy algorytmy do określania marszrut orbit okresowych.

W *pierwszym* artykule badamy dyskretny model dynamiki neuronalnej wprowadzony przez Chialvo [Chaos, Solitons & Fractals 5, 1995]. W szczególności pokazujemy, że jego zredukowana jednowymiarowa wersja może być traktowana jako niezależny, prosty model aktywności neuronowej, w którym wejście oraz ustalona wartość zmiennej regeneracyjnej stanowią parametry. Ten jednowymiarowy model nadal wykazuje bardzo bogatą i zróżnicowaną dynamikę. Wykorzystując fakt, że odwzorowanie, którego iteracje definiują dynamikę napięcia, jest S-unimodalne, szczegółowo opisujemy zarówno zachowanie okresowe, jak i występowanie różnych rodzajów chaosu, wskazując odpowiadające im regiony w przestrzeni parametrów. Nasze badanie uzupełniamy również analizą bifurkacyjną wspomnianego modelu dynamicznego.

Model Courbage'a, Nekorkina i Vdovina (CNV) jest analizowany w *drugim* artykule. Przeglądamy i rozszerzamy niektóre istniejące wyniki dotyczące β -transformacji oraz rozszerzających odwzorowań typu Lorenza. Następnie stosujemy je do wyprowadzenia istotnych własności sekwencji impulsów (spike-trains) generowanych przez model CNV oraz wyjaśniamy ich implikacje dla zachowania neuronów. W szczególności, wykorzystując najnowsze twierdzenia teorii rotacji dla odwzorowań typu Lorenza, dokonujemy klasyfikacji okresowych wzorców impulsów w tym modelu.

W *trzecim* artykule analizujemy dynamikę modelu CNV, w którym pierwotnie funkcja przedziałami liniowa definiująca dynamikę napięcia zostaje zastąpiona przez wielomian trzeciego stopnia z dodatkowym parametrem kontrolującym nachylenie. Pokazujemy, że na dużym podzbiorze wielowymiarowej przestrzeni parametrów odwzorowanie powrotne dynamiki napięcia jest rozszerzającym odwzorowaniem typu Lorenza. Analizujemy zarówno zachowanie chaotyczne, jak i okresowe tego układu oraz opisujemy złożoność wzorców impulsowania generowanych przez neuron. Osiągamy to poprzez wykorzystanie i rozszerzenie wyników z teorii odwzorowań typu Lorenza oraz ich rozszerzających wariantów.

W *czwartym* artykule, nawiązując do wyników teoretycznych Gellera i Misiurewicza [Int. J. Bifurcation Chaos 28, 2018], przedstawiamy procedurę umożliwiającą określenie marszrut zdecydowanej większości orbit okresowych odwzorowań typu Lorenza. Dostarczamy sprecyzowane algorytmy wraz z gotowymi do użycia narzędziami obliczeniowymi dostępnymi w otwartych repozytoriach. Ponieważ odwzorowania typu Lorenza pojawiają się jako podukłady wielu złożonych modeli i są powszechne w różnych zastosowaniach, nasze wyniki otwierają nowe możliwości badania ich struktury okresowej.

Abstract

Map-based neuron models are an important tool in modelling neural dynamics and sometimes can be considered as an alternative to usually computationally costlier models based on continuous or hybrid dynamical systems. However, due to their discrete nature, rigorous mathematical analysis might be challenging. Overall, we concentrate our work on studying two well-known map based models both theoretically and numerically and provide algorithms for determining itineraries of periodic orbits.

In the *first* article we study a discrete model of neuronal dynamics introduced by Chialvo [Chaos, Solitons & Fractals 5, 1995]. In particular, we show that its reduced one-dimensional version can be treated as an independent simple model of neural activity where the input and the fixed value of the recovery variable are parameters. This one-dimensional model still displays very rich and varied dynamics. Using the fact that the map whose iterates define voltage dynamics is S-unimodal, we describe in detail both the periodic behaviour and the occurrence of different notions of chaos, indicating corresponding regions in parameter space. Our study is also complemented by a bifurcation analysis of the mentioned dynamical model.

The Courbage, Nekorkin and Vdovin (CNV) model is studied in the *second* article with a special focus on the piece-wise linear version. We review and extend some of the existing results concerning β -transformations and (expanding) Lorenz mappings. Then we apply them for deducing important properties of spike-trains generated by the CNV model and explain their implications for neuron behaviour. In particular, using recent theorems of rotation theory for Lorenz-like maps, we provide a classification of periodic spiking patterns in this model.

When the originally piecewise linear function defining voltage dynamics is replaced by a cubic polynomial, with an additional parameter responsible for varying the slope, the CNV model displays interesting dynamics that is addressed in the *third* article. Showing that on a large subset of the multidimensional parameter space the return map of the voltage dynamics is an expanding Lorenz map, we analyze both chaotic and periodic behaviour of the system and describe complexity of spiking patterns fired by a neuron. This is achieved by using and extending some results from the theory of Lorenz-like and expanding Lorenz mappings.

In the *fourth* article, following theoretical findings of Geller and Misiurewicz [Int. J. Bifurcation Chaos 28, 2018], we outline a procedure that allows for determining the itineraries of vast majority of periodic orbits of Lorenz-like maps. We provide explicit algorithms with ready-to-use computational tools available in open repositories. Since Lorenz-like maps arise as subsystems of many complex models and are prevalent in various applications, our results open a way of investigation of their periodic structure.

Periodic and chaotic dynamics in a map-based neuron model

Frank Llovera Trujillo¹  | Justyna Signerska-Rynkowska^{2,3}  | Piotr Bartłomiejczyk² 

¹Doctoral School, Gdańsk University of Technology, Gdańsk, Poland

²Faculty of Applied Physics and Mathematics and BioTechMed Centre, Gdańsk University of Technology, Gdańsk, Poland

³Dioscuri Centre in Topological Data Analysis, Institute of Mathematics of the Polish Academy of Sciences, Warsaw, Poland

Correspondence

Piotr Bartłomiejczyk, Faculty of Applied Physics and Mathematics and BioTechMed Centre, Gdańsk University of Technology, Gabriela Narutowicza 11/12, 80-233 Gdańsk, Poland.
Email: piobartl@pg.edu.pl

Communicated by: J. Banasiak

Funding information

Max-Planck-Gesellschaft, Grant/Award Number: Dioscuri Programme; Narodowe Centrum Nauki, Grant/Award Number: grant no. 2019/35/D/ST1/02253

Map-based neuron models are an important tool in modeling neural dynamics and sometimes can be considered as an alternative to usually computationally costlier models based on continuous or hybrid dynamical systems. However, due to their discrete nature, rigorous mathematical analysis might be challenging. We study a discrete model of neuronal dynamics introduced by Chialvo in 1995. In particular, we show that its reduced one-dimensional version can be treated as an independent simple model of neural activity where the input and the fixed value of the recovery variable are parameters. This one-dimensional model still displays very rich and varied dynamics. Using the fact that the map whose iterates define voltage dynamics is S-unimodal, we describe in detail both the periodic behavior and the occurrence of different notions of chaos, indicating corresponding regions in parameter space. Our study is also complemented by a bifurcation analysis of the mentioned dynamical model.

KEYWORDS

chaos, flip bifurcation, fold bifurcation, neuronal dynamics, S-unimodal map

MSC CLASSIFICATION

Primary: 37E05, 37N25, Secondary: 37G99, 92C20

1 | INTRODUCTION

In the last decades, many different types of neuron models have been developed, including conductance-based models (with the pioneering example of the experimentally derived Hodgkin-Huxley model¹ or Morris-Lecar model²) and other models based on continuous dynamical systems, that is, differential equations (e.g., FitzHugh-Nagumo model^{3,4}), models based on discrete dynamical systems, that is, iterates of functions (so-called *map-based models*), up to hybrid models which combine ordinary differential equations (accounting for input integration) with discrete events (resetting mechanism accounting for action potential); see, for example, earlier studies.^{5–8} In this paper, we study the following map-based neuron model, introduced in Chialvo⁹:

$$x_{n+1} = f(x_n, y_n) = x_n^2 \exp(y_n - x_n) + k, \quad (1a)$$

$$y_{n+1} = g(x_n, y_n) = ay_n - bx_n + c. \quad (1b)$$

This model will be referred to as the 2D Chialvo model (or full Chialvo model). In the 2D Chialvo models (1a) and (1b), x is a membrane voltage potential (the most important dynamical variable in all the neuron models) and y is so-called recovery variable. The time-constant $a \in (0, 1)$, the activation-dependence $b \in (0, 1)$, and the offset $c > 0$ are the real parameters connected with the recovery process. In turn, $k \geq 0$ can be interpreted as an additive perturbation of the

voltage. In our analysis, the one-dimensional subsystem

$$x_{n+1} = f(x_n, r) = x_n^2 \exp(r - x_n) + k, \quad (2)$$

where $r \in \mathbb{R}$ is a parameter, will be referred to as the 1D or reduced Chialvo model.

Other examples of map-based models are, among others, Cazelles–Courbage–Rabinovich model,¹⁰ different types of Rulkov models,^{11–13} or Courbage–Nekorkin–Vdovin model.¹⁴ In particular, the work of Zhong et al¹⁵ is devoted to the non-chaotic Rulkov model,¹² where the analysis, similarly as in our case, firstly concerns bifurcations in the one-dimensional reduced model, that is, fast subsystem describing the evolution of the membrane voltage, and shows that it produces fold and flip bifurcations. This subsystem also produces chaos as it is shown by numerical simulations. Different examples of map-based neuron models are discussed, for example, in review articles^{16,17} (see also references therein).

In this work, we obtain rigorous characterization of chaos and co-dimension-one bifurcations of fixed points in the subsystem (2), relevant for the classification of bursting neurons. Before we start, let us summarize the known results on Chialvo model and introduce notations. Obviously, the fixed points (x_f, y_f) of the full model must satisfy

$$\begin{aligned} x_f &= x_f^2 \exp(y_f - x_f) + k, \\ y_f &= (c - bx_f)/(1 - a). \end{aligned}$$

In particular, for $k = 0$, the point $(x_{f_0}, y_{f_0}) := (0, c/(1 - a))$ is always a stable fixed point of the system as can be seen by calculating corresponding eigenvalues which are 0 and a (and $a < 1$ by the assumption). Further, as Chialvo observed,⁹ when $b \ll a$, the initial part of the trajectory with initial condition (x, y_{f_0}) where $x \approx 0$ can be well described by the 1D Chialvo model (2) with $k = 0$ and $r = y_{f_0} = c/(1 - a)$. Therefore, in this parameter regime, among others, the 1D subsystem gives the information about initial dynamics following the small perturbation of the resting state $x = 0$ in the full model. A few other observations for $k > 0$ (referring mainly to the situation where systems (1a) and (1b) have exactly one fixed point (x_f, y_f)) were made already in Chialvo's work,⁹ including identification of some regions of bistability (coexistence of stable resting state and stable periodic oscillations) and regions of chaotic-like behavior interspersed with subregions of periodic behavior.

For more results on the full model, we also refer the reader to the more recent works.^{18,19} In particular, Jing et al¹⁸ studied analytically the existence and stability of the fixed points, conditions for existence of flip, fold, and Hopf bifurcations and chaos in the sense of Marotto's definition. Further, it numerically reports various period doubling bifurcations and routes to chaos, periodic windows in transient chaotic regions and strange chaotic and nonchaotic attractors, whereas the work of Wang and Cao¹⁹ illustrates numerically the existence of interesting structures in parameter space.

As our work is mainly concerned with the one-dimensional subsystem (2), we have only briefly described above the findings on the full 2D model. However, we go back to the analysis of the full model at the end of the paper. Let us also observe that for $0 < \varepsilon = 1 - a = b = c \ll 1$, systems (1a) and (1b) can be seen as a *slow-fast* (discrete) system, that is, the system of the form

$$x_{n+1} = \tilde{f}(x_n, y_n), \quad (3a)$$

$$y_{n+1} = y_n + \varepsilon \tilde{g}(x_n, y_n), \quad (3b)$$

where $\varepsilon \rightarrow 0$ is a small parameter. For this particular assumptions on parameters, the separation of timescales in the Chialvo models (1a) and (1b) is explicit. However, for many other choices of parameter values, the timescale separation is not so explicit but still visible in simulations. In this case, the voltage variable x and the recovery variable y can be referred to as *fast* and *slow* variables, respectively. Consequently, while x_n describes spiking behavior, y_n acts as a slowly changing parameter (with time-scale variation $\varepsilon \ll 1$) that modulates the spiking dynamics.

Models of the form (3a) and (3b) are usually analyzed by firstly assuming that $\varepsilon = 0$ and treating (3a) as a quazi-static approximation of (3a) and (3b) with parameter $y_n \equiv y$. If for some values of y (3a) exhibits equilibrium dynamics (due to the existence of a stable fixed point) and for some other values it exhibits periodic dynamics (due to the existence of a stable periodic orbit), then bursting in systems (3a) and (3b) occur because slowly varying y_n acts as bifurcation parameter that makes the dynamics of x switching between these two regimes (similar approach can be applied for ODE bursting systems, compare, e.g., with Rinzel²⁰). Therefore, bursting behavior in the above neuron model is indeed directly connected with the types of bifurcations present in the fast system (3a) (correspondingly, in (1a) or (2)). According to this observation, in Izhikevich and Hoppensteadt,²¹ the classification of bursting mappings was obtained, taking into account

that there are only four possible co-dimension-one bifurcations of a stable fixed point in maps (3a) that lead to its loss of stability or disappearance (fold, SNIC-saddle node on invariant circle bifurcation and supercritical and subcritical flip bifurcations) and only five co-dimension one bifurcations of a stable periodic orbit, which make the dynamics settle on a stable equilibrium afterwards (SNIC, homoclinic bifurcation, supercritical flip bifurcation, fold periodic orbit bifurcation, and subcritical flip of periodic orbits bifurcation). The former bifurcations correspond to transition from resting to spiking frequently (i.e., the onset of bursting), the later ones to the transition back to resting and their combination defines the type of burster in a given neuron model. We also remark that classification of bursting types in ODEs neuron models was discussed, for example, in Bertram et al.²² and Rinzel²⁰ as well as in the recent article²³ (see also review article²⁴ and references therein).

It is also worth pointing out that, contrary to most of the 2D map-based models, the recovery variable y in Chialvo model enters the voltage Equation (1a) not in additive but in multiplicative way and changes the shape of the first return map $x_n \mapsto x_{n+1} = f(x_n, y)$ of the x variable in a complicated nonlinear way instead of just shifting the x -nullcline upward or downward. Therefore understanding how the map $f_{r,k}(x) := x^2 \exp(r-x) + k$ depends not only on the additive parameter k but also on the parameter r is helpful for the analysis of the overall model. In fact y variable in the Chialvo model can also be intended to represent fast, not slow dynamics (as already mentioned in the review article¹⁷). When playing with the 2D model we have often observed that for many parameters configurations y variable quickly stabilized at certain value y_s while the voltage variable x still evolved in an oscillatory way. In such a case types of voltage oscillations can be well explained by understanding the dynamics of the 1D model with corresponding value of parameter $r = y_s$ (we exemplify this in section 3.4).

The main aim of this paper is to study the 1D Chialvo model using the methods of one-dimensional dynamics. According to our best knowledge, it has never been pointed out that the map describing the membrane voltage evolution in the Chialvo model is an S -unimodal map and thereby there are no results on this model, which use the theory of S -unimodal maps. This basic observation that we make allows to draw relevant conclusions for this map, as well as, in some cases, for the whole model itself. Another example of the occurrence of unimodal maps in the context of neuron dynamics is the adaptation map of the bidimensional integrate-and-fire model²⁵ (however, this unimodal map is given in a very implicit way and hardly ever exhibits negative Schwarzian derivative). In addition, it may be worth pointing out that various discrete systems similar to the 1D Chialvo model, for example, the logistic family $Q(x) = \lambda x(1-x)$, the Ricker family $R(x) = \lambda x \exp(-\beta x)$, and the Hassell family $H(x) = \lambda x/(1+x)^\beta$, have been the subject of both theoretical and numerical intensive research study since the mid-1970s (see for instance earlier studies^{26–30}).

Let us also note that $f(z) = z^2 \exp(r-z) + k$ (for the fixed complex values of parameters r and k) can be seen as an example of a complex entire transcendental analytic function of finite type, that is, having finite number of critical and asymptotic values. Since such maps exhibit, in general, different dynamical properties than polynomials, their complex dynamics (Julia and Fatou sets, etc.) has been studied extensively since the early 1980s (see^{31–33} and the references given there). However, the approach presented in this paper is focused on one-dimensional methods and, in consequence, we do not make use of complex dynamics theory in our paper.

The organization of the paper is as follows. In Section 3 we examine the existence and stability of fixed points and corresponding bifurcations in the one-dimensional Chialvo model (2). Section 4 is devoted to the study of the dynamical core of the 1D Chialvo map. Further, in Section 5 we provide the description of periodic and chaotic behavior of the model making use of the fact that (2) is given by an S -unimodal map. To ease our analysis, we introduce basic concepts and definitions of the theory of S -unimodal maps in Section 2. Finally, concluding remarks are presented in Section 6 at the end of the paper.

2 | BASIC DEFINITIONS

2.1 | Unimodality and Schwarzian derivative

We say that an interval map $f : I \rightarrow I$ has *negative Schwarzian derivative* if f is of class C^3 and

$$Sf(x) := \frac{f'''(x)}{f'(x)} - \frac{3}{2} \left(\frac{f''(x)}{f'(x)} \right)^2 < 0$$

for all $x \in I \setminus \{c | f'(c) = 0\}$. Points at which $f'(c) = 0$ are called *critical points*. The Schwarzian derivative was introduced in one-dimensional dynamics by D. Singer,³⁴ but its origins go back to H. Schwarz and 19th century complex analysis.

A continuous interval map $f : I = [a, b] \rightarrow I$ is called *unimodal* if there is a unique maximum c in the interior of I such that f is strictly increasing on $[a, c]$ and strictly decreasing on $(c, b]$. For simplicity, the term unimodal will also require that either a is a fixed point with b as its other pre-image or that $I = [f^2(c), f(c)]$. A unimodal map with negative Schwarzian derivative is called *S-unimodal*.

The *itinerary* of x under f is the sequence $s(x) = (s_0 s_1 s_2 \dots)$ where

$$s_j = \begin{cases} 0 & \text{if } f^j(x) < c, \\ 1 & \text{if } f^j(x) > c, \\ C & \text{if } f^j(x) = c. \end{cases}$$

The *kneading sequence* $K(f)$ of f is the itinerary of $f(c)$, i.e., $K(f) = s(f(c))$.

2.2 | Bifurcations

Let x_0 be a fixed point for f . The point x_0 is called *hyperbolic* if $|f'(x_0)| \neq 1$. The number $\mu = f'(x_0)$ is called the *multiplier* of the fixed point. Consider a one-dimensional discrete dynamical system depending on a parameter a

$$x \mapsto f(x, a), \quad x \in \mathbb{R}, \quad a \in \mathbb{R}, \quad (4)$$

where f is smooth with respect to both x and a . Let x_0 be a hyperbolic fixed point of the system. While the parameter a varies, the hyperbolicity condition can be violated. The bifurcation associated with the appearance of the multiplier $\mu = 1$ is called *fold* or *tangent* and with the appearance of the multiplier $\mu = -1$ *flip* or *period doubling*. Alternatively, a fold bifurcation is called a *saddle node* bifurcation. Let us recall a classical result concerning these bifurcations (³⁵, Th. 4.1 and 4.3).

Theorem 1. Suppose that a one-dimensional system (4) with smooth f , has at $a = 0$ the fixed point $x_0 = 0$. Let $\mu := \frac{\partial f}{\partial x}(0, 0)$. If $\mu = 1$ and the following conditions are satisfied,

$$(A1) \quad \frac{\partial^2 f}{\partial x^2}(0, 0) \neq 0,$$

$$(A2) \quad \frac{\partial f}{\partial a}(0, 0) \neq 0,$$

then a fold bifurcation occurs at the fixed point $x_0 = 0$ for the bifurcation value $a = 0$.

On the other hand, if $\mu = -1$ and the following conditions are satisfied,

$$(B1) \quad \frac{1}{2} \left(\frac{\partial^2 f}{\partial x^2}(0, 0) \right)^2 + \frac{1}{3} \frac{\partial^3 f}{\partial x^3}(0, 0) \neq 0,$$

$$(B2) \quad \frac{\partial^2 f}{\partial x \partial a}(0, 0) \neq 0,$$

then a flip bifurcation occurs at the fixed point $x_0 = 0$ for the bifurcation value $a = 0$.

Remark 1. Based on the nonlinear stability of the fixed point at the bifurcation point, we distinguish two cases for the flip bifurcation. If the quantity

$$Qf(0, 0) := \frac{1}{2} \left(\frac{\partial^2 f}{\partial x^2}(0, 0) \right)^2 + \frac{1}{3} \frac{\partial^3 f}{\partial x^3}(0, 0)$$

in the (B1) condition above is positive, the fixed point loses its stability at the bifurcation value and new stable two-periodic orbit emerges, in which case the flip bifurcation is called *supercritical*. Otherwise, that is, when $Qf(0, 0) < 0$, the fixed point turns unstable as it coalesces with an unstable two-periodic orbit and the bifurcation is called *subcritical*.

2.3 | Attractors

A set Γ is called *forward invariant* if $f(\Gamma) \subset \Gamma$. The ω -limit set (or *forward limit set*) of x is defined as $\omega(x) = \bigcap_{n \in \mathbb{N}} \overline{\{f^k(x) | k > n\}}$, where \bar{A} stands for the closure of A . Let $B(\Gamma)$ denote the *basin of attraction* of a forward invariant set Γ , that is, $B(\Gamma) = \{x | \omega(x) \subset \Gamma\}$. A forwards invariant set Ω is called a *metric attractor* if $B(\Omega)$ satisfies:

1. $B(\Omega)$ has positive Lebesgue measure;

2. if Ω' is another forward invariant set, strictly contained in Ω , then $B(\Omega) \setminus B(\Omega')$ has positive measure.

We will need two well-known results concerning attractors for unimodal maps with negative Schwarzian derivative (e.g., Thunberg²⁹, Th. 4, Cor. 5 and Th. 6). Let x be a periodic point of period n . Its periodic orbit is called *neutral* if $|(f^n)'(x)| = 1$.

Theorem 2. *An S-unimodal map can have at most one periodic attractor, and it will attract the critical point. Moreover, each neutral periodic orbit is attracting.*

By a periodic attractor in the above statement, we obviously mean an attracting periodic orbit, that is, a periodic orbit which is a forward limit set for each point in some of its neighborhood.

Theorem 3. *Let $f : I \rightarrow I$ be an S-unimodal map with nonflat critical point. Then f has a unique metric attractor Ω , such that $w(x) = \Omega$ for almost all $x \in I$. The attractor Ω is of one of the following types: an attracting periodic orbit, a Cantor set of measure zero, and a finite union of intervals with a dense orbit. In the first two cases, $\Omega = \omega(c)$.*

The attractor described in Theorem 3 as a finite union of intervals will be called an *interval attractor* for brevity.

3 | BIFURCATIONS IN THE CHIALVO MODEL

We start with the observation that will be crucial for our further analysis.

Proposition 1. *The map $f(x) = x^2 \exp(r - x) + k$ has negative Schwarzian derivative for all $r, k \in \mathbb{R}$.*

Proof. By the definition of the Schwarzian derivative,

$$Sf(x) = -\frac{1}{2} \frac{x^4 - 8x^3 + 24x^2 - 24x + 12}{(2x - x^2)^2} = -\frac{1}{2} \frac{(x^2 - 4x + 2)^2 + 4(x - 1)^2 + 4}{(2x - x^2)^2}.$$

This is obviously negative for all x (even for x equal to 0 or 2 we have $Sf(x) = -\infty$), which completes the proof. \square

Thus, the function whose iterations define the reduced Chialvo model (2) is an S-unimodal map, when restricted to an appropriate invariant subinterval of $[0, \infty)$, as will be discussed in details in the next section. However, let us firstly examine bifurcations of fixed points of the map $f_{r,k}$, when $k \geq 0$ is fixed and r acts as a bifurcation parameter.

We will discuss flip and fold bifurcations of fixed points for the reduced Chialvo model. Loosing stability of the fixed point and emergence of the stable periodic orbit in case of the flip bifurcation is relevant for the onset of bursting in the full 2D model. Let us also mention that other co-dimension-one bifurcations of fixed points, as well as bifurcations of periodic orbits responsible for the onset or termination of bursting in map-based models, are summarized in Izhikevich and Hoppensteadt²¹ (with examples of models and corresponding voltage plots), which provides classification of one-dimensional and two-dimensional slow-fast bursting mappings with the implications for neuron's computational abilities.

3.1 | Flip bifurcation

Theorem 4 (flip bifurcation). *Let $k \geq 0$ be fixed. For $r_0 = x_0 - \ln(x_0(x_0 - 2))$ (or equivalently $r_0 = x_0 + \ln((x_0 - k)/x_0^2)$), the 1D Chialvo map undergoes a supercritical flip bifurcation at the fixed point $x_0 = (k + 3 + \sqrt{k^2 - 2k + 9})/2$.*

Proof. Any fixed point x_0 of the map $f_{r,k}(x) = x^2 \exp(r - x) + k$ must satisfy the fixed point condition $x_0 = x_0^2 \exp(r - x_0) + k$. Simultaneously, the multiplier condition for the flip bifurcation gives

$$f'_{r_0,k}(x_0) = x_0 \exp(r_0 - x_0)(2 - x_0) = -1.$$

It follows that (when $k \geq 0$) the candidate x_0 for the flip bifurcation satisfies $x_0 > \max\{2, k\}$ and $(x_0 - k)(x_0 - 2)/x_0 = 1$. The last equation, regardless of the value of k , has always two roots $x_{0,1} = (k + 3 - \sqrt{k^2 - 2k + 9})/2$ and $x_{0,2} = (k + 3 + \sqrt{k^2 - 2k + 9})/2$. However, $x_{0,1}$ violates the condition that $x_0 > k$. Thus, $x_0 = x_{0,2}$. The formula for the parameter value r_0 follows from the multiplier condition (or equivalently the fixed point condition), and the condition (B2) of Theorem 1 can be easily verified as direct calculations give $\frac{\partial^2 f}{\partial r \partial x}(x_0, r_0) = -1 \neq 0$. Similarly, the negative value of the Schwarzian derivative immediately implies that the condition (B1) is also satisfied, as $Qf(x_0, r_0) = -Sf/3$, and the bifurcation is supercritical. \square

The flip bifurcation, for $k = 0$, is numerically illustrated in Figure 1 with the help of the cobweb diagram.

3.2 | Fold bifurcation

Theorem 5 (fold bifurcation). *Let $k \in [0, 3 - 2\sqrt{2}]$ be fixed. Then the 1D Chialvo model undergoes a fold bifurcation with r as a bifurcation parameter. In particular, for $k = 0$ and $r_0 = 1$, the map in (2) displays a fold bifurcation at the fixed point $x_0 = 1$. In turn, for fixed $0 < k \leq 3 - 2\sqrt{2}$, there are two values of the bifurcation parameter, $r_{0,1} = x_{0,1} - \ln((2 - x_{0,1})x_{0,1})$ and $r_{0,2} = x_{0,2} - \ln((2 - x_{0,2})x_{0,2})$, with corresponding values of bifurcating fixed points given, respectively, as $x_{0,1} = (k + 1 - \sqrt{k^2 - 6k + 1})/2$ and $x_{0,2} = (k + 1 + \sqrt{k^2 - 6k + 1})/2$.*

Proof. Assume $k = 0$. From the fixed point condition $x^2 \exp(r - x) = x$ and the multiplier condition $f'(x) = x \exp(r - x)(2 - x) = 1$, we easily obtain that the only candidate for the bifurcation point and parameter value is a pair $(x_0, r_0) = (1, 1)$. It is also immediate to verify that for these values, the conditions (A1) and (A2) of Theorem 1 are satisfied.

For $k > 0$, the situation is a bit more complicated. Firstly, the fixed point condition $x^2 \exp(r - x) + k = x$ and the multiplier condition $\mu = 1$ yield that the fold bifurcation is only possible for $k < 2$ and the candidate x_0 for the fixed point undergoing bifurcation must satisfy $k < x_0 < 2$. Combining the multiplier condition with the fixed point condition gives $(2 - x_0)(x_0 - k)/x_0 = 1$ or equivalently $x_0^2 - (k + 1)x_0 + 2k = 0$. The discriminant of this equation $k^2 - 6k + 1$ must be nonnegative which leads to further restriction on admissible values of k , namely, $k \leq 3 - 2\sqrt{2}$. Now, the above quadratic equation has the roots $x_{0,1}$ and $x_{0,2}$ as stated in the theorem, which both belong to the interval $(k, 2)$. When $x_0 = x_{0,1}$ or $x_0 = x_{0,2}$ the corresponding values of the bifurcation parameter ($r_{0,1}$ and $r_{0,2}$) can be easily derived from the multiplier condition $x_0 \exp(r - x_0)(2 - x_0) = 1$. We need to verify the conditions (A1) and (A2) at points $(x_{0,1}, r_{0,1})$ and $(x_{0,2}, r_{0,2})$. The latter one can only be violated when $x_{0,1} = 0$ or $x_{0,1} = k$ (correspondingly, $x_{0,2} = 0$ or $x_{0,2} = k$). But these two cases have been excluded. As for (A1), $\frac{\partial^2 f}{\partial x^2}(x, r) = \exp(r - x)((x - 2)^2 - 2)$, and thus, direct calculations show

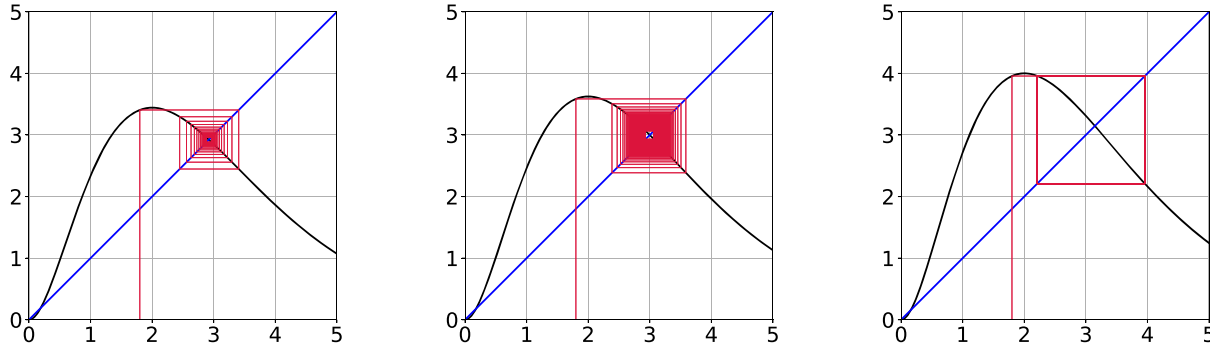


FIGURE 1 Flip bifurcation in the 1D Chialvo model with r as a bifurcation parameter ($k = 0$). Left: $r = 1.85$. Center: $r = 3 - \ln 3$ (bifurcation value). Right: $r = 2$. [Colour figure can be viewed at wileyonlinelibrary.com]

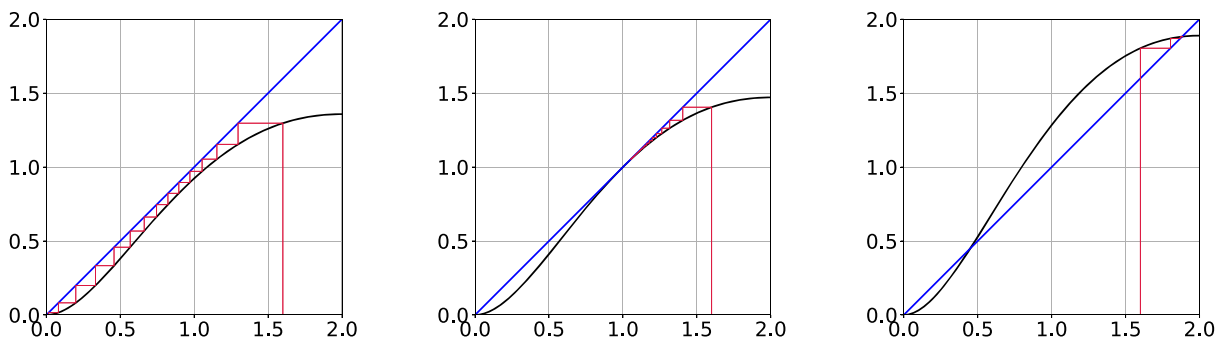


FIGURE 2 Fold bifurcation in the 1D Chialvo model with r as a bifurcation parameter ($k = 0$). Left: $r = 0.92$. Center: $r = 1$ (bifurcation value). Right: $r = 1.25$. [Colour figure can be viewed at wileyonlinelibrary.com]

that $\frac{\partial^2 f}{\partial x^2}(x_0, r_0) = 0$ (for $(x_0, r_0) \in \{(x_{0,1}, r_{0,1}), (x_{0,2}, r_{0,2})\}$) only for $k = 3 - 2\sqrt{2}$. Hence, the restriction $k < 3 - 2\sqrt{2}$ in the theorem on the fold bifurcation (we notify that $k = 3 - 2\sqrt{2}$ is the degenerate case when $x_{0,1} = x_{0,2} = 2 - \sqrt{2}$). \square

The fold bifurcation with respect to r ($k = 0$) is presented in Figure 2.

3.3 | Bifurcations with respect to k

Let us consider now k as a bifurcation parameter in the reduced Chialvo model. Since $\frac{\partial^2 f}{\partial x \partial k}(x, k) = 0$, the fundamental condition for the occurrence of a flip bifurcation is not satisfied here. However, the analysis of a fold bifurcation versus the parameter k is still possible, which is discussed below.

Theorem 6 (fold bifurcation with respect to k). *Let $r > 2 - \sqrt{2} - \ln(2\sqrt{2} - 2)$ be fixed. Then there is a unique point $x(r)$ and a unique parametr value k^* such that $x(r)$ is the fixed point of the 1D Chialvo map in the interval $(0, 2 - \sqrt{2})$ for $k = k^*$ and $x(r)$ undergoes a fold bifurcation with respect to k at the bifurcation value k^* . Moreover, the fixed point and the the bifurcation value are related by the equation*

$$k^* = x(r) - \frac{x(r)}{2 - x(r)}.$$

Proof. Observe that for $r > 2 - \sqrt{2} - \ln(2\sqrt{2} - 2)$, the multiplier equation

$$(2x - x^2) \exp(r - x) = 1$$

has a unique solution $x(r)$ in the interval $(0, 2 - \sqrt{2})$. Since the fixed point and the multiplier conditions read as follows:

$$\begin{aligned} x^2 \exp(r - x) + k &= x, \\ (2x - x^2) \exp(r - x) &= 1, \end{aligned}$$

one obtains that $x(r)$ is the fixed point if and only if $k = x - \frac{x(r)}{2 - x(r)}$. It remains to check the fold bifurcation conditions from Theorem 1. But both conditions (A1) and (A2) are obviously satisfied under our assumptions, which completes the proof. \square

Figure 3 illustrates an example of the fold bifurcation with respect to k . Namely, for $r = 0.8$, the fixed point $x(r) \approx 0.4695$ undergoes a fold bifurcation, with bifurcation parameter $k^* = 0.1627$.

3.4 | Implications for the 2D Chialvo model and neural activity

We notify that often, the knowledge about the reduced subsystem (2) gives insight into the dynamics of the full model in a properly chosen parameters range. Figures 4 and 5 present the behavior of the voltage x and the recovery variable y over simulation time of $n = 80$ iterates for $a = 0.876$ and $c = 0.28$ and initial conditions $(x_{\text{init}}, y_{\text{init}}) = (5, 3)$. The trace

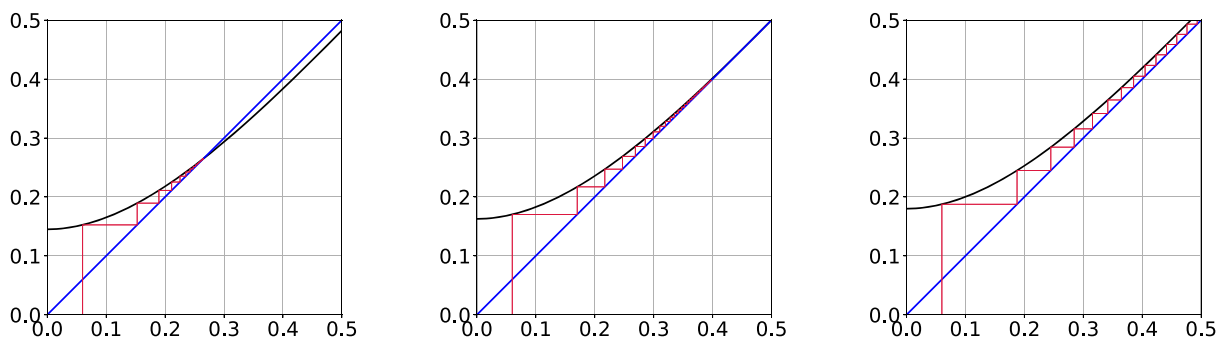


FIGURE 3 Fold bifurcation in the 1D Chialvo model with k as a bifurcation parameter ($r = 0.08$). Left: $k = 0.151$. Center: $k = 0.1627$ (numerical bifurcation value). Right: $k = 0.18$. [Colour figure can be viewed at wileyonlinelibrary.com]

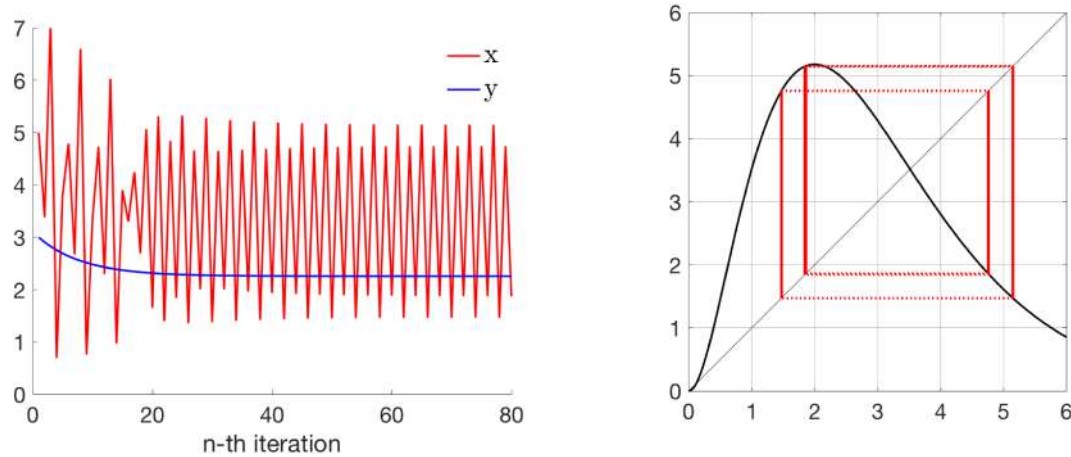


FIGURE 4 Bursting of period 4 in the 2D Chialvo model (left) and the corresponding period 4 orbit in the reduced model (right). See text for details. [Colour figure can be viewed at wileyonlinelibrary.com]

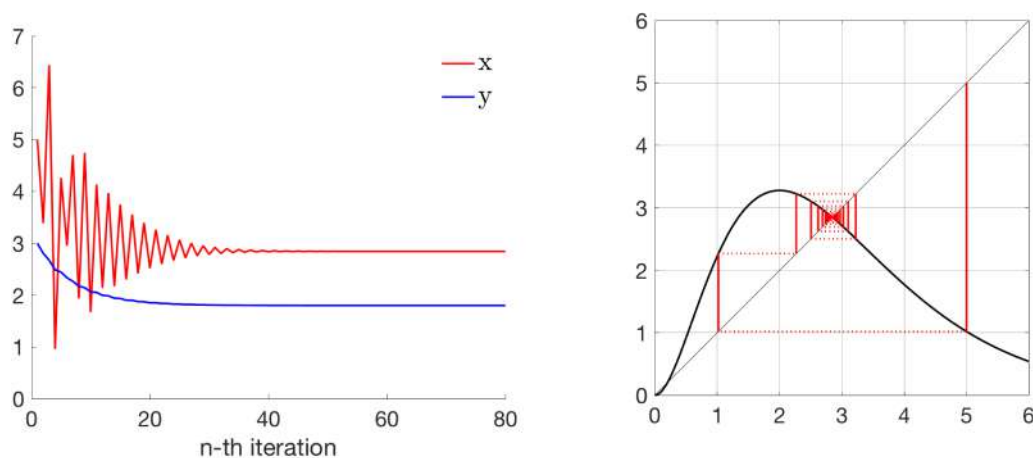


FIGURE 5 Resting of the voltage in the 2D Chialvo model (left) and the corresponding stable fixed point in the reduced model (right). See text for details. [Colour figure can be viewed at wileyonlinelibrary.com]

of the voltage x is marked in red and of the recovery variable y in blue. For $b = 0$ (Figure 4), we observe stabilization of y at $r_1 := y \approx 2.258$ and bursting of period 4 for the voltage variable. Small increase in the parameter b to $b = 0.02$ (Figure 5) yielded, for the same initial conditions, stabilization of the recovery variable at $r_2 := y \approx 1.8$, and resting of the voltage at $x \approx 2.84$ after initial damped oscillations. The corresponding reduced models given by iterates of $f_{r_1, k=0}$ and $f_{r_2, k=0}$, respectively, display (except for the superattracting fixed point $x_0 = 0$) attracting period 4 periodic orbit and nonzero stable fixed point $x_f \approx 2.84$, correspondingly. Both cobwebs present the orbit starting at $x = 5$. In Figure 5, the first 80 iterates are depicted, whereas Figure 4 shows only iterates between 60 and 80 for clarity.

Our bifurcation results (Theorems 4–6) confirm that a single neuron in the reduced Chialvo model is able to exhibit diverse activity regimes and periodic state transitions. Since quiescence plays the fundamental role in the analysis of neuronal activity, it seems to be crucial to describe the basic possible scenarios that fixed states of the model can undergo. Recall that the bifurcation parameters r (Theorems 4 and 5) and k (Theorem 6) coincide, respectively, with the recovery variable of the 2D Chialvo system and the additive voltage perturbation. Note that, in general, the flip bifurcation, which usually starts the period doubling route to chaos (compare with Section 5), corresponds to transition from quiescence to regular tonic spiking, while the fold bifurcation corresponds to appearance of new resting states.

However, our main motivation behind studying the 1D Chialvo model is not to show that it well approximates the dynamics of the full 2D model but to point out that the 1D system itself represents very rich dynamics. Indeed, within some parameters range, the behavior of the 1D map might be even more complicated. For example, while experimenting numerically with the Chialvo model, we have found that with the parameters set as $a = 0.866$, $b = 0.05$, $c = 0.48$, and

$k = 0$, the trajectory starting from the initial conditions $(x_{\text{init}}, y_{\text{init}}) = (2.8, 1.5)$ converges numerically to the period 4 cycle $\{(x_0, y_0), (x_1, y_1), (x_2, y_2), (x_3, y_3)\}$ with

x_0	y_0	x_1	y_1	x_2	y_2	x_3	y_3
1.4646	2.2539	4.7230	2.3586	2.0970	2.2864	5.3144	2.3552

On the other hand, the corresponding 1D model (with $k = 0$ and $x_{\text{init}} = 2.8$) showed period 4 periodic attractor for $r \in \{y_0, y_2\}$ and period 12 periodic attractor for $r = y_3$ and chaotic interval attractor for $r = y_1$, which agrees with our numerically obtained bifurcation diagram for the Chialvo map f_r with $k = 0$ (not shown here but similar to that from Figure 7). In Figure 6, we present, starting from top left in clockwise direction, the time-series of x - and y -variables for the 2D model and the corresponding trajectories of the reduced model (with $x_{\text{init}} = 2.8$ after removing a transient of 970 iterates) with $r = y_0$, $r = y_1$, and $r = y_3$, respectively. This behavior exemplifies that sometimes the reduced model might, counter-intuitively, show more complicated dynamics than some of its 2D extensions. Therefore, understanding of the 1D model bifurcation structure seems to be a relevant standalone topic.

We close this section with Figure 7 which shows one-parameter bifurcation diagrams for the 1D Chialvo model, obtained in Python. One can observe that the r dependence for the Chialvo family is similar to the parameter dependence in the logistic family, while the k dependence is similar to that in the Gauss family (with respect to the additive parameter).

4 | DYNAMICAL CORE OF THE CHIALVO MAP

Recall that our definition of unimodality requires that either the left endpoint of the interval domain I of the map f is a fixed point with the right endpoint of the interval as its other pre-image or that $I = [f^2(c), f(c)]$, where c is the critical

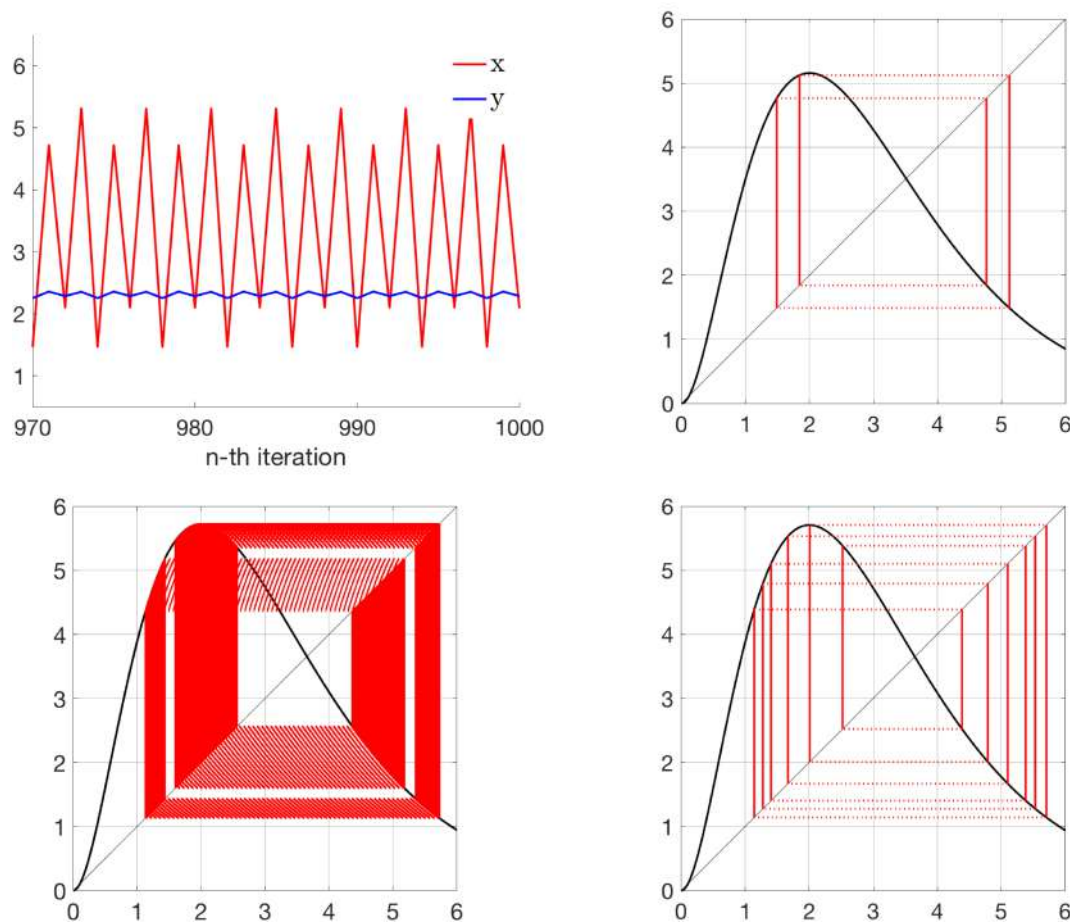


FIGURE 6 Regular period 4 bursting in the 2D model and the behavior of the reduced model in the corresponding range of r parameter values. See main text for details. [Colour figure can be viewed at [wileyonlinelibrary.com](https://onlinelibrary.wiley.com/doi/10.1002/jnm.9118)]

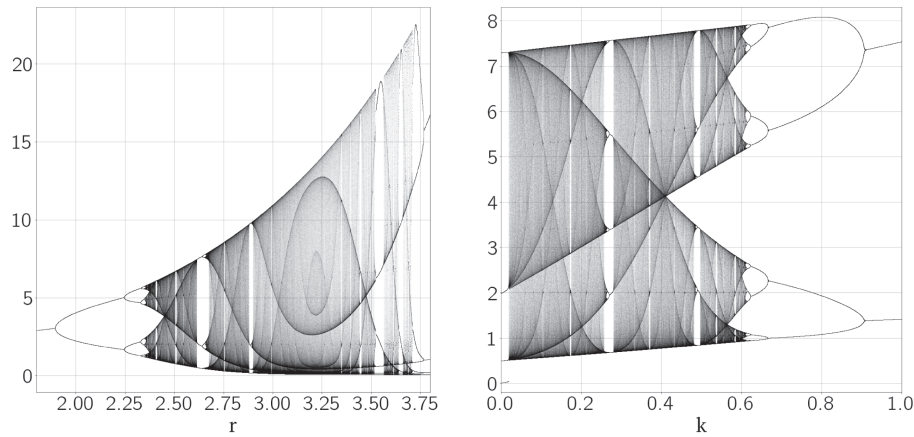


FIGURE 7 Bifurcation diagrams for the Chialvo family: versus r with fixed $k = 0.05$ (left) and versus k with fixed $r = 2.6$ (right).

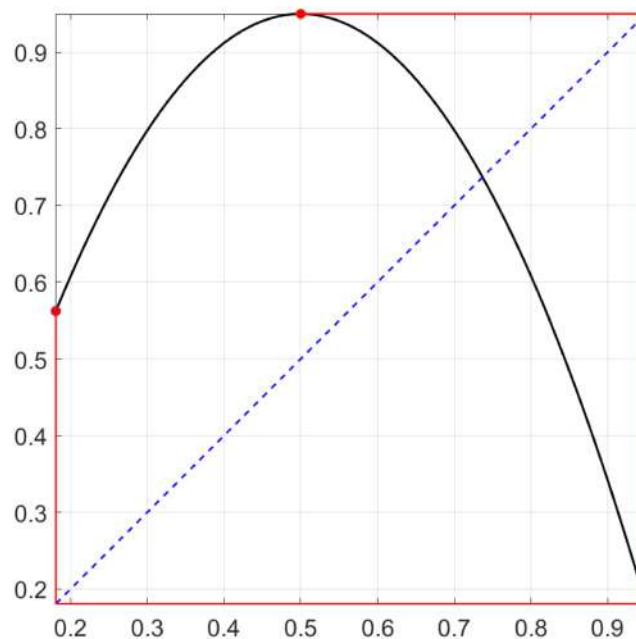


FIGURE 8 Interval $[f^2(c), f(c)]$ as a dynamical core ($c = 1/2$ is a critical point). [Colour figure can be viewed at [wileyonlinelibrary.com](https://onlinelibrary.wiley.com/terms-and-conditions)]

point (maximum) of f . In this case, we say that the interval I is the *dynamical core* of f , that is, the invariant interval where all nontrivial dynamics concentrates. An example of the dynamical core for some unimodal map is showed in Figure 8.

Below we discuss the form of the dynamical core $I_{r,k}$ for $f_{r,k}(x) = x^2 \exp(r - x) + k$ with respect to parameters k and r in order to justify that the map $f_{r,k}$ describing the 1D Chialvo model is S-unimodal on an appropriate subinterval of $[0, +\infty)$.

4.1 | Case $k = 0$

Let us firstly consider the case $k = 0$ and the corresponding map $f_{r,0}(x) = x^2 \exp(r - x)$. The map $f_{r,0}$ has exactly

- one fixed point $x_0 = 0$,
- two fixed points: $x_0 = 0$ and x_1 satisfying $0 < x_1 < 2$,
- three fixed points: x_0, x_1 and x_2 satisfying $x_0 = 0, 0 < x_1 < x_2$.

In the first two instances, the dynamics is trivial. Namely, every initial condition is attracted either by the superattracting fixed point x_0 or by the semistable fixed point x_1 (if exists). Configuration with three fixed points splits into two cases, the second with two subcases:

1. $x_2 \leq 2$,
2. $x_2 > 2$: subcase 2.1. x_2 is stable, subcase 2.2. x_2 is unstable.

Of course, there is also a special case when $x_2 = 3$ undergoes flip bifurcation (when $2 < x_2 < 3$, then x_2 is stable and if $x_2 > 3$ then it is unstable as follows from simple calculations in the part concerning flip bifurcation). Cases 1. and 2.1. are again trivial. Therefore, for our further developments, we shall be interested in case 2.2. Note that under this condition, x_2 satisfies $x_2 \exp(-x_2) = \exp(-r)$, and for the derivative, we have $|f'_{r,0}(x_2)| = |2 - x_2| > 1$. Therefore, with the increase of r , the fixed point $x_2 > 3$ moves further to the right and remains unstable. Simultaneously, the fixed point x_1 remains to the left of $c = 2$ and is unstable. If, moreover, $x_1 < f_{r,0}^2(2)$, then the interval $[f_{r,0}^2(2), f_{r,k}(2)]$ can be treated as the dynamical core of the map $f_{r,0}$, because every initial condition $x \in (x_1, \infty)$ is after a few iterates mapped into $[f_{r,0}^2(2), f_{r,k}(2)]$. On the other hand, all the points in $(0, x_1)$ are monotonically attracted to the resting state $x_0 = 0$. We are mainly interested in this case, that is, when $x_1 \notin [f_{r,0}^2(2), f_{r,0}(2)]$, which holds at least for some interval of r -values (see Lemma 1 and Remark 2).

4.2 | Case $k > 0$

Now let us consider the case $k > 0$. Note that when $k \geq 2$, the dynamics of $f_{r,k}$ is actually trivial: indeed, for $k \geq 2$, there is exactly one fixed point x_0 which is located on the right (decreasing) part of the graph (i.e., $x_0 > k \geq 2$). As also $f_{r,k}^2(2) > k \geq 2$, the interval $[2, f_{r,k}(2)]$ is an invariant interval and every initial condition $x \in \mathbb{R}$ is after at most one iterate mapped into this interval. On the other hand, as $f_{r,k}$ is strictly decreasing on this interval, every initial condition $x \in \mathbb{R} \setminus \{x_0\}$ is actually attracted to x_0 (if x_0 is attracting) or to period 2 periodic orbit (if x_0 is not attracting). Obviously, in this case, the dynamical core can be set as $[f^2(2), f(2)]$.

Therefore, assume that $0 < k < 2$. Then (especially for small values of r) one possibility is that $f_{r,k}$ has only one fixed point x_0 , which is located on the left branch: $x_0 \leq 2$. Note that in this case, x_0 is globally attracting, and thus, this is the trivial case. If x_0 is a unique fixed point but $x_0 > 2$, then, depending on r , the fixed point x_0 can be either stable or unstable, but, as $f_{r,k}^2(2) > k = f_{r,k}(0)$, we can set the interval $[f_{r,k}^2(2), f_{r,k}(2)]$ as the dynamical core, which contains exactly one fixed point $x_0 > 2$. Lemma 1 asserts that this always holds for r large enough.

The situation when $f_{r,k}$ has exactly two fixed points is very rare (it holds, e.g., when there is a fixed point $x_0 > 0$ and the other fixed point $x_1 = x_2$ is just undergoing the fold bifurcation). Thus, the effective complementary case for unique fixed point x_0 is the situation when there are exactly three fixed points $0 < x_0 < x_1 < x_2$ and necessarily then $x_1 \leq 2$. If also $x_2 \leq 2$, then every initial condition (except x_1) is attracted either to x_0 or to x_2 . It follows that for $0 < k < 2$, the nontrivial generic case with three fixed points is the situation when $0 < x_0 < x_1 < 2 < x_2$ (with x_2 that can be stable or unstable). If $f_{r,k}^2(2) < x_1$, then as a dynamical core, we set $[x_0, y_0]$, where $y_0 \in f_{r,k}^{-1}(x_0)$ and $y_0 \neq x_0$ (note that such a point y_0 exists since $f_{r,k}(x) \rightarrow k < x_0$ as $x \rightarrow \infty$). Then $f_{r,k} : [x_0, y_0] \rightarrow [x_0, y_0]$ matches the definition of the unimodal map. On the other hand, if $f_{r,k}^2(2) \geq x_1$, we can assume that the dynamical core is $[f_{r,k}^2(2), f_{r,k}(2)]$ (the map $f_{r,k}$ restricted to this interval is unimodal).

4.3 | Auxiliary results on dynamical core

This subsection contains several results concerning the dynamical core of the 1D Chialvo map, which will be of our interest in the next section (e.g., in the proof of Theorem 11). The technical proofs of Lemmas 1 and 2 are postponed to Appendix A.

Lemma 1. For any $0 \leq k < 2$, there exists $r^* = r^*(k)$ such that for all $r \geq r^*(k)$, we have

$$f_{r,k}^2(c) < c < f_{r,k}(c), \quad (5)$$

where $f_{r,k}(x) = x^2 \exp(r - x) + k$ is the 1D Chialvo map and $c = 2$ is its critical point. Moreover, for $k \neq 0$, the value of $r^*(k)$ can be chosen such that, in addition, for $r \geq r^*(k)$, the interval $[f_{r,k}^2(c), f_{r,k}(c)]$ contains exactly one fixed point x_f .

Remark 2. For $k = 0$, demanding that (5) is satisfied and simultaneously there are no fixed points in $[f_{r,0}^2(c), f_{r,0}(c)]$ to the left of c requires some more specific range of r values. Indeed, for $k = 0$, the map can have three fixed points $x_0 = 0$, $0 < x_1 < 2$, and $x_2 > 2$ with x_1 that actually can fall into the interval $[f_{r,0}^2(c), f_{r,0}(c)]$. We have verified numerically that for any $r \in [2.1, 2.97]$, inequality (5) is satisfied with $f_{r,0}^2(c) > x_1$. In turn, for $r = 2$, we have $f_{r,0}^2(c) \approx 2.1654 > c = 2$ (violating (5)) and for $r = 2.98$ $f_{r,0}^2(c) < x_1$ as $f_{r,0}^2(c) \approx 0.0526$ and $x_1 \approx 0.0535$.

Remark 3. Consequently, the interval $[f_{r,k}^2(c), f_{r,k}(c)]$ (in the proper parameter regime, i.e., $r \geq r^*(k)$ for $k \in (0, 2)$ and $r \in [2.1, 2.97]$ for $k = 0$) can be treated as dynamical core of $f_{r,k}$, which contains exactly one fixed point, namely, $x_f > 2$.

The next lemma assures that with r large enough, the fixed point x_f mentioned above is unstable.

Lemma 2. For any $0 \leq k < 2$, there exists $r^*(k)$ such that for all $r \geq r^*(k)$, the map $f_{r,k}$ has an unstable fixed point $x_f > 2$.

Corollary 1. For every $k \in [0, 2)$, there exists an interval $[r_1, r_2]$ of positive r -values such that for any $r \in [r_1, r_2]$, the map $f_{r,k}$ has an attracting fixed point $x_f > 2$.

The above corollary can be easily justified taking into account the proof of Lemma 2 and the fact that for a S-unimodal map f every fixed point x_f with $|f'(x_f)| \leq 1$ is attracting.

5 | PERIODIC VERSUS CHAOTIC BEHAVIOR

The 1D Chialvo map (2) except for regular behavior due to the existence of stable fixed points or periodic orbits can also exhibit chaotic behavior. There are many different notions of chaos (see Aulbach and Kieninger³⁶), with the most prominent one probably due to Devaney.³⁷ The common point of most of these definitions is some sort of sensitive dependence on initial conditions. In our approach, we will consider both metric chaos associated with the existence of the absolutely continuous invariant probability measure (acip), which, as we recall below, for S-unimodal maps can be identified with some strong sensitive dependence on initial conditions and topological chaos corresponding to the classical definitions of Li and Yorke, Block and Coppel, and Devaney.

5.1 | Periodic attractors

Since the reduced Chialvo map is S-unimodal and its critical point is nondegenerate, the following two theorems are immediate consequences of Theorems 2 and 3.

Theorem 7. The 1D Chialvo map (2) can have at most one periodic attractor and this attractor attracts the critical point $c = 2$.

Let Γ be a periodic orbit with period n and let $\lambda(\Gamma) = (f^n)'(x)$ for $x \in \Gamma$. It is clear that $|\lambda(\Gamma)| \in [0, 1)$ implies that Γ is attracting. However, since f is S-unimodal, by Theorem 2, also neutral periodic orbits (i.e., such that $|\lambda(\Gamma)| = 1$) are attracting.

Theorem 8. The 1D Chialvo map has a unique metric attractor \mathcal{A} which is a limit set $\omega(x)$ for almost all initial conditions x . This attractor is an attracting periodic orbit, a Cantor set of measure zero, or a finite union of intervals with a dense orbit (so-called interval attractor).

We say that two unimodal maps f and g are *combinatorially equivalent* if there exists an order-preserving bijection $h : \cup_{n \geq 0} f^n(c) \rightarrow \cup_{n \geq 0} g^n(c')$ such that $h(f^n(c)) = g^n(c')$ for all $n \geq 0$, where c and c' are critical points of f and g . In other words, f and g are combinatorially equivalent if the order of their forward critical orbit is the same.

Let us present the following general mathematical observation, which might be known to specialists in one-dimensional dynamics but probably lacks clear references as follows, for example, from Remark 4 below.

Lemma 3. Assume that f and g are S-unimodal maps. If f has a period 2 attracting orbit and g has a period 3 attracting orbit, then f and g are not combinatorially equivalent.

Proof. Let \mathcal{A} denote a periodic attractor and c a critical point. Since $\omega(c) = \mathcal{A}$, starting from some iteration, the order of the critical point orbit is the same as the order on the periodic attractor. Obviously, the orders of a two- and a three-periodic orbit are different, which is our claim. \square

Remark 4. In Schreiber,³⁸ it is stated that a map with an attracting equilibrium and a map with a period 2 attracting orbit are not combinatorially equivalent, which in general is not true.

Let us also formulate a conjecture which generalizes Lemma 3 and which we believe is true.

Conjecture 1. Let f and g be S -unimodal maps, $m > k$ and $m \neq 2k$. If f has an attracting periodic orbit with a prime period m and g has an attracting periodic orbit with a prime period k , then f and g are not combinatorially equivalent.

The following useful result can be found in Kozlovski.³⁹, Th. C

Theorem 9 (Kozlovski). Let $\Lambda \subset \mathbb{R}^k$ be open and $\{f_\lambda\}_{\lambda \in \Lambda}$ be an analytic family of unimodal maps with a nondegenerate critical point and negative Schwarzian derivative. If there exist two maps in $\{f_\lambda\}$ that are not combinatorially equivalent, then there exists a dense subset Θ of Λ such that f_λ has a stable attracting periodic orbit for every $\lambda \in \Theta$.

The next result describes the subset in parameter space corresponding to periodic attractors.

Theorem 10. The set of parameters for which the 1D Chialvo map $f_{r,k}$ has a stable attracting periodic orbit forms a dense subset of

1. the r parameter space \mathbb{R} when $k \in [0, 2)$ is fixed,
2. the (r, k) parameter space $\mathbb{R} \times [0, 2)$.

Proof. Let $k \in [0, 2)$ be fixed. Clearly, for some r , the map $f_{r,k}$ has a period 2 attracting orbit and for some other r it has a period 3 one. Consequently, Lemma 3 guarantees that the family $\{f_{r,k}\}$ contains two maps that are not combinatorially equivalent. Alternatively, to obtain two such maps, we can use the kneading sequences from the proof of Corollary 2. Since all other assumptions of Theorem 9 are obviously satisfied, the assertion of the first statement of our theorem follows the Kozlovski theorem. Finally, the second statement of our theorem follows from the first one. \square

5.2 | Metric chaos

The following theorem guarantees that 1D Chialvo maps are strongly chaotic with positive frequency in parameter space. As we have mentioned above, strong chaos here is associated with the existence of acip measure. Below we present the rigorous proof in the case $k = 0$ and conclusions of numerical analysis for the case $k \in (0, 0.58)$. Here and subsequently, δ_x denotes the Dirac measure at the point x and $\text{supp}(\mu)$ the support of a measure μ . Moreover, recall that a map f is called a *Misiurewicz map* if it has no periodic attractors and if critical orbits do not accumulate on critical points, that is, when

$$C_f \cap \omega(C_f) = \emptyset,$$

where C_f denotes the set of critical points of f . For a parametrized family of maps $\{f_r\}$, the values of parameters for which f_r are Misiurewicz maps are called *Misiurewicz parameters*. An example of such a parameter in the logistic family $Q(x) = \mu x(1 - x)$ is $\mu = 4$.

For fixed k , let $f_r(x) := x^2 \exp(r - x) + k$ and let $I_r \subset [0, \infty)$ denote the dynamical core of f_r (see Section 4 for details).

Theorem 11. Let $k = 0$ be fixed. There exists a positive Lebesgue measure set \mathcal{R} such that for all $r \in \mathcal{R}$:

- the map $f_r : I_r \rightarrow I_r$ admits an absolutely continuous invariant probability measure μ_r such that

$$\mu_r = \lim_{n \rightarrow \infty} \frac{1}{n} \sum_{i=0}^{n-1} \delta_{f_r^i(x)} \quad \text{for a.a. } x \in I_r, \quad (6)$$

that is, μ_r describes the asymptotic distribution of almost all orbits under f_r ,

- the unique metric attractor of the map f_r is an interval attractor \mathcal{A}_r ; moreover, $\mathcal{A}_r = \text{supp}(\mu_r)$ and μ_r is equivalent to the Lebesgue measure on \mathcal{A}_r .

In consequence, for each $r \in \mathcal{R}$, the Lyapunov exponent of f_r is positive, that is,

$$\lim_{n \rightarrow \infty} \frac{1}{n} \log |Df_r^n(x)| = \kappa_r > 0 \quad \text{for a.a. } x \in I_r, \quad (7)$$

where D denotes the derivative with respect to x .

Proof. The statements of the above theorem follow from some nowadays classical results on S-unimodal maps, for example, from Theorem 18 and Corollary 19 in Thunberg,²⁹ provided that the below-listed conditions C1–C6 are satisfied for some interval of parameters r :

- C1. $\{f_r\}$ is a one-parameter family of C^2 unimodal maps of an interval I (in general the interval I can vary with the change of the parameter r , i.e. $I = I_r$),
- C2. each f_r has a nondegenerate critical point c ,
- C3. the map $(x, r) \mapsto (f_r(x), D_x f_r(x), D_{xx} f_r(x))$ is C^1 ,
- C4. each f_r has a repelling fixed point on the boundary of I ,
- C5. there is a parameter value r^* such that the critical orbit is mapped onto an unstable periodic cycle P^* in a finite number of steps (this implies that f_{r^*} is a Misiurewicz map),
- C6. the map moves with the parameter at r^* in the following technical sense

$$\frac{d}{dr}(x(r) - f_r(c))|_{r=r^*} \neq 0,$$

where $x(r)$ is a point of I and $P(r)$ is an unstable periodic orbit such that

- $r \mapsto x(r)$ is differentiable,
- $x(r^*) = f_{r^*}(c)$,
- $P(r)$ moves continuously with r ,
- $x(r)$ is mapped onto $P(r)$ in the same number of steps as $x(r^*)$ and onto the corresponding point of $P(r)$

(existence of such a point and orbit is guaranteed by the perturbation theory).

We are left with the task of checking all these conditions. We will see that in fact only C5 and C6 might pose a problem.

Ad C1–C3. It is easy to see that in our situation, the first three conditions do not require any justification.

Ad C4. The condition C4 can also be formally achieved by properly extending the map f_r beyond its dynamical core $[f_r^2(c), f_r(c)]$ which does not effect its dynamics as all the points in I will after a few iterates be mapped into the dynamical core. Recall that by Lemma 1 for each $k = 0$ and $r = r(k)$ large enough, we can set $[f_r^2(c), f_r(c)]$ as a dynamical core such that there are no fixed points in $[f_r^2(c), f_r(c)]$ except for x_f located on the decreasing branch of f , i.e., $x_f > 2$.

Ad C5. We will show that there exists a map f_{r^*} such that the critical point c is mapped in a few steps onto the unstable fixed point. Such a map is necessarily a Misiurewicz map. Let us only remind that Misiurewicz maps can be found in a number of ways, and our idea of the proof is chosen for simplicity. We will call r^* the *Misiurewicz parameter*.

Let us firstly justify that the fixed point $x_f > 2$ is unstable for the r -parameter values used in further estimation of the Misiurewicz parameter. Let x_f be a fixed point of $f(x) = x^2 \exp(r - x)$. Then for $x_f \neq 0$, we have $x_f \exp(-x_f) = \exp(-r)$. The right-hand side of this equality decreases with r , and similarly, the left one is a decreasing function of x_f for $x_f > 1$ (we are interested in $x_f > 2$). Therefore, the value of the fixed point $x_f > 2$ also increases as r increases, that is, with the increase of r , the fixed point $x_f > 2$ moves further to the right. Since $f'(x_f) = x_f \exp(r - x_f)(2 - x_f) = 2 - x_f$, x_f is unstable whenever $x_f > 3$. In our below estimation of the Misiurewicz parameter, we consider $r \in (2.43, 2.44)$. As for $r \geq 2.43$, we certainly have $x_f > 3$, x_f is unstable in this parameter range (taking into account the above arguments and our previous estimation of flip bifurcation r value, x_f remains unstable fixed point for all $r > r_0 \approx 1.901$).

We show the existence of the Misiurewicz parameter in the interval $r \in (2.43, 2.44)$. Namely, we prove that for the parameter value $r^* \approx 2.436$, the critical point $c = 2$ is mapped onto the unstable fixed point after exactly three iterations. We make use of the cobweb diagram, instead of using numerical approximations methods. Let $d(r)$ be the distance between the third iteration of the critical point $x_c = 2$ and the corresponding fixed point $x_f(r)$, that is, $d(r) = f^3(2, r) - x_f(r)$. Although we do not have an explicit expression for the fixed point, $d(r)$ represents a smooth function in r . Since $d(r)$ changes sign in the interval $2.43 < r < 2.44$, that is illustrated in Figures 9 and 10, by the intermediate value theorem, there exists $r^* \in (2.43, 2.44)$ such that $d(r^*) = 0$, and therefore, the critical point is mapped onto the fixed point in three iterations. Note that in this way, we have obtained actually a rigorous proof of the existence of a Misiurewicz map and the numerics were only used for estimation of the Misiurewicz parameter.

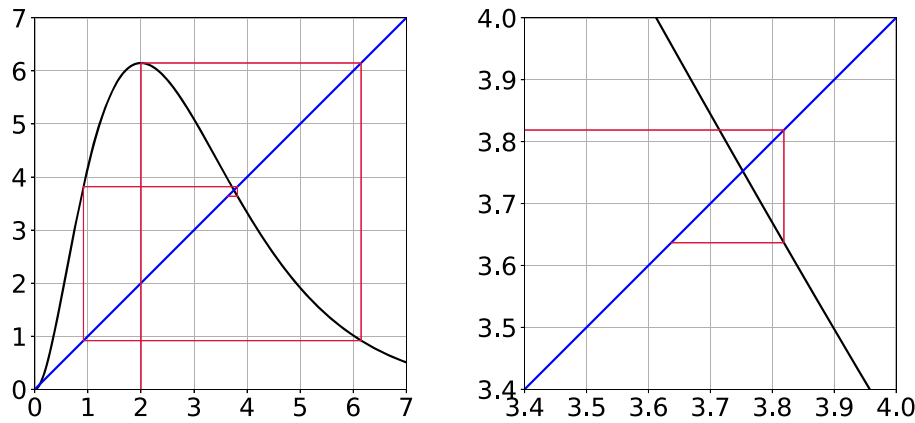


FIGURE 9 Lower estimation of the Misiurewicz parameter (case $k = 0$): $d(r) > 0$ for $r = 2.43$. Left: iterations of the critical point. Right: close-up of cobweb around the fixed point. [Colour figure can be viewed at wileyonlinelibrary.com]

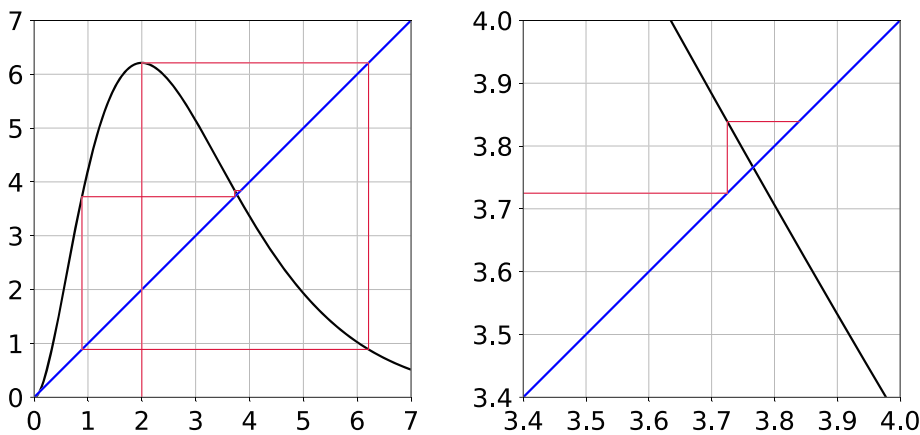


FIGURE 10 Upper estimation of the Misiurewicz parameter (case $k = 0$): $d(r) < 0$ for $r = 2.44$. Left: iterations of the critical point. Right: close-up of cobweb around the fixed point. [Colour figure can be viewed at wileyonlinelibrary.com]

Ad C6. We will verify the condition C6 numerically as in Thunberg.²⁹ Let us define $f(x, r) = f_r(x)$, and $f^n(x, r) = f(f^{n-1}(x, r), r) = f_r^n(x)$ for $n > 1$. For r close to r^* , we may define $\zeta(r)$ by the formulas

$$\zeta(r^*) = f_{r^*}(c) \text{ and } f^2(\zeta(r), r) = z(r),$$

where c is the critical point and $z(r)$ is an unstable fixed point of f_r (see Lemma 2). This means that $\zeta(r)$ is a point close to $f_r(c)$ with the same type of forward orbit as $f_{r^*}(c)$. We abbreviate $f(\zeta(r), r)$ to $\zeta_1(r)$. The condition C6 now reads

$$\frac{d}{dr} (\zeta(r) - f(c, r))|_{r=r^*} \neq 0.$$

By the definition of ζ , we have the following:

$$\begin{aligned} \frac{d\zeta}{dr} &= \left(\frac{\partial f}{\partial x}(\zeta, r) \right)^{-1} \left\{ \left(\frac{\partial f}{\partial x}(\zeta_1, r) \right)^{-1} \left(\frac{dz}{dr} - \frac{\partial f}{\partial r}(\zeta_1, r) \right) - \frac{\partial f}{\partial r}(\zeta, r) \right\} \\ &= \frac{dz}{dr} \cdot \frac{\exp(\zeta + \zeta_1 - 2r^*)}{\zeta \zeta_1 (2 - \zeta)(2 - \zeta_1)} - \frac{\zeta_1 \exp(\zeta - r^*)}{\zeta (2 - \zeta)(2 - \zeta_1)} - \frac{\zeta}{2 - \zeta}. \end{aligned} \quad (8)$$

Observe that all the partial derivatives in (8) can be computed explicitly. To find the value of $\frac{dz}{dr}$, we differentiate the implicit formula for fixed points $z^2 \exp(r - z) = z$, which gives $\frac{dz}{dr} = \frac{z}{z-1}$. In consequence, to check the condition

C6, we need only the previous estimation of the Misiurewicz parameter ($r^* \approx 2.436$) and the similar estimation of the corresponding fixed point ($z(r^*) \approx 3.761$). The final calculations (done in MATLAB) are presented in the first column of Table 1. As we see, $\frac{d}{dr}(\zeta(r) - f(c, r))|_{r=r^*} \approx -3.851$, so it is nonzero, which shows that the condition C6 is satisfied and completes the proof. \square

Remark 5. Unfortunately, when $k > 0$ we are not able to prove rigorously that the conditions C5 and C6 are satisfied for all k in this range. However, we can provide numerical justification of both the existence of the Misiurewicz parameter r^* (C5) and the nonzero value of the term $\Gamma = \frac{d}{dr}(\zeta(r) - f(c, r))|_{r=r^*}$ (C6) for some values of the parameter k between 0 and 0.58. Recall that, by Lemma 2, for any $0 < k < 2$, there exists $\hat{r} = \hat{r}(k)$ such that for all $r \geq \hat{r}$, the map f_r has an unstable fixed point $x_f > 2$. It occurs that for $k \in (0, 0.58]$, one can proceed in much the same way as in the case $k = 0$ to show that there exists r^* such that the map f_{r^*} is a Misiurewicz map. We simply search for r^* such that the third iteration of the critical point is mapped onto the unstable fixed point (this method does not work for $k > 0.58$). The calculation of the term Γ is also similar as in the case $k = 0$. Formula (8) still holds, but $\frac{dz}{dr} = \frac{z^2}{\exp(z-r)+z^2-2z}$ for $k > 0$. The results of our numerical analysis are summarized in Table 1. Note that only the last row of Table 1 does not display monotonic behavior. Finally, in Figure 11, we present plots of the Misiurewicz parameter r^* and the term Γ from the condition C6 as functions of the parameter $k \in [0, 0.58]$ (in both cases the step size is 0.001). Observe the rapid growth of the value of Γ near $k = 0.58$.

We finish this subsection with a result showing that in the Chialvo model, two cases (periodic attractors and acips) occupy a set of full measure in parameter space. Namely, the following classical theorem from Avila et al.^{40, Th. B} can be applied in the analysis of the reduced Chialvo map. The original result is more general, as it considers the class of quasiquadratic maps, which contains S-unimodal maps with a nondegenerate critical point. Recall that a one-parameter family of S-unimodal maps is called *trivial* if all maps have the same kneading sequence, and the multipliers of any nonrepelling orbits are the same for all maps.

TABLE 1 Data for estimation of $\Gamma = \frac{d}{dr}(\zeta(r) - f(c, r))|_{r=r^*}$ for some k in $[0, 0.58]$.

Term	k = 0	k = 0.01	k = 0.1	k = 0.3	k = 0.5	k = 0.55	k = 0.58
r^*	2.436	2.439	2.461	2.535	2.681	2.759	2.851
$z(r^*)$	3.761	3.768	3.830	3.999	4.254	4.367	4.491
$\zeta = \zeta(r^*)$	6.186	6.215	6.443	7.130	8.403	9.095	9.948
$\zeta_1 = \zeta_1(r^*)$	0.900	0.895	0.874	0.814	0.731	0.697	0.662
$\frac{d\zeta}{dr}(r^*)$	2.335	2.335	2.383	2.594	3.491	4.433	6.426
$\frac{\partial f}{\partial r}(c, r^*)$	6.186	6.205	6.343	6.830	7.903	8.545	9.368
$\Gamma = \frac{d\zeta}{dr}(r^*) - \frac{\partial f}{\partial r}(c, r^*)$	-3.851	-3.870	-3.960	-4.236	-4.412	-4.112	-2.942

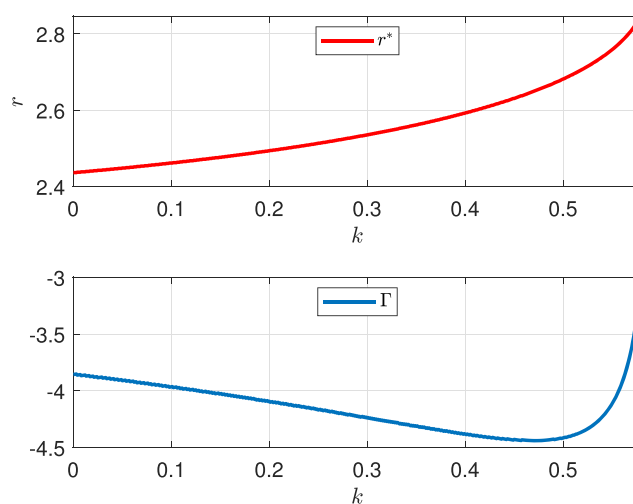


FIGURE 11 The Misiurewicz parameter r^* (upper plot) and $\Gamma = \frac{d}{dr}(\zeta(r) - f(c, r))|_{r=r^*}$ (lower plot) as functions of the parameter $k \in [0, 0.58]$ (step size 0.001). [Colour figure can be viewed at wileyonlinelibrary.com]

Theorem 12 (Avila, Lyubich, de Melo). Let $\Lambda \subset \mathbb{R}$ be open and let $\{f_\lambda\}_{\lambda \in \Lambda}$ be a nontrivial real-analytic family of S -unimodal maps with a no-degenerate critical point. Then for Lebesgue-almost all parameter values $\lambda \in \Lambda$ the map, f_λ has either a periodic attractor (such a map is called regular) or an interval attractor supporting an acip (such a one is called stochastic).

Proposition 2. If $k \in [0, 2)$ is fixed, then for Lebesgue-almost all parameters r , the 1D Chialvo map f_r has either a periodic attractor or an interval attractor supporting an acip.

Proof. It suffices to show that the 1D Chialvo family with respect to r is nontrivial. However, when $k \in [0, 2)$, our family contains two maps with the kneading sequences of the form $(CC \dots)$ (the critical point is fixed) and $(C1 \dots)$ (the critical point is on the left from the fixed point), which is our claim. \square

5.3 | Topological chaos

Let us start this subsection with three classical definitions of topological chaos for discrete dynamical systems given by Li and Yorke⁽⁴¹⁾, Block and Coppel⁽⁴²⁾, and Devaney⁽³⁷⁾. The relations among these three definitions of chaos for continuous maps are comprehensively explained in Aulbach and Kieninger.³⁶ Recall that Σ denotes the *sequence space* on the two symbols $\{\alpha = (a_0 a_1 a_2 \dots) | a_i = 0 \text{ or } a_i = 1\}$ with the metric $d(\alpha, \beta) = \sum_{i=0}^{\infty} |a_i - b_i| / 2^i$. The *shift map* $\sigma : \Sigma \rightarrow \Sigma$ is given by $(a_0 a_1 a_2 \dots) \rightarrow (a_1 a_2 a_3 \dots)$. From now on, assume that X is a compact metric space and $f : X \rightarrow X$ is continuous.

Definition 1 (L/Y-chaos). A map f is called *chaotic in the sense of Li and Yorke* (L/Y-chaotic for short) if there exists an uncountable subset S (called *scrambled set*) of X with the following properties:

1. $\limsup_{n \rightarrow \infty} d(f^n(x), f^n(y)) > 0$ for all $x, y \in S, x \neq y$,
2. $\liminf_{n \rightarrow \infty} d(f^n(x), f^n(y)) = 0$ for all $x, y \in S, x \neq y$,
3. $\limsup_{n \rightarrow \infty} d(f^n(x), f^n(p)) > 0$ for all $x \in S, p \in X, p$ periodic.

Definition 2 (B/C-chaos). A map f is called *chaotic in the sense of Block and Coppel* (B/C-chaotic for short) if there exists $m \in \mathbb{N}$ and a compact f^m -invariant subset Y of X such that $f^m|_Y$ is semiconjugate to the shift on Σ , that is, if there exists a continuous surjection $h : Y \rightarrow \Sigma$ satisfying $h \circ f^m = \sigma \circ h$ on Y .

Definition 3 (D-chaos). A map f is called *chaotic in the sense of Devaney* (D-chaotic for short) if there exists a compact invariant subset Y (called a *D-chaotic set*) of X with the following properties:

1. $f|_Y$ is topologically transitive,
2. the set of periodic points $\text{Per}(f|_Y)$ is dense in Y , i.e., $\overline{\text{Per}(f|_Y)} = Y$,
3. $f|_Y$ has sensitive dependence on initial conditions.

The following result provides the sufficient condition for the existence of topological chaos in the 1D Chialvo model in all the above senses.

Theorem 13. If the 1D Chialvo map f satisfies the condition

$$f^2(c) < f^3(c) < c < f(c) \quad (c = 2 \text{ is the critical point}), \quad (9)$$

then it is chaotic in the sense of Li and Yorke, Block and Coppel, and Devaney.

Proof. Let $x_0 = c$ and $x_i = f(x_{i-1})$ for $i = 1, 2, 3$. By the intermediate value theorem, the map $f : [x_0, x_1] \rightarrow [x_2, x_1]$ has a unique fixed point $z \in (x_0, x_1)$. Observe that

$$f([x_2, x_0]) = [x_3, x_1] \supset [z, x_1] \text{ and } f([x_0, z]) = [z, x_1],$$

and in consequence,

$$[x_2, z] = [x_2, x_0] \cup [x_0, z] \subset f^2([x_2, x_0]) \cap f^2([x_0, z]).$$

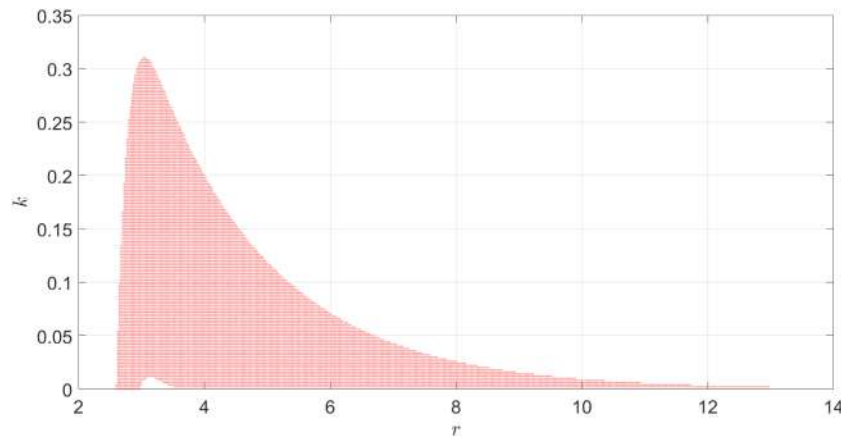


FIGURE 12 Topological chaos values (red dots) for the 1D Chialvo model in (r, k) parameter plane. [Colour figure can be viewed at [wileyonlinelibrary.com](https://onlinelibrary.wiley.com/doi/10.1002/ana.9118)]

Hence, f^2 is turbulent, that is, there are nonempty closed subintervals J, K of $[x_2, x_1]$ with disjoint interiors such that $J \cup K \subset f^2(J) \cap f^2(K)$. By Aulbach and Kieninger,^{36, Prop. 3.3} the map $f : [x_2, x_1] \rightarrow [x_2, x_1]$ is B/C-chaotic. Moreover, by Aulbach and Kieninger,^{36, Th. 4.1} this is equivalent to being D-chaotic and by Aulbach and Kieninger,^{36, Th. 4.2} this implies being L/Y-chaotic. \square

Remark 6. It is worth pointing out that according to the above definitions of chaos, the map is chaotic if it displays chaotic behavior on a nonempty compact invariant subset of the dynamical core (not necessarily on the whole domain interval), and this set can be small both in the sense of measure and category. Notice also that the above proof works for an arbitrary unimodal map, whose critical point satisfies (9).

It occurs that the sufficient condition from Theorem 13 is actually satisfied for some range of parameters in the Chialvo model.

Proposition 3. For $k = 0$ and $2.6 \leq r \leq 2.9$, the 1D Chialvo map f_r satisfies (9) and, in consequence, is chaotic in the sense of Li and Yorke, Block and Coppel, and Devaney.

The technical proof of Proposition 3 is postponed to Appendix B.

Remark 7. When $k > 0$, by means of numerical simulations, we are able to observe a dependence between values of r and k for which the condition (9) from Theorem 13 is satisfied. However, it is difficult to obtain an interval for r where all the inequalities are satisfied independently of the values of k . Figure 12 below depicts the result of a numerical simulation in MATLAB. We plot values of r and k for which condition (9) is satisfied. The intervals of study for both parameters are: $2 \leq r \leq 14$ with step size 0.025 and $0 \leq k \leq 0.35$ with step size 0.002. The short of the program and the table with computed parameter values can be found in an open repository.⁴³

5.4 | Conclusions for the neuron activity analysis

It should be emphasized that the standalone 1D model (2) is able to reproduce a wide range of interesting neuronal behaviors (similarly to its 2D counterpart). In Figure 13, we show two examples of voltage trajectories. The trajectory with initial condition $x_{\text{init}} = 2.2$ and parameter values $k = 0.1$ and $r = 2.45$ displays “chaotic” spiking with subthreshold oscillations (depicted on the left), which can be also classified as (nonregular) MM(B)Os (mixed-mode (bursting) oscillations), that is, spikes (or bursts) interspersed with small (“subthreshold”) oscillations. Note that Theorem 11 guarantees that for $k = 0$, the set of parameters r for which the model that exhibits “strongly chaotic” behavior (chaotic spiking/ bursting, irregular MMOs, etc.) is “observable” (has a positive Lebesgue measure). However, the estimation of its actual size is a completely different and much harder task (see, e.g., Luzzatto and Takahasi⁴⁴). Moreover, for $k = 0$, “weak chaotic” behavior of the model is even more clearly “visible” as, according to Proposition 3, it occurs for the set of parameters r containing a “quite big” interval.

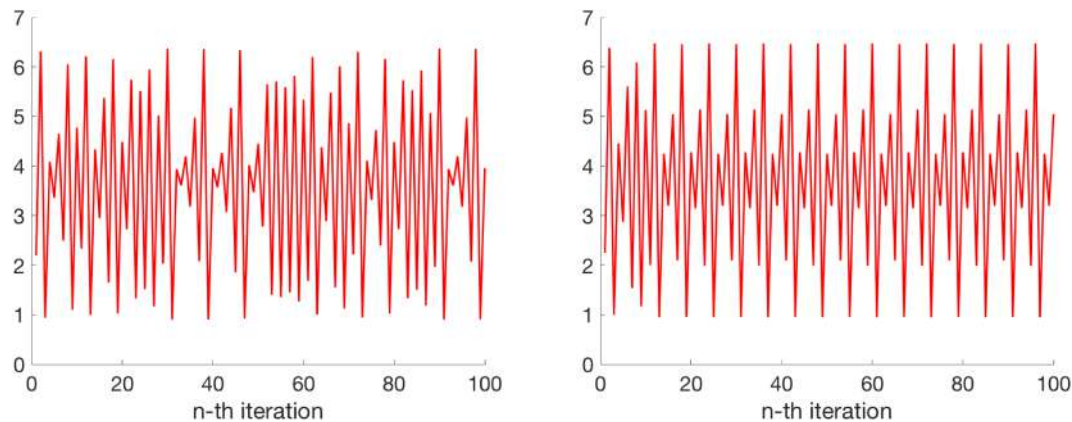


FIGURE 13 Chaotic spiking with subthreshold oscillations (left) and regular mixed-mode oscillations after initial adaptation (right) in 1D Chialvo model (for parameter values see main text). [Colour figure can be viewed at [wileyonlinelibrary.com](https://onlinelibrary.wiley.com/doi/10.1002/ana.9118)]

On the other hand, for the same value of r and k increased to $k = 0.2$, the neuron with initial voltage value $x_{\text{init}} = 2.25$ exhibits, after initial adaptation, regular MMOs (depicted on the right). In this case, both spikes and subthreshold (nonspikes, i.e., low amplitude) oscillations occur periodically. Observe that, according to Theorem 10, periodicity and asymptotic periodicity (periodic spiking/bursting, phasic spiking/bursting, regular MMOs, etc.) are the most “common” types of behavior of the model under consideration.

It is worth notifying that MM(B)Os can play an important role in neuron's information processing but for nondiscrete models can occur only in higher dimensions (continuous models require at least three dimensions and for hybrid models, with continuous subthreshold dynamics, starting from two dimensions; see Rubin et al.⁷). Actually, during our numerical experiments with the 1D Chialvo model, we have also encountered, for example, regular tonic spiking and phasic spiking.

Moreover, observe that, due to Theorem 8, if we restrict ourselves to the dynamical core, then the reduced Chialvo model cannot directly exhibit bistable behavior (coexistence of periodic and chaotic attractors) for fixed values of parameters r and k , because the 1D Chialvo map admits a unique metric attractor, which in general is periodic, solenoidal, or interval but with full probability periodic or interval (see Proposition 2). However, chaotic behavior in the dynamical core can, of course, coexist with an attracting fixed point outside the dynamical core. Moreover, the substitute of bistability effect, that is, interweaving of periodic and chaotic attractors in the 1D model can be also observed while varying the parameter r corresponding to the second (recovery) variable of the 2D model. This is formally assured by Theorems 10 and 11.

Various oscillations modes in the reduced Chialvo model, as we have seen, are closely related to the existence of periodic attractors. Restricting the domain of the initial conditions to the dynamical core, we know that there is at most one attracting periodic orbit since the map is S -unimodal. Hence, if the 1D model exhibits periodic oscillations, then this (asymptotically) periodic spike pattern is unique among observed oscillations modes (for fixed parameters r and k). The arrangement of smaller and larger oscillations (spikes) and their amplitudes depend on the itinerary of this attracting periodic orbit. In particular, period 2 attracting orbit (with points on different sides of the critical point c) corresponds to tonic regular spiking (when each spike has the same amplitude and length of each interspike interval is the same). However, for many parameter values, the system exhibits also chaotic-like (not regular) oscillations since there are ranges of parameters when the map is chaotic. Therefore, determining values of parameters corresponding to various oscillations modes firstly demands providing exact bifurcation diagram of the map $f_{r,k}$ in the (r, k) -plane. This, however, would be a very challenging task since even with one parameter fixed the system undergoes cascades of rapid bifurcations. This is exemplified in Figure 7. In fact, left panel of this figure allows to conclude, approximately, values of r (for $k = 0.05$ fixed) corresponding to resting and periodic oscillations with periods 2, 4, 8 (and perhaps more) as well as ranges of chaotic (or very large period) oscillations. The second panel of this figure provides analogous information for varying k and $r = 2.6$ fixed. Note, however, that in all the cases, small change of the parameter might cause onset of chaos or quite sudden disappearance of chaotic behavior. Approximate regions in (r, k) -parameter space when chaotic oscillations might occur might be deduced from the red area depicted in Figure 12.

5.5 | Remarks on the 2D Chialvo model

Although, this work is concerned with 1D reduction of the Chialvo model, for completeness, let us discuss some properties of systems (1a) and (1b) which might indicate interesting pathways for further studies.

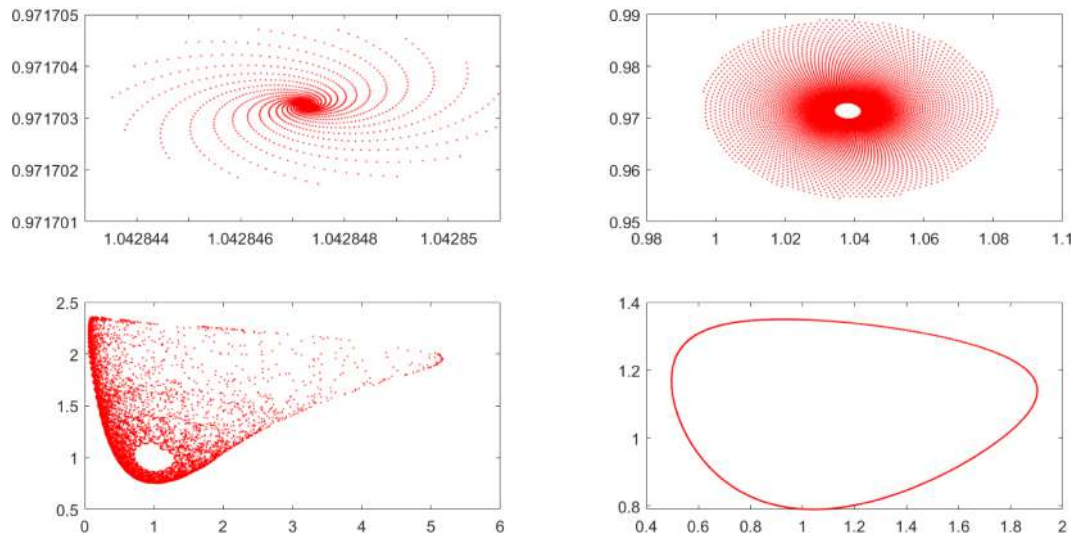


FIGURE 14 Numerical attractors in the 2D Chialvo model for the fixed values of $a = 0.89$, $c = 0.28$, $k = 0.03$ and four different values of b : 0.166, 0.1668, 0.169, 0.1738 (clockwise from upper left corner). [Colour figure can be viewed at [wileyonlinelibrary.com](https://onlinelibrary.wiley.com/doi/10.1002/mina.9118)]

The work of Chialvo⁹ discusses the case of $k = 0$ and k of small positive value keeping fixed values of parameters a and c and only varying b when needed. The parameter k is treated as the bifurcation parameter. As mentioned in Section 1, for $k = 0$, the point $(x_{f0}, y_{f0}) := (0, c/(1 - a))$ is always a stable fixed point of the system. For $k \neq 0$, systems (1a) and (1b) can have up to three fixed points.

Chialvo⁹ treats only the case when the phase portrait has exactly one equilibrium point and the values of parameters a and c are fixed as $a = 0.89$ and $c = 0.28$. Nevertheless, even in this prescribed regime of parameters, the system features rich behavior which is directly matched with activity properties of neurons. With this choice of parameters a and c , small values of k (e.g., $k = 0.02$) and $b = 0.6$, the unique fixed point is globally attracting and the system is *quiescent-excitable* since it can generate an action potential when properly stimulated but is not able to maintain oscillatory spiking. Increasing k (while keeping other parameters fixed) causes fixed point loses stability and oscillatory behavior appears (bifurcation from quiescent-excitable to oscillatory solution). Obviously, the 2D model is also able to exhibit chaotic-like behavior which Chialvo⁹ observed, for example, for $k = 0.03$ and $b = 0.18$ (and $a = 0.89$, $c = 0.28$ as stated). In this case, the model displays chaotic mixed-mode oscillations (bursting oscillations with large spikes often followed by oscillations of smaller amplitude; see Figure 10 therein).

However, as we already mentioned, systems (1a) and (1b) can have up to three fixed points. Their existence, stability, and bifurcations were studied in Jing et al.¹⁸ In particular, the authors provided explicit conditions when the 2D Chialvo system has a given number of fixed points and theorems establishing the existence of fold, flip bifurcation, and Hopf bifurcations. They have also proved the existence of chaos in the sense of Marotto. These analytical studies are then complemented by numerical simulations which in addition reveal, for example, various period doubling bifurcations and different routes to chaos, sudden disappearance of chaos and strange chaotic, and nonchaotic attractors. In the analytical part, they treat k as a bifurcation parameter but interestingly allow also negative values of k . On the other hand, in the numerical part, they consider also nonautonomous Chialvo model where the external stimulus is periodic and the amplitude or frequency of this input can be a bifurcation parameter.

In a recent short communication paper,¹⁹ the authors, contrary to other studies, consider (a, b) -parameter space where c and k are fixed. These studies are numerical but illustrate the existence of interesting structures. In particular, they suggest Neimark–Sacker bifurcation of the fixed point and mode locking behavior. The location of parameter regions corresponding Neimark–Sacker bifurcation and the birth of Arnold tongues are determined analytically. They have also numerically identified comb-shaped periodic regions (corresponding to period-incrementing bifurcations) and shrimp-shaped structures immersed in large chaotic regions.

Finally, the recent preprint⁴⁵ undertakes the analysis of the 2D Chialvo model combining rigorous numerical methods and a topological approach based on the Conley index and Morse decompositions which allows to split considered range of parameters into classes of equivalent dynamics. However, again, due to the computational complexity of this four-parameter-dependant system, the authors fix $a = 0.89$ and $c = 0.28$ (similarly as in Chialvo paper⁹)

and explore some rectangular area of $b > 0$ and $k > 0$. Their study is enriched with the analysis of chain-recurrence properties of sets and additionally incorporates machine learning for identifying parameter ranges that yield chaotic behavior.

Although the current work is concerned with 1D Chialvo model, we have performed numerous simulations of the 2D model. We have decided to include only some of them in this work. This is due to the fact that the model is extremely sensitive to any, sometimes even arbitrary small, changes of parameters that can lead to very different behaviors. Indeed, in Figure 14, we present numerically obtained representative phase portraits for $a = 0.89$, $c = 0.28$, $k = 0.03$ and four different values of b (0.166, 0.1668, 0.169, 0.1738, respectively). Each picture presents a typical trajectory of the system after removing the transient part. Thus, these pictures show various types of possible attractors for the 2D model. We see that increasing b in such a small range of values, while keeping all the other parameters fixed, causes shifting the dynamics from the one corresponding to the attracting focus, through periodic limit cycle, to chaotic oscillations where both the interspike intervals and the number of small oscillations between consecutive spikes vary. Looking at Figure 14, we can suspect that the system firstly undergoes bifurcation when the globally attracting fixed point loses its stability and the stable limit cycle appears and soon after that another bifurcation when asymptotically periodic dynamics is replaced by chaotic one. Corresponding voltage traces are presented in Figure 15.

Our brief investigation of the 2D model and the mentioned works^{9,18,19,45} provide insightful and valuable observations. However, detailed dynamical picture of the 2D Chialvo model is still very incomplete. This is mainly due to the fact that discrete systems, even in low-dimensions such as the Chialvo model, yield more challenges in their analytical (and numerical) analysis. Indeed, in planar continuous systems (i.e., systems defined by ODEs), one has, for example, Poincaré–Bendixson theorem which allows to draw conclusions on the asymptotic behavior of trajectories (by describing possible types of invariant limit sets). In particular, in 2D continuous systems, chaotic dynamics is excluded, whereas in discrete settings, one can observe chaos even in one dimension (i.e., on the interval or on the circle). The second reason is the nature of the Chialvo model itself, by which we mean, and as we demonstrated, that the model is very sensitive to even very small change of parameters as it happens that in the very small region of parameter space it might undergo not one but a couple of bifurcations. This in turn makes validation of the numerical analysis of the model challenging and emphasize the need for rigorous analytical studies which, however, due to the above mentioned reasons are especially hard. Therefore, our aim was to show that even the reduced Chialvo model can be interesting for the mathematical analysis and not necessarily less plausible than its full version.

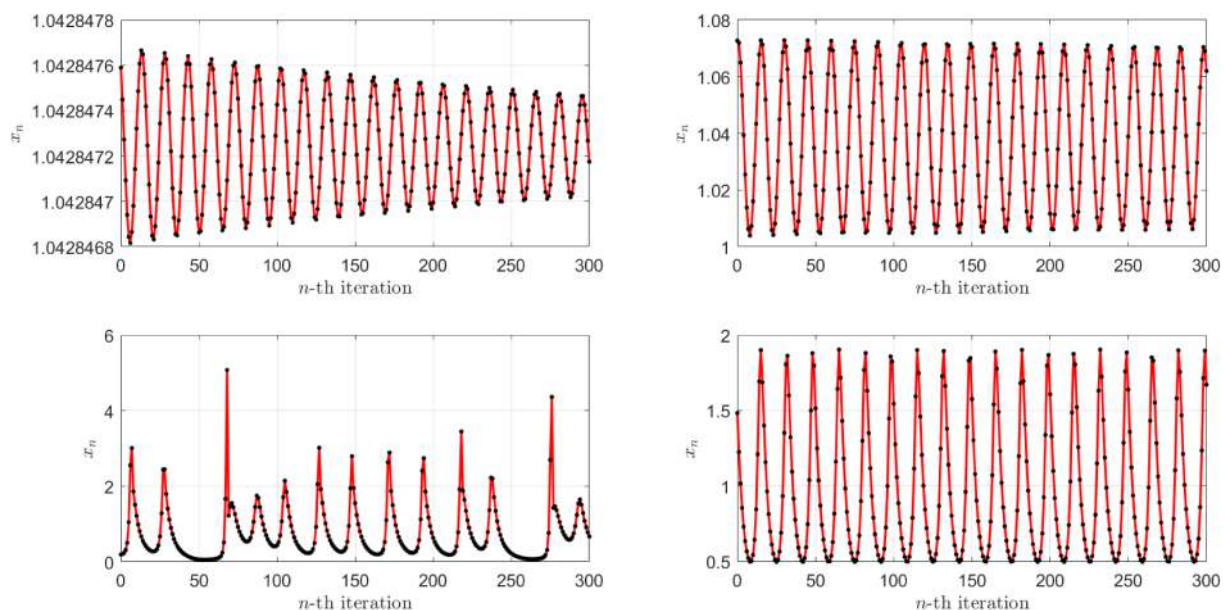


FIGURE 15 Time series of the voltage x for the numerical attractors of the 2D Chialvo model from Figure 14. [Colour figure can be viewed at [wileyonlinelibrary.com](https://onlinelibrary.wiley.com/doi/10.1002/ana.9118)]

6 | DISCUSSION

We have performed detailed analysis of the reduced Chialvo model (2) which describes the evolution of the membrane voltage when recovery variable is frozen, that is, becomes a parameter. Let us briefly summarize these results here.

Firstly, we established that model (2) can be seen as iterations of the S-unimodal map f_r , which opened the way to prove its various properties with the use of the powerful theory of S-unimodal maps (and, more general, maps with negative Schwarzian derivative). In Theorems 4–6, we rigorously showed that the model undergoes flip and fold bifurcations of fixed points when r is a bifurcation parameter and a fold bifurcation with respect to k parameter, providing formulas for the bifurcation parameter values and fixed points involved. In particular, due to the fact that Schwarzian derivative is negative, all the flip bifurcations are supercritical.

Next, discussing different configurations of the map with respect to the number and location of its fixed points and precising what should be treated as dynamical core of the map, we justified that the map can be in fact viewed as an S-unimodal map. Moreover, Lemmas 1 and 2 assert that for wide range of (r, k) parameter space in the dynamical core of the map, there is only one fixed point which is unstable. This instability of the fixed point played role in justifying the existence of Misiurewicz maps in the family $\{f_r\}$ (with k fixed) and showing that for positive Lebesgue measure set of parameters, these maps admit an absolutely continuous invariant probability measure (acip) with positive Lyapunov exponent for almost all initial conditions (see Theorem 11 and following discussion). In all these cases, the map has an interval attractor which is the support of the acip. This situation is often referred to as metric chaos. The effective complementary case (see Proposition 2) is when the map f_r has a periodic attractor which is then necessarily unique (Theorem 7). This fact has some implications for the numerics, that is, in the regime of the existence of stable periodic orbit, its uniqueness and the fact that it attracts almost all initial conditions guarantees that by randomly choosing initial point x_0 and iterating it under the one-dimensional Chialvo map, we can reconstruct this periodic attractor. Abundance of this periodic case is captured in Theorem 10. On the other hand, Theorem 13 gives the combinatorial condition for the map to be chaotic in the sense of Li and Yorke, Block and Coppel, and Devaney. Proposition 3 and further numerical analyses estimate the subset of (r, k) parameter space where this topological chaos occurs.

As argued in some references and mentioned in Section 1, Equation (2) sometimes qualitatively approximates the dynamics of voltage variable in the full model (1a) and (1b), especially when it can be viewed as a slow-fast system with the slow variable y , virtually frozen, or acting as a slowly varying bifurcation parameter of the fast subsystem. However, the form of the full model (1a) and (1b) does not allow for an easy and explicit separation of timescales unless the a , b , and c parameter values are specifically chosen. Therefore, although the slow-fast nature of the system for some parameters' values is reflected in numerical simulations (see, e.g., Chialvo⁹), rigorous application of singular perturbation theory for this model and, perhaps, revealing implications of our finding for the full model can be a separate task for future research. Another approach can rely on using the theory of discrete-time nonautonomous dynamical systems (see, e.g., Kloeden et al.⁴⁶) for inferring the x -dynamics in the full system. However, as revealed, for example, by the numerical experiments related to Figure 6, sometimes the behavior of the reduced model might be more complicated than that of the 2D model within the corresponding area of the phase plane. This of course depends on the parameter choice in the 2D model and also, together with the variety of activity modes which the model is able to display (as illustrated, for example, in Figures 4, 5, and 13), serves in favor of the argument that 1D model might be treated as the independent model and that, perhaps, it would be worth considering other variants of the 2D model with the same equation for the membrane voltage but different types of the recovery dynamics. In any case, the starting point for creating such new variants of the Chialvo model would be to fully understand the evolution of the membrane voltage given by (2), which this paper aims at.

Moreover, as pointed also in Ibarz et al.,¹⁷ the Chialvo model does not fit exactly into the scheme of slow-fast neuron models with x being the fast variable and y the slow variable (in fact, y might even represent the fast, not the slow, variable), because the impact of y onto the voltage evolution equation is not additive but multiplicative and thus changing y does not simply shifts the map f upward or downward. Therefore, understanding the bifurcation structure of the map $f_{r,k}$, especially with respect to r parameter is very important and was another motivation behind this work.

On the other hand, providing complete description of the dynamics of the full models (1a) and (1b) (corresponding to different parameters configuration in the (a, b, c, d, k) space or its (b, k) subspace) seems challenging. The works by Chialvo⁹ and Jing et al.¹⁸ gave some initial results in this direction, but this extensive task demands other supporting methods, for instance, topological and computational dynamics tools (identifying invariant sets and their Conley indices) and might be a base for future works. From that point of view, presented here, rather complete, dynamical description of the somehow independent 1D model seems to be very natural and useful.

ACKNOWLEDGEMENTS

Frank Llovera Trujillo and Justyna Signerska-Rynkowska were supported by NCN (National Science Centre, Poland) grant no. 2019/35/D/ST1/02253. Frank Llovera Trujillo was also supported by Polonium International Doctoral Fellowships (first edition) scholarship awarded by Gdańsk University of Technology within “Initiative of Excellence - Research University” program. Justyna Signerska-Rynkowska also acknowledges the support of Dioscuri program initiated by the Max Planck Society, jointly managed with the National Science Centre (Poland), and mutually funded by the Polish Ministry of Science and Higher Education and the German Federal Ministry of Education and Research.

CONFLICT OF INTEREST STATEMENT

The authors declare no potential conflict of interests.

ORCID

Frank Llovera Trujillo  <https://orcid.org/0000-0001-5979-3584>

Justyna Signerska-Rynkowska  <https://orcid.org/0000-0002-9704-0425>

Piotr Bartłomiejczyk  <https://orcid.org/0000-0001-5779-4428>

REFERENCES

- Hodgkin AL, Huxley AF. A quantitative description of membrane current and its application to conduction and excitation in nerve. *The J Physiol.* 1952;117(4):500-544. doi:10.1113/jphysiol.1952.sp004764
- Morris C, Lecar H. Voltage oscillations in the barnacle giant muscle fiber. *Biophys J.* 1981;35(1):193-213.
- FitzHugh R. Impulses and physiological states in theoretical models of nerve membrane. *Biophys J.* 1961;1(6):445-466.
- Nagumo J, Arimoto S, Yoshizawa S. An active pulse transmission line simulating nerve axon. *Proc IRE.* 1962;50(10):2061-2070.
- Brette R, Gerstner W. Adaptive exponential integrate-and-fire model as an effective description of neuronal activity. *J Neurophysiol.* 2005;94(5):3637-3642. doi:10.1152/jn.00686.2005
- Izhikevich EM. Simple model of spiking neurons. *IEEE Trans Neural Netw.* 2003;14(6):1569-1572.
- Rubin JE, Signerska-Rynkowska J, Touboul JD, Vidal A. Wild oscillations in a nonlinear neuron model with resets: (ii) Mixed-mode oscillations. *Discret Contin Dyn Syst - B.* 2017;22(10):4003-4039. doi:10.3934/dcdsb.2017205
- Touboul J, Brette R. Spiking dynamics of bidimensional integrate-and-fire neurons. *SIAM J Appl Dyn Syst.* 2009;8(4):1462-1506. doi:10.1137/080742762
- Chialvo DR. Generic excitable dynamics on a two-dimensional map. *Chaos Solitons Fractals.* 1995;5(3):461-479.
- Cazelles B, Courbage M, Rabinovich M. Anti-phase regularization of coupled chaotic maps modelling bursting neurons. *Europhysics Lett.* 2001;56(4):504. doi:10.1209/epl/i2001-00548-y
- Rulkov NF. Regularization of synchronized chaotic bursts. *Phys Rev Lett.* 2001;86:183-186. doi:10.1103/PhysRevLett.86.183
- Rulkov NF. Modeling of spiking-bursting neural behavior using two-dimensional map. *Phys Rev E.* 2002;65:041922. doi:10.1103/PhysRevE.65.041922
- Shilnikov AL, Rulkov NF. Subthreshold oscillations in a map-based neuron model. *Phys Lett A.* 2004;328(2):177-184.
- Courbage M, Nekorkin VI, Vdovin LV. Chaotic oscillations in a map-based model of neural activity. *Chaos An Interdiscip J Nonlinear Sci.* 2007;17(4):043109. doi:10.1063/1.2795435
- Zhong J, Zhang L, Tigan G. Bifurcations of a discrete-time neuron model. *J Differ Equ Appl.* 2017;23(9):1508-1528. doi:10.1080/10236198.2017.1339698
- Courbage M, Nekorkin VI. Map based models in neurodynamics. *Int J Bifurcation Chaos.* 2010;20(06):1631-1651. doi:10.1142/S0218127410026733
- Ibarz B, Casado JM, Sanjun MAF. Map-based models in neuronal dynamics. *Phys Reports.* 2011;501(1):1-74.
- Jing Z, Yang J, Feng W. Bifurcation and chaos in neural excitable system. *Chaos Solitons Fractals.* 2006;27(1):197-215.
- Wang F, Cao H. Mode locking and quasiperiodicity in a discrete-time Chialvo neuron model. *Commun Nonlinear Sci Numer Simul.* 2018;56:481-489.
- Rinzel J. A formal classification of bursting mechanisms in excitable systems. *Mathematical Topics in Population Biology, Morphogenesis and Neurosciences: Proceedings of an International Symposium Held in Kyoto, November 10-15, 1985.* Berlin, Heidelberg: Springer Berlin Heidelberg; 1987:267-281. doi:10.1007/978-3-642-93360-8_26
- Izhikevich EM, Hoppensteadt F. Classification of bursting mappings. *Int J Bifurcation Chaos.* 2004;14(11):3847-3854. doi:10.1142/S0218127404011739
- Bertram R, Butte MJ, Kiemel T, Sherman A. Topological and phenomenological classification of bursting oscillations. *Bulletin Math Biol.* 1995;57(3):413-439.
- Desroches M, Rinzel J, Rodrigues S. Classification of bursting patterns: a tale of two ducks. *PLOS Comput Biol.* 2022;18(2):1-32. doi:10.1371/journal.pcbi.1009752

24. Izhikevich EM. Neural excitability, spiking and bursting. *Int J Bifurcation Chaos*. 2000;10(06):1171-1266. doi:10.1142/S0218127400000840
25. Rubin JE, Signerska-Rynkowska J, Touboul JD, Vidal A. Wild oscillations in a nonlinear neuron model with resets: (i) bursting, spike-adding and chaos. *Discret Contin Dyn Syst - B*. 2017;22(10):3967-4002. doi:10.3934/dcdsb.2017204
26. May R. Simple mathematical models with very complicated dynamics. *Nature*. 1976;261:459-467.
27. Cohen JE. Unexpected dominance of high frequencies in chaotic nonlinear population models. *Nature*. 1995;378:610-612.
28. Brauer F, Castillo-Chavez C. *Mathematical Models in Population Biology and Epidemiology*, Vol. 40. New York Dordrecht Heidelberg London: Springer; 2001.
29. Thunberg H. Periodicity versus chaos in one-dimensional dynamics. *SIAM Review*. 2001;43(1):3-30.
30. H. R. Thieme. *Mathematics in Population Biology*. Princeton: Princeton University Press; 2018. doi:10.1515/9780691187655
31. Schleicher D. Dynamics of entire functions. *Holomorphic Dynamical Systems: Cetraro, Italy, July 7-12, 2008*. Berlin, Heidelberg: Springer Berlin Heidelberg; 2010:295-339. doi:10.1007/978-3-642-13171-4_5
32. Alhamed M, Rempe L, Sixsmith D. Geometrically finite transcendental entire functions. *J London Math Soc*. 2022;106:485-527.
33. Misiurewicz M. On iterates of e^z . *Ergodic Theory Dyn Syst*. 1981;1(1):103-106. doi:10.1017/S01438570000119X
34. Singer D. Stable orbits and bifurcation of maps of the interval. *SIAM J Appl Math*. 1978;35(2):260-267.
35. Kuznetsov YA. *Elements of Applied Bifurcation Theory*, Appl. Math. Sci. New York: Springer-Verlag; 2004.
36. Aulbach B, Kieninger B. Periodicity versus chaos in one-dimensional dynamics. *Nonlinear Dyn Syst Theory*. 2001;1(1):23-37.
37. Devaney RL. *An Introduction to Chaotic Dynamical Systems*, Studies in Nonlinearity. Boulder: Westview Press; 2003. Reprint of the second (1989) edition.
38. Schreiber SJ. Periodicity, persistence, and collapse in host parasitoid systems with egg limitation. *J Biol Dyn*. 2007;1(3):273-287. doi:10.1080/17513750701450235
39. Kozlovski OS. Axiom a maps are dense in the space of unimodal maps in the c^k topology. *Ann Math*. 2003;157(1):1-43.
40. Avila A, Lyubich M, de Melo W. Regular or stochastic dynamics in real analytic families of unimodal maps. *Invent Math*. 2003;154:451-550.
41. Li T-Y, Yorke JA. Period three implies chaos. *The Am Math Monthly*. 1975;82(10):985-992.
42. Block LS, Coppel WA. *Dynamics in One Dimension*, Lecture Notes in Mathematics. Berlin: Springer-Verlag; 1992.
43. Llovera F, Bartłomiejczyk P, Signerska-Rynkowska J. Parameter values for topological chaos in the reduced Chialvo model. Gdańsk University of Technology. [Dataset]; 2021. doi:10.34808/by1g-e883
44. Luzzatto S, Takahasi H. Computable conditions for the occurrence of non-uniform hyperbolicity in families of one-dimensional maps. *Nonlinearity*. 2006;19(7):1657. doi:10.1088/0951-7715/19/7/013
45. Pilarczyk P, Signerska-Rynkowska J, Graff G. Topological-numerical analysis of a two-dimensional discrete neuron model. preprint arXiv:2209.03443[math.DS]; 2022.
46. Kloeden PE, Pötzsche C, Rasmussen M. Discrete-time nonautonomous dynamical systems. *Stability and Bifurcation Theory for Non-autonomous Differential Equations: Cetraro, Italy 2011*, editors: Russell Johnson, Maria Patrizia Pera. Berlin, Heidelberg: Springer Berlin Heidelberg; 2013:35-102. doi:10.1007/978-3-642-32906-7_2

How to cite this article: Trujillo LF, Signerska-Rynkowska J, Bartłomiejczyk P. Periodic and chaotic dynamics in a map-based neuron model. *Math Meth Appl Sci*. 2023;46(11):11906-11931. doi:10.1002/mma.9118

APPENDIX A: PROOFS OF RESULTS ON THE DYNAMICAL CORE

Proof of Lemma 1. The second inequality $c < f_{r,k}(c)$ is straightforward, and moreover, if we demand only this inequality, it is enough to set $r^*(k) = r^*(0)$ for any $k \geq 0$. In order to prove the first inequality, we compute $f_{r,k}^2(c) = (4 \exp(r-2) + k)^2 \exp\{r - 4 \exp(r-2) - k\} + k$, which can be further expanded as

$$f_{r,k}^2(c) = \{16 \exp(3r-4-k) + 8k \exp(2r-2-k) + k^2 \exp(r-k)\} \exp\{-4 \exp(r-2)\} + k.$$

Since for large r (with fixed $k \in [0, 2)$)

$$\exp\{-4 \exp(r-2)\} \leq \min\{\exp(-4r+4+k), \exp(-3r+2+k), \exp(-2r+k)\},$$

we have

$$f_{r,k}^2(c) \leq \{16 + 8k + k^2\} \exp(-r) + k < 2$$

for sufficiently large r , which proves (5).

Note that the second statement about the unique fixed point in the interval $[f_{r,k}^2(c), f_{r,k}(c)]$ means that there are no fixed points x_f on the increasing part of the graph of $f_{r,k}$ with $x_f \geq f_{r,k}^2(c)$ (as necessarily the interval $[f_{r,k}^2(c), f_{r,k}(c)]$ contains the fixed point $x_f > 2$). Thus, let $0 < k < 2$. In this case for r large enough and $k \leq x \leq 2$, the following sequence of inequalities holds:

$$\exp(r-x) \geq \exp(r-2) > \frac{1}{k} - \frac{k}{4} \geq \frac{1}{x} - \frac{k}{x^2} = \frac{x-k}{x^2},$$

which implies

$$f_{r,k}(x) = x^2 \exp(r-x) + k > x.$$

Consequently, for large r enough, there are no fixed points in $[k, 2]$. However, $x^2 \exp(r-x) + k > x$ for all $0 \leq x < k$, independently of r , yielding that for $k > 0$ and sufficiently large r , there are no fixed points in $[0, 2]$ and completing the proof.

Proof of Lemma 2. Since it is clear that for any fixed $0 \leq k < 2$ and $r = r(k)$ large enough there is a fixed point located in the right subinterval $[c, f_{r,k}^2(c)]$, it remains to show that the fixed point $x_f > 2$ is unstable for all r large enough.

Let $0 \leq k < 2$ be fixed and assume that $x_f > 2$ is a fixed point of $f = f_{r,k}$, where r is some parameter value. We have to show that $|f'(x_f)| = x_f(x_f - 2) \exp(r - x_f) > 1$ for r large enough (note that the value of x_f also changes with r). Since the fixed point x_f satisfies $x_f = x_f^2 \exp(r - x_f) + k$, we only need to show that $(x_f - k)(x_f - 2)/(x_f) > 1$ (note that $x_f > 2 > k$). This last inequality is satisfied when

$$x_f < \frac{3 + k - \sqrt{(k-1)^2 + 8}}{2} \quad (\text{A1})$$

or

$$x_f > \frac{3 + k + \sqrt{(k-1)^2 + 8}}{2}. \quad (\text{A2})$$

The inequality (A1) must be rejected as we are interested in $x_f > 2$ and this contradicts (A1). Instead, let us focus on the inequality (A2). From Theorem 4 on the period doubling bifurcation, it follows that there exists a parameter value r_1 such that $x_f = x_{f,r_1} > 2$ is an unstable fixed point of $f = f_{r_1,k}$. Thus, necessarily x_{f,r_1} satisfies (A2). Let $r_2 > r_1$. Then $x_{f,r_2} > x_{f,r_1}$, where x_{f,r_2} is a fixed point of $f_{r_2,k}$, located in the subinterval $[2, f_{r_2,k}(2)]$. Indeed, if $x_f > 2$ is a fixed point of $f_{r,k}$, then $\exp(r) = (x_f^{-1} - kx_f^{-2}) \exp(x_f)$. The left-hand side of this equation is an increasing function of r , and the function $(x^{-1} - kx^{-2}) \exp(x)$ is an increasing function of x (k is kept constant). Thus, increasing r moves the fixed point $x_f > 2$ further to the right. It follows that x_{f,r_2} also satisfies (A2) and thus the fixed point x_{f,r_2} is also unstable.

APPENDIX B: PROOF OF THE CONDITION FOR TOPOLOGICAL CHAOS

Proof of Proposition 3. To show that

$$f_r^2(2) < f_r^3(2) < 2 < f_r(2) \text{ for } 2.6 \leq r \leq 2.9,$$

we need only consider three cases:

Case I: $2 < f_r(2)$. One can check that $2 < f_r(2)$ iff $r > 2 - \ln(2) \approx 1.3$. But we assume $r \geq 2.6$.

Case II: $f_r^3(2) < 2$. An easy computation shows that

$$f_r^3(2) = 256 \exp(7r - 8 - 8 \exp(r - 2) - 16 \exp(3r - 4 - 4 \exp(r - 2))).$$

Let us define $h(r) = f_r^3(2) - 2$. Then

$$\frac{dh}{dr} = 256s(r) \exp(7r - 8 - 8 \exp(r - 2) - 16 \exp(3r - 4 - 4 \exp(r - 2))),$$

where $s(r) = 7 - 8 \exp(r - 2) + 64 \exp(4r - 6 - 4 \exp(r - 2)) - 48 \exp(3r - 4 - 4 \exp(r - 2))$. Assume that $r \geq 2.6$. Since $\exp(r - 2) \geq \exp(0.6) > 1.8$, we have

- $7 - 8 \exp(r - 2) < -7.4$,
- $64 \exp(4r - 6 - 4 \exp(r - 2)) < 64 \exp(-2.8) < 3.9$.

Hence, $s(r) < 0$ for $r \geq 2.6$, and in consequence, h is decreasing in this range. As $h(2.6) \approx -0.027 < 0$, we obtain $h(r) < 0$ for $r \geq 2.6$, which is our claim in this case.

Case III: $f_r^2(2) < f_r^3(2)$. Similar considerations applied to the function $g(r) = f_r^2(2) - f_r^3(2)$ on $[2.6, 2.9]$ give $g(r) < 0$ for $2.6 \leq r \leq 2.9$, and the proof is complete. □

SPIKE PATTERNS AND CHAOS IN A MAP-BASED NEURON MODEL

PIOTR BARTŁOMIEJCZYK ^{a,*}, FRANK LLOVERA TRUJILLO ^b,
JUSTYNA SIGNERSKA-RYNKOWSKA ^{a,c}

^a Faculty of Applied Physics and Mathematics/BioTechMed Centre
Gdańsk University of Technology
G. Narutowicza 11/12, 80-233 Gdańsk, Poland
e-mail: {piobartl, justyna.signerska}@pg.edu.pl

^b Doctoral School
Gdańsk University of Technology
G. Narutowicza 11/12, 80-233 Gdańsk, Poland
e-mail: frankllovera91@gmail.com

^c Dioscuri Centre in Topological Data Analysis, Institute of Mathematics
Polish Academy of Sciences
Śniadeckich 8, 00-656 Warsaw, Poland

The work studies the well-known map-based model of neuronal dynamics introduced in 2007 by Courbage, Nekorkin and Vdovin, important due to various medical applications. We also review and extend some of the existing results concerning β -transformations and (expanding) Lorenz mappings. Then we apply them for deducing important properties of spike-trains generated by the CNV model and explain their implications for neuron behaviour. In particular, using recent theorems of rotation theory for Lorenz-like maps, we provide a classification of periodic spiking patterns in this model.

Keywords: neuronal dynamics, β -transformations, Farey–Lorenz permutations, periodic spiking, chaos.

1. Introduction

Courbage *et al.* (2007) proposed the following two-dimensional discrete neuron model:

$$\begin{aligned} x_{n+1} &= f_1(x_n, y_n) \\ &= x_n + F(x_n) - y_n - \beta H(x_n - d), \end{aligned} \quad (1a)$$

$$y_{n+1} = f_2(x_n, y_n) = y_n + \varepsilon(x_n - J). \quad (1b)$$

The variables x and y stand, respectively, for the membrane potential of the neuron and the so-called recovery variable, aggregating the dynamics of all outward ionic currents (x_n and y_n describe the values of x and y , respectively, at consecutive time instances). Parameter J can be considered as a constant external stimulus and $\varepsilon > 0$ sets the time scale of the recovery variable. Parameters $\beta > 0$ and $d > 0$, in turn, control the threshold properties of oscillations. The function $H(x)$ is

the usual Heaviside step function:

$$H(x) = \begin{cases} 1 & \text{if } x \geq 0, \\ 0 & \text{if } x < 0, \end{cases}$$

and $F(x)$ is a piecewise linear continuous function defined as follows:

$$F(x) = \begin{cases} -m_0 x & \text{if } x \leq J_{\min}, \\ m_1(x - a) & \text{if } J_{\min} \leq x \leq J_{\max}, \\ -m_0(x - 1) & \text{if } x \geq J_{\max}, \end{cases} \quad (2)$$

where $m_0, m_1 > 0$, $1 > a > 0$, $J_{\min} = am_1/(m_0 + m_1)$ and $J_{\max} = (m_0 + am_1)/(m_0 + m_1)$.

The following assumptions are considered: $m_0 < 1$ and hence $\det \frac{\partial(f_1, f_2)}{\partial(x, y)} = 1 + F'(x) + \varepsilon > 0$ for any $\varepsilon \geq 0$, which guarantees the map to be one to one; lastly, the region of study is restricted to $0 < J < d$, $J_{\min} < d < J_{\max}$ resulting in $F'(d) > 0$ that is crucial in order to form chaotic behavior of the map.

*Corresponding author

It may be worth pointing out that in the later alternative version of the model (Courbage and Nekorkin, 2010), the piecewise linear function F is replaced with a cubic-shape function (e.g., $F(x) = x(x - a)(1 - x)$). It is due to the fact that the model is actually based on the FitzHugh–Nagumo model (FitzHugh, 1955) given by two ODEs with a third-degree polynomial in the first equation. The Courbage–Nekorkin–Vdovin (CNV for short) model is an example of so-called map-based (or discrete) models since it is given by the iterates of some map $f : \mathbb{R}^2 \rightarrow \mathbb{R}^2$, $f(x, y) = (f_1(x, y), f_2(x, y))$ (see also the review articles by Courbage and Nekorkin (2010) or Ibarz et al. (2011)).

The CNV model appeared in many theoretical and data-based later studies. Its relative simplicity makes it possible to analytically or partially analytically study small ensembles of interacting neurons when each neuron is modelled by the CNV system. For instance, Courbage et al. (2012) consider two-interacting neurons of the type 1. However, such small networks can also represent larger ensembles of neurons with synchronized subpopulations as in the modelling of respiratory neural networks, reproducing some key experimental findings. See, for example, the work of Hess et al. (2013), where a mathematical model of respiratory rhythmogenesis is studied with the use of the piecewise linear CNV model refined to incorporate post-inhibitory rebound bursting oscillations.

One of the prominent applications of the CNV model in medical sciences is the work of Yu et al. (2016) on examining and modelling the interplay between the brainstem automatic network and cortical voluntary command on controlling the breathing process, relevant in numerous respiratory diseases, including the chronic obstructive pulmonary disease. In this study hypotheses drawn from the functional MRI imaging of patients were mathematically validated on the model of a neural network with the piecewise linear CNV model for each neural cluster. In turn, the work by Maslennikov and Nekorkin (2012) builds a discrete model of the olivo-cerebellar system based on the CNV model with cubic $F(x)$.

Apart from numerous applications, the model is still very challenging and attractive for analytical studies. In particular, Maslennikov and Nekorkin (2013) analyze the boundary crisis and transient chaos in the one-dimensional model (1a) with the cubic function $F(x)$ and a slowly varying control parameter y_n : $y_{n+1} = y_n + \varepsilon$. Transient chaos in a version of the one-dimensional model with periodic forcing is described by Maslennikov et al. (2018). In turn Yue et al. (2017) study a two-dimensional piecewise linear model with time-varying (pulse) external stimulus and claim that the CNV model could capture fundamental behaviours of the information processing of most conductance-based models.

For system (1), it turns out that the map describing

the dynamics of the voltage variable x while the second variable y is kept constant (which we denote later by g in (6)) is a Lorenz-like map for a large range of parameter values of interest. Therefore, the first sections of the paper recall and develop some essential results on Lorenz-like maps which will be further applied directly to this model and its one-dimensional reduction. This shows how advanced results in discrete low-dimensional dynamical systems might be used for studying map-based neuron models. Another example in this vein is our recent work (Llovera-Trujillo et al., 2023) on the Chialvo model which takes advantage of the theory of S -unimodal interval maps.

Apart from understanding and modelling biological neurons, another important field of research which develops rapidly in recent decades are artificial neural networks where the dynamics of single neurons is simple but the architecture of the network allows us to solve complex computational tasks and model dynamics of real systems (Korbicz et al., 1999; Patan et al., 2008).

The paper is organized as follows. Sections 2 and 3 contain basic definitions and facts on Lorenz maps and rotation theory. In turn, in Section 4 we present key properties of finite unions of periodic orbits. Sections 5 and 6 are devoted to the study of chaotic properties of Lorenz maps and β -transformations. In Section 7 we introduce the one-dimensional CNV model. Our main results concerning the pCNV model (piecewise linear case) are stated and proved in Sections 8. Finally, Sections 9 and 10 contain interpretation of our results in terms of spiking patterns and implications of the model for neuron behaviour.

2. Lorenz-like and expanding Lorenz maps

2.1. Chaos and its components. Let (X, d) be a compact metric space and $f : X \rightarrow X$ a function (not necessarily continuous). As the condition will recur, a set $U \subset X$ will be called *opene* when it is open and nonempty. Recall that f is called

- *transitive* if for every two opene sets $U, V \subset X$ there is $n \in \mathbb{N}$ such that $f^n(U) \cap V \neq \emptyset$,
- *mixing* if for every two opene sets $U, V \subset X$ there is $N \in \mathbb{N}$ such that for every $n \geq N$ we have $f^n(U) \cap V \neq \emptyset$,
- *sensitive* if there exists $\delta > 0$ such that for every $x \in X$ and every neighbourhood U of x , there exists $y \in U$ and $n \in \mathbb{N}$ such that $d(f^n(x), f^n(y)) > \delta$,
- *expansive* if there exists $\delta > 0$ such that for any $x, y \in X$, $x \neq y$, there exists $n \in \mathbb{N}$ such that $d(f^n(x), f^n(y)) > \delta$.

Remark 1. By definition, mixing implies transitivity and expansiveness implies sensitivity.

A function $f: X \rightarrow X$ is called *chaotic in the sense of Devaney* on X if

1. f is transitive,
2. the set of periodic points of f is dense in X ,
3. f is sensitive.

For notational simplicity, we will formulate the definitions and results below for the unit interval $[0, 1]$. However, all definitions make sense and all results still hold if we replace the unit interval by $[a, b]$ for fixed a and b . Namely, consider the linear change of variables (conjugacy) $h: [0, 1] \rightarrow [a, b]$ given by $h(t) = a + t(b - a)$ and define \tilde{f} using the following diagram:

$$\begin{array}{ccc} [0, 1] & \xrightarrow{f} & [0, 1] \\ h \downarrow & & \downarrow h \\ [a, b] & \xrightarrow{\tilde{f}} & [a, b] \end{array} \quad (3)$$

Note that the condition $f(t) = x$ translates to $\tilde{f}(h(t)) = h(x)$. Moreover, $f'(t) = \tilde{f}'(h(t))$ if f is differentiable at $t \in [0, 1]$ and, in consequence, both monotonicity and slope are preserved by h . Finally, if f is a Lorenz-like map (expanding Lorenz map, β -transformation) according to the definitions given below then so is \tilde{f} and vice versa.

2.2. Topological entropy. For a piecewise continuous piecewise monotone map $f: [0, 1] \rightarrow [0, 1]$ we usually define *topological entropy* using the formula

$$h(f) = \lim_{n \rightarrow \infty} \frac{1}{n} \ln c_n(f),$$

where $c_n(f)$ denotes the number of *laps* of f^n . Recall that the *lap* of f is the maximal interval, on which f is simultaneously monotone and continuous.

2.3. Lorenz-like maps. A *Lorenz-like map* is a map f of an interval $[0, 1]$ to itself, for which there exists a point $c \in (0, 1)$ such that

- f is continuous and increasing (not necessarily strictly) on $[0, c)$ and on $(c, 1]$,
- $\lim_{x \rightarrow c^-} f(x) = 1$ and $\lim_{x \rightarrow c^+} f(x) = f(c) = 0$.

Set $I_L = [0, c)$ and $I_R = [c, 1]$. If $f(0) > f(1)$, that is, $f(I_L) \cap f(I_R) = \emptyset$, the Lorenz-like map f is called *nonoverlapping*. If $f(0) \leq f(1)$, that is, $f(I_L) \cap f(I_R) \neq \emptyset$, the map is called *overlapping*.

2.4. Expanding Lorenz maps. An *expanding Lorenz map* is a map $f: [0, 1] \rightarrow [0, 1]$ satisfying the following three conditions:

- there is a *critical point* $c \in (0, 1)$ such that f is continuous and strictly increasing on $[0, c)$ and $(c, 1]$,
- $\lim_{x \rightarrow c^-} f(x) = 1$ and $\lim_{x \rightarrow c^+} f(x) = f(c) = 0$,
- f is differentiable for all points not belonging to a finite set $\Omega \subset [0, 1]$ and such that $\inf \{f'(x) \mid x \in [0, 1] \setminus \Omega\} > 1$.

By definition, expanding Lorenz maps are overlapping Lorenz-like. Moreover, the assumption on the derivative yields expansiveness.

Proposition 1. *Every expanding Lorenz map is expansive.*

Proof. Let f be an expanding Lorenz map and $\beta = \inf \{f'(x) \mid x \in [0, 1] \setminus \Omega\} > 1$. By definition, there exists $\delta_1 > 0$ such that $f(x) > 2/3$ for all $x \in [c - \delta_1, c)$ and $f(x) < 1/3$ for all $x \in [c, c + \delta_1]$. Let $\delta = \min\{1/3, \delta_1\}$. Assume that $x \neq y$ and $|x - y| < \delta$. Now suppose, contrary to our claim, that for all $n \in \mathbb{N}$ we have

$$d_n := |f^n(x) - f^n(y)| \leq \delta. \quad (4)$$

Consider two cases:

- If $f^n(x), f^n(y) \in I_L$ or $f^n(x), f^n(y) \in I_R$ for all $n \in \mathbb{N}$, then, by the mean value theorem, $d_n \geq \beta d_{n-1} \geq \beta^n |x - y|$, which contradicts (4).
- If $f^n(x) \in I_L$ and $f^n(y) \in I_R$ for some $n \in \mathbb{N}$ (or vice versa), then $f^n(x) \in [c - \delta_1, c)$ and $f^n(y) \in [c, c + \delta_1]$ and, in consequence, $|f^{n+1}(x) - f^{n+1}(y)| > 1/3$, which also contradicts (4). ■

3. Rotation number and interval

In this and the next section we mainly recall essential definitions and results of Geller and Misiurewicz (2018), which we will use in our analysis of the CNV model. Let f be a Lorenz-like map.

Definition 1. For a point $x \in [0, 1]$ and a positive integer n we will denote by $R(x, n)$ the number of integers $i \in \{0, \dots, n-1\}$ such that $f^i(x) \in I_R$. If the limit

$$\rho(x) = \lim_{n \rightarrow \infty} \frac{R(x, n)}{n}$$

exists, we will call it the *rotation number* of x .

Remark 2. By definition, $0 \leq \rho(x) \leq 1$ if it exists.

Observe that it is extremely easy to compute the rotation number of a periodic point.

Proposition 2. *If x is a periodic point of f of period p then $\rho(x)$ exists and is equal to $R(x, p)/p$.*

The following classical result characterizes the uniqueness of the pointwise rotation number.

Theorem 1. (Rhodes–Thompson) *If $f(0) \geq f(1)$ (in particular, if the map is nonoverlapping), then all points have the same rotation number.*

In that case we will denote it by $\rho(f)$.

Let f be a Lorenz-like map. If $t \in f(I_L) \cap f(I_R)$, then we define the *water map* at level t by

$$f_t(x) = \begin{cases} \max(t, f(x)) & \text{if } x \in I_L, \\ \min(t, f(x)) & \text{if } x \in I_R. \end{cases}$$

It is obvious that this map is also Lorenz-like and $f_t(0) = f_t(1)$. Consequently, for fixed t , all points have the same rotation number $\rho(f_t)$ for it. It is known that $\rho(f_t)$ is an increasing continuous function of t , and if $f(0) \leq f(1)$, then the set of rotation numbers for f of all points having rotation number is equal to the interval $[\rho(f_{f(0)}), \rho(f_{f(1)})]$ (for details, see, e.g., Alsedà et al., 1989). We will call it the *rotation interval* of f and denote it by $\text{Rot}(f)$.

4. Finite unions of periodic orbits and Farey–Lorenz permutations

Let f be a Lorenz-like map. Below we summarize important properties of Farey–Lorenz permutations that allow us to deduce about the existence of periodic orbits with given itineraries. By the itinerary of a periodic orbit $\{x, f(x), \dots, f^{q-1}(x)\}$ we mean a sequence of symbols L and R of length q such that the i -th element of this sequence ($i = 1, \dots, q$) is L if $f^i(x) \in I_L$ and R otherwise (the sequence is given up to cyclic permutation). Proofs of Proposition 3 as well as Theorems 2 and 3 can be found in the work of Geller and Misiurewicz (2018).

4.1. Finite unions of periodic orbits (fupos). A finite union of periodic orbits of f is called, by acronym, a *fupo*. For each fupo we will consider its permutation, that is, if a fupo P consists of points $x_1 < \dots < x_n$, and $f(x_i) = x_{\sigma(i)}$ for $i = 1, \dots, n$, then σ is the permutation of P .

4.2. L-permutations. Permutations of fupos of Lorenz-like maps have a specific form. Namely, if a fupo has $n > 1$ elements, then there exists $k \in \{1, \dots, n-1\}$ such that σ is increasing on $\{1, \dots, k\}$ and on $\{k+1, \dots, n\}$. We will call such permutations (and the permutation of $\{1\}$) *L-permutations*. If our fupo is a periodic orbit, then its rotation number is $(n-k)/n$.

For every L-permutation σ there exists a Lorenz-like map f with the fupo P such that P has permutation σ . A *canonical model* can be built as the “connect the dots” map with the dots being the points $(x, f(x))$ with coordinates as in Table 1.

Among L-permutations there are some special ones, which look like cyclic permutations for circle rotations. A cyclic L-permutation σ of $\{1, \dots, n\}$ will be called a *twist permutation* if $\sigma(1) > \sigma(n)$. Similarly, a periodic orbit with such a permutation will be called a *twist orbit*. It is easy to describe explicitly a twist permutation of $\{1, \dots, n\}$ with rotation number j/n . Namely,

$$\sigma(i) = i + j \pmod n.$$

4.3. Farey–Lorenz permutations. An L-permutation σ of $\{1, \dots, p+q\}$ will be called a *Farey–Lorenz permutation* (or *FL-permutation*) if σ consists of two cycles, both of them twist, of period p and q , with rotation numbers a/p and b/q respectively, and $a/p < b/q$ are Farey neighbours, that is, $bp = aq + 1$. An example of a fupo of FL-type (similar to those occurring in the pICNV model) is presented in Fig. 11.

Let us assume that σ is an FL-permutation with cycles of rotation numbers a/p and b/q , where $a/p < b/q$ are Farey neighbours and $p < q$. We will call those cycles *slow* and *fast*, respectively. Note that (Geller and Misiurewicz, 2018):

- the slow cycle contains 1, and the fast cycle contains $p+q$,
- the fast cycle contains 2.

We will refer to P as the slow orbit and Q as the fast orbit. Let the points of P be $x_1 < x_2 < \dots < x_p$ and the points of Q , $y_1 < y_2 < \dots < y_q$. Write $J_1 = [x_1, y_1]$ and $J_j = [y_{j-1}, y_j]$ for $j = 2, \dots, q$.

Proposition 3. *With the notation we adopted,*

$$f(x_i) = x_{i+a \pmod p} \quad \text{and} \quad f(y_j) = y_{j+b \pmod q}.$$

The relative order of the points of the orbits P and Q is given by the following rule: $x_1 < y_1$; then for $i = 1, \dots, p-1$, if $j = 1 + ia \pmod p$ and $l = ib \pmod q$, then $y_{l-1} < x_j < y_l$.

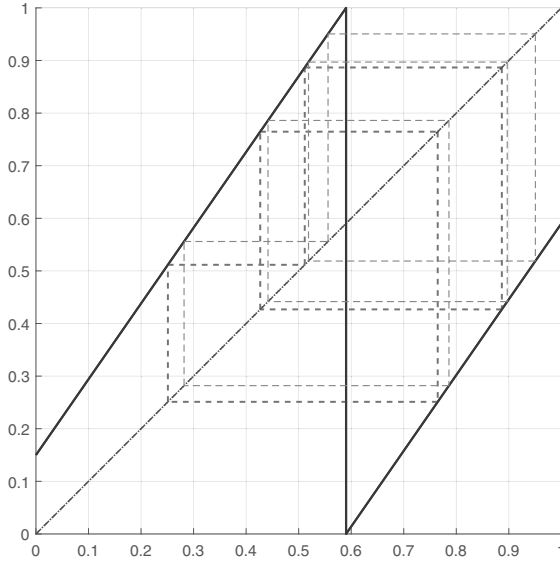
Theorem 2. *Let g be a Lorenz-like map. If a number r/s is in the rotation interval of g , and r, s are coprime, then g has a twist periodic orbit of period s and rotation number r/s .*

Proposition 4. *If g is an expanding Lorenz map and S is a periodic L-R sequence, then there is at most one periodic orbit with itinerary S .*

Proof. Assume we have two distinct q -periodic orbits $\{x_1 < \dots < x_q\}$ and $\{y_1 < \dots < y_q\}$ with the same itinerary. Hence, by the mean value theorem, $|f^q(x_1) - f^q(y_1)| > |x_1 - y_1|$, a contradiction. ■

Table 1. “Connect the dots” map.

x	0	$\frac{1}{n+1}$	\dots	$\frac{k}{n+1}$	$\frac{k+\frac{1}{2}}{n+1}$	$\frac{k+\frac{1}{2}}{n+1}$	$\frac{k+1}{n+1}$	\dots	$\frac{n}{n+1}$	1
$f(x)$	$\frac{\sigma(1)}{n+1}$	$\frac{\sigma(1)}{n+1}$	\dots	$\frac{\sigma(k)}{n+1}$	1	0	$\frac{\sigma(k+1)}{n+1}$	\dots	$\frac{\sigma(n)}{n+1}$	$\frac{\sigma(n)}{n+1}$

Fig. 1. Fupo of FL-type $(\frac{2}{5} < \frac{3}{7})$.

Corollary 1. If g is an expanding Lorenz map and r/s is in the rotation interval of g (r and s coprime) then there is only one twist periodic orbit with rotation number r/s .

Corollary 2. If g is an expanding Lorenz map, then there is at most $\binom{q}{p}/q$ periodic orbits with rotation number p/q (q, p coprime).

Theorem 3 below follows from Theorem 2 of Geller and Misiurewicz (2018) and considerations in the second paragraph of Section 5 therein.

Theorem 3. Let g be a Lorenz-like map. Assume that the rotation interval of g contains the interval $[a/p, b/q]$, where $a/p < b/q$ are Farey neighbours, and $p < q$. Then g has a twist periodic P orbit of period p and rotation number a/p and a twist periodic orbit Q of period q and rotation number b/q . The union of these orbits forms a fupo with the FL-permutation. Moreover, there exist periodic orbits with itineraries being concatenations of finitely many periodic itineraries (starting at x_1 or y_1) of P and Q .

5. Lorenz maps and chaos

We say that a map $f: [0, 1] \rightarrow [0, 1]$ is *strongly transitive* if for every nonempty open subinterval $J \subset (0, 1)$ there

exists $n \in \mathbb{N}$ such that $\bigcup_{i=0}^n f^n(J) \supset (0, 1)$. Note that strong transitivity implies transitivity.

The following three results, which are essential for our considerations, can be found in the work of Oprocha *et al.* (2019, Thms. 4.5, 4.6, 4.7, 4.8), Kameyama (2002, Thm. 3) or Afraimovich and Hsu (2002, Thm. 3.1.1), respectively. Let

$$f_1(x) = \sqrt{2}x + \frac{2 - \sqrt{2}}{2} \pmod{1},$$

$$f_2(x) = \sqrt[3]{2}x + \frac{2 + \sqrt[3]{4} - 2\sqrt[3]{2}}{2} \pmod{1},$$

$$f_3(x) = \sqrt[3]{2}x + \frac{2 - \sqrt[3]{4}}{2} \pmod{1}.$$

for $x \in [0, 1]$.

Theorem 4. Let f be an expanding Lorenz map and $\beta = \inf \{f'(x) \mid x \in [0, 1] \setminus \Omega\}$. If

- $\sqrt{2} \leq \beta \leq 2$ and $f \neq f_1$ or
- $\sqrt[3]{2} \leq \beta < \sqrt{2}$ and $f(0) \geq \frac{1}{1+\beta}$ and $f \neq f_2$ or
- $\sqrt[3]{2} \leq \beta < \sqrt{2}$ and $f(1) \leq 1 - \frac{1}{1+\beta}$ and $f \neq f_3$,

then f is mixing. Moreover, the maps f_1 , f_2 and f_3 are transitive but not mixing.

Theorem 5. Assume that $f: [0, 1] \rightarrow [0, 1]$ is piecewise continuous piecewise strictly monotone. If f is transitive then it is strongly transitive.

Theorem 6. If an expanding Lorenz map is strongly transitive then the set of its periodic points is dense in $[0, 1]$.

Remark 3. Theorem 6 has been originally formulated for the so-called Lorenz-type maps, but it is easy to check that expanding Lorenz maps are also Lorenz-type.

It is well known that for continuous maps on intervals transitivity implies chaos. As we see below, a similar result holds for expanding Lorenz maps.

Proposition 5. An expanding Lorenz map is transitive if and only if it is chaotic in the sense of Devaney on $[0, 1]$.

Proof. Chaos obviously implies transitivity, so we only need to show the opposite implication. By Theorem 5, each transitive expanding Lorenz map is strongly transitive. Hence, by Theorem 6, the set of its periodic points is dense in $[0, 1]$. It remains to prove the sensitive dependence on initial conditions, but, by Proposition 1, our map is even expansive. ■

The following result provides a sufficient condition for Devaney's chaos for expanding Lorenz maps.

Theorem 7. *Let f be an expanding Lorenz map and $\beta = \inf \{f'(x) \mid x \in [0, 1] \setminus \Omega\}$. If one of the following conditions is satisfied:*

- (i) $\sqrt{2} \leq \beta \leq 2$,
- (ii) $\sqrt[3]{2} \leq \beta < \sqrt{2}$ and $f(0) \geq \frac{1}{1+\beta}$,
- (iii) $\sqrt[3]{2} \leq \beta < \sqrt{2}$ and $f(1) \leq 1 - \frac{1}{1+\beta}$,

then f is chaotic in the sense of Devaney on the interval $[0, 1]$. Moreover,

- f is strongly transitive and expansive,
- if $f \neq f_1$ and $f \neq f_2$ and $f \neq f_3$ then f is mixing.

Proof. It is an immediate consequence of Theorem 4 and Proposition 5. Strong transitivity and expansiveness can be concluded from the proof of Proposition 5. ■

6. β -transformations

6.1. Definition. Let $1 < \beta \leq 2$, $\alpha \geq 0$ and $\alpha + \beta \leq 2$. The map $T: [0, 1] \rightarrow [0, 1]$ of the form

$$T(x) = \beta x + \alpha \pmod{1}$$

is called a β -transformation.

Remark 4. Every β -transformation has a point of discontinuity at $c = (1 - \alpha)/\beta$ and $T(c) = 0$. Moreover, $T(0) = \alpha$ and $T(1) = \alpha + \beta - 1$. Note that β -transformations are expanding Lorenz maps and Lorenz-like of a constant slope.

6.2. Acip. Here we summarize some metric (measure-theoretic) properties of β -transformations from Theorem 3 of Hofbauer (1979) and Theorem 2 of Hofbauer (1981).

Theorem 8. *The β -transformation T has topological entropy $h(T) = \ln \beta$ and unique T -invariant probability measure (acip for short) μ with maximal entropy, i.e., such that the metric entropy $h_\mu(T)$ is equal to the topological entropy $h(T)$. The measure μ is absolutely continuous with respect to Lebesgue measure. The density of μ is given by the formula*

$$K \sum_{n=0}^{\infty} \beta^{-n} (\chi_{[0, T^n(1)]}(x) - \chi_{[0, T^n(0)]}(x)),$$

where K is a normalizing factor. Moreover, the support of μ is a finite union of intervals and it is the whole interval $[0, 1]$ if

- (i) $\sqrt{2} \leq \beta \leq 2$ or

- (ii) $1 < \beta < \sqrt{2}$ and $0 \leq \alpha \leq 1 - 1/\beta$ or
- (iii) $1 < \beta < \sqrt{2}$ and $1 - \beta + 1/\beta \leq \alpha \leq 2 - \beta$.

Remark 5. Assume $1 < \beta \leq 2$. Observe that the acip μ of T is equivalent to the Lebesgue measure if and only if $\text{supp}(\mu) = [0, 1]$ (see the proof of Lemma 4.1 in the work of Ding et al. (2010)). Moreover, Parry (1979) proved that if $1 < \beta < \sqrt{2}$ and $c = 1/2$ (or equivalently $\alpha = 1 - \beta/2$) then μ is not equivalent to the Lebesgue measure. Since the measure μ is unique, the β -transformation T is ergodic with respect to μ , i.e., if $T^{-1}B = B$ for some Borel set $B \subset [0, 1]$ then $\mu(B) = 0$ or $\mu(B) = 1$. Under some assumptions on β and α , the transformation T has even stronger metric properties (for details, see Palmer, 1979), but we will not study and use them in this paper.

6.3. Transitivity and chaos. The following result by Ding et al. (2010, Lem. 4.1.) provides a nice metric characterization of topological transitivity.

Proposition 6. *Let $1 < \beta \leq 2$ and μ be the acip of the β -transformation T . Then T is transitive if and only if $\text{supp}(\mu) = [0, 1]$.*

The following result concerning β -transformations of Oprocha et al. (2019, Thm. 7.1.) corresponds to Theorem 4 proven by the same authors for expanding Lorenz maps. However, it is worth pointing out that Theorem 4 gives a sufficient condition for mixing in a broader class of functions (expanding Lorenz maps) while Theorem 9 gives a necessary and sufficient condition for mixing in a narrower class (β -transformations).

Theorem 9. *Let T be a β -transformation and $\sqrt[3]{2} \leq \beta \leq 2$. Then T is mixing if and only if one of the following conditions is satisfied:*

- $\sqrt{2} \leq \beta \leq 2$ and $f \neq f_1$ or
- $\sqrt[3]{2} \leq \beta < \sqrt{2}$ and $(\alpha < \frac{1}{\beta(1+\beta)} \text{ or } 2 - \beta - \frac{1}{\beta(1+\beta)} < \alpha)$ and $f \neq f_2$ and $f \neq f_3$.

Let us present the complete characterization of chaos parameters for β -transformations in the parameter region $\sqrt[3]{2} \leq \beta \leq 2$ and $0 \leq \alpha \leq 2 - \beta$.

Theorem 10. *Assume that T is a β -transformation and $\sqrt[3]{2} \leq \beta \leq 2$. Then T is chaotic in the sense of Devaney on the interval $[0, 1]$ if and only if one of the following conditions is satisfied:*

- (i) $\sqrt{2} \leq \beta \leq 2$,
- (ii) $\sqrt[3]{2} \leq \beta < \sqrt{2}$ and $(\alpha < \frac{1}{\beta(1+\beta)} \text{ or } 2 - \beta - \frac{1}{\beta(1+\beta)} < \alpha)$.

Moreover, under these assumptions

- T is strongly transitive and expansive,
- if $T \neq f_1$, $T \neq f_2$ and $T \neq f_3$ then T is mixing.

Proof. Our claim can be shown in the same manner as Theorem 7 using Theorem 4, Proposition 5 and Theorem 9. ■

In the case $1 < \beta < \sqrt[3]{2}$ we can formulate a sufficient condition for chaos for β -transformations.

Theorem 11. *Let T be a β -transformation with $1 < \beta < \sqrt[3]{2}$. Then T is chaotic in the sense of Devaney on the interval $[0, 1]$ if*

- $0 \leq \alpha \leq 1 - 1/\beta$ or
- $1 - \beta + 1/\beta \leq \alpha \leq 2 - \beta$.

Proof. By Theorem 8, our assumptions guarantee that $\text{supp}(\mu) = [0, 1]$, which is equivalent to transitivity of T from Proposition 6. Finally, by Proposition 5, transitivity implies chaos. ■

6.4. Fixed and periodic points. The simplicity of the formula defining β -transformation allows us to easily derive the following two results concerning fixed points and 2-periodic orbits.

Lemma 1. *β -transformation $T(x)$ admits fixed points only when $\alpha = 0$ or when $\alpha + \beta = 2$. In the first case, i.e., $\alpha = 0$, there is a fixed point $x_{f_1} = 0$ and the rotation interval $\text{Rot}(T)$ contains 0. In the second case, $\alpha + \beta = 2$, there is a fixed point $x_{f_2} = 1$ and the rotation interval contains 1. In particular, $\text{Rot}(T) = [0, 1]$ only when $\alpha = 0$ and $\beta = 2$, in which case $T(x) = 2x \pmod{1}$ is a standard chaotic dyadic transformation.*

The above lemma is a simple observation and does not require a proof. On the other hand, some short calculations lead to the following result.

Lemma 2. *Suppose that $\alpha > 0$ and $\alpha + \beta < 2$. If*

$$\tilde{\beta} < \beta < \min \left\{ 2 - \alpha, \frac{1 - \alpha}{\alpha} \right\}, \quad (5)$$

where

$$\tilde{\beta} := \frac{1 - \alpha + \sqrt{(\alpha - 1)(\alpha - 5)}}{2},$$

then T admits a 2-periodic orbit and 2 is minimal among periods of periodic points of T . In particular, under these assumptions $1/2 \in \text{Rot}(T)$ and $\{0, 1\} \cap \text{Rot}(T) = \emptyset$.

Proof. Note that the requirements $\beta < (1 - \alpha)/\alpha$ and $1 < \beta$ imply that $\alpha < 1/2$ and consequently, that $\tilde{\beta} > 1$. Further, under these conditions none of the points 0, c and 1 acts as a fixed point of T and thus the map T does not have fixed points. It suffices to show that under (5) there exists a period-two point $z \in (0, c)$, i.e.,

$$0 < z < c \quad \text{and} \quad T^2(z) = z,$$

which is equivalent to

$$0 < z < \frac{1 - \alpha}{\beta} \quad \text{and} \quad \beta^2 z + \beta \alpha + \alpha - 1 = z.$$

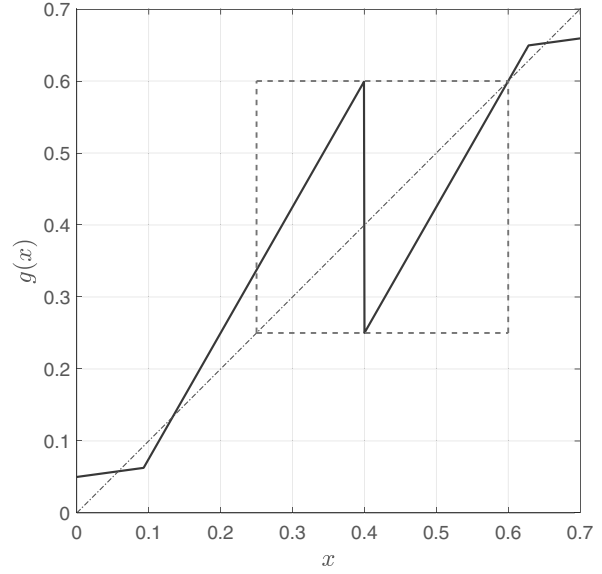


Fig. 2. Plot of the pICNV function and the invariant interval.

Solving the last equality for z gives

$$z := \frac{1}{\beta - 1} \left(\frac{1}{\beta + 1} - \alpha \right).$$

Now, it remains to solve with respect to β the following double inequality

$$0 < \frac{1}{\beta - 1} \left(\frac{1}{\beta + 1} - \alpha \right) < \frac{1 - \alpha}{\beta}.$$

As $\beta > 1$, this yields

$$\beta < \frac{1 - \alpha}{\alpha} \quad \text{and} \quad \beta^2 + \beta(\alpha - 1) + \alpha - 1 > 0.$$

The first inequality gives the upper bound for β in (5). On the other hand, since the discriminant $\Delta = (\alpha - 1)(\alpha - 5)$ in the second inequality is positive, this inequality is satisfied (considering the assumption $\beta > 1$) if

$$\beta > \frac{1 - \alpha + \sqrt{(\alpha - 1)(\alpha - 5)}}{2}.$$

■

We have now obtained a picture of periodic and chaotic properties for Lorenz maps. At the end of this theoretical part, let us mention that in their recent works Cholewa and Oprocha (2021a; 2021b) developed the theory of limit sets and renormalization for Lorenz maps.

7. One-dimensional Courbage–Nekorkin–Vdovin model

Now we will analyze more closely the 1D CNV model. When the variable $y = y_0$ is assumed to be constant, $0 <$

$J < d$ and $J_{\min} < d < J_{\max}$, the CNV model can be reduced to a one-dimensional map $g: \mathbb{R} \rightarrow \mathbb{R}$ given by

$$g(x) = x + F(x) - y_0 - \beta H(x - d). \quad (6)$$

In general, in the above function we will vary the parameters β and/or y_0 keeping all other parameters fixed. One can consider two versions of the 1D CNV model:

- a *piecewise linear* case (pICNV for short), when F is defined by Eqn. (2),
- a *nonlinear* case (nICNV for short), when $F(x) = \mu x(x - a)(1 - x)$ with $0 < a < 1$ and $\mu \geq 1$.

Observe that in both the cases the function g is discontinuous at d and the plot of F has the shape of the upside down reversed N letter. Moreover, both maps exhibit quite similar dynamics. For that reason we will mainly focus on the piecewise linear map.

Let us have a more detailed look at the 1D pICNV model, which is our main object of interest in this paper. Note that in the piecewise linear case the map g can be re-written explicitly as

$$g(x) = \begin{cases} (1 - m_0)x - y_0 & \text{if } x \leq J_{\min}, \\ qx - y_0 - am_1 & \text{if } J_{\min} < x < d, \\ qx - y_0 - am_1 - \beta & \text{if } d \leq x \leq J_{\max}, \\ (1 - m_0)x - y_0 + m_0 - \beta & \text{if } x \geq J_{\max}, \end{cases}$$

where $q = 1 + m_1$. Recall that $J_{\min} = am_1/(m_0 + m_1)$ and $J_{\max} = (m_0 + am_1)/(m_0 + m_1)$. Let us assume that the parameters a, d, m_0, m_1 are fixed and satisfy the following conditions:

1. $0 < a < 1$,
2. $J_{\min} < d < J_{\max}$,
3. $0 < m_0 < 1$,
4. $0 < m_1 \leq 1$.

The first condition means that a is a zero of F , which lies between J_{\min} and J_{\max} . The second one means that the discontinuity point of g also lies between these two points. The third and fourth conditions guarantee that two of the four possible fixed points of g are stable while the other two are unstable (if they exist). An illustrative plot of the function g involved in the pICNV model is provided in Fig. 2.

8. Periodicity and chaos in the 1D pICNV model

The main goal of this section is to study the dynamics of the pICNV map in the parameter plane (β, y_0) . We work with the assumptions from Section 7. However, the further restriction of the parameter region allows us to obtain interesting dynamical properties of the pICNV map. Namely, we list the following additional assumptions:

Assumption A1: $\beta > \beta_0 = F(J_{\max}) - F(J_{\min})$,

Assumption A2: $\beta \leq \beta_1 = \min\{J_{\max} - d, d - J_{\min}\}$,

Assumption A3: $y_0 > F(d) - \beta$,

Assumption A4: $y_0 < F(d)$,

Assumption A5: $y_0 \geq F(d) - \beta/q$,

Assumption A6: $y_0 \leq F(d) - \beta(q - 1)/q$,

Assumption A7: $y_0 > F(J_{\min})$,

Assumption A8: $y_0 < F(J_{\max}) - \beta$.

Let us explain thoroughly the geometric meaning of these assumptions. A special role in our considerations is played by an interval $I = [b, c] \subset \mathbb{R}$, where

$$b = \lim_{x \rightarrow d^+} g(x) = g(d) = qd - y_0 - am_1 - \beta,$$

$$c = \lim_{x \rightarrow d^-} g(x) = qd - y_0 - am_1.$$

Note that if β is positive then I is well defined and its length is equal to β .

Assumption A1 guarantees that $\beta > 0$ and that for a fixed β satisfying this condition there is a nonempty open interval $(F(J_{\max}) - \beta, F(J_{\min}))$ of values of y_0 for which the map g has no fixed points.

Assumption A3 reads $b < d$ and Assumption A4 reads $d < c$, so they both imply that the discontinuity point d lies inside $[b, c]$. Assume for a moment that Assumptions A3 and A4 hold. Now Assumption A2 implies that $J_{\min} \leq b$ and $J_{\max} \geq c$. Namely, then $d - b \leq c - b = \beta \leq d - J_{\min}$ and, in consequence, $J_{\min} \leq b$. Similarly, we justify that $J_{\max} \geq c$. This means that g restricted to $[b, c]$ is a constant slope map with the slope q .

Observe that, by the definitions of b and c , the interval $[b, c]$ is invariant, i.e., $g([b, c]) = [b, c]$ if and only if $g(b) \geq b$ and $g(c) \leq c$. This is true if Assumptions A2–A6 are satisfied. Namely, then $g(b) - b = g(b) - g(d) = q(b - d) + \beta = q(F(d) - y_0 - \beta(q - 1)/q) \geq 0$ and, analogously, $g(c) - c = q(F(d) - y_0 - \beta/q) \leq 0$.

Furthermore, Assumption A5 (resp. A6) means that an unstable fixed point on the right (resp., left) branch of the plot of g is outside the interval $[b, c]$. Finally, Assumptions A7 and A8 are related to the existence of a stable fixed point for g (see Theorem 12 below).

The following summary result is an immediate consequence of the above considerations and simple calculations.

Theorem 12. (Fixed points)

- Under Assumption A7 g has a stable fixed point $x_{ls} = -y_0/m_0$ on the left branch of the plot.
- Under Assumption A4 and A7 g has an unstable fixed point $x_{lu} = a + y_0/m_1$ on the left branch of the plot.

- Under Assumption A8 g has a stable fixed point $x_{rs} = 1 - (y_0 + \beta)/m_0$ on the right branch of the plot.
- Under Assumptions A3 and A8 g has an unstable fixed point $x_{ru} = a + (y_0 + \beta)/m_1$ on the right branch of the plot.
- Under Assumption $F(J_{\max}) - \beta < y_0 < F(J_{\min})$, g has no fixed points in \mathbb{R} .

Remark 6. Moreover, observe that

- the existence of an unstable fixed point always implies the existence of a stable fixed point for g ;
- if Assumption A1 is met, then the fixed points on the left branch of the plot of g cannot coexist with the fixed points on the right branch of the plot;
- if $y_0 = F(J_{\min})$ (resp. $y_0 = F(J_{\max}) - \beta$) then J_{\min} (resp. J_{\max}) is a semistable fixed point and a fold bifurcation occurs at this parameter value;
- if $y_0 = F(d) - \beta/q$ (resp. $y_0 = F(d) - \beta(q-1)/q$) then the unstable fixed point on right (resp. left) branch of the plot coincides with the right (resp. left) end of the interval $[b, c]$.

For the rest of this section we make Assumptions A1–A6. Let G denote g restricted to $[b, c]$. Observe that G governs the dynamics of the 1D pICNV on the invariant interval $[b, c]$. The next proposition is an easy consequence of our assumptions.

Proposition 7. (β -transformation) *The map $G: [b, c] \rightarrow [b, c]$*

- *is a well-defined β -transformation with slope q and point of discontinuity d ,*
- *has no fixed points in (b, c) .*

Figure 3 presents a plot of the map G for the following choice of parameters in the pICNV model: $a = 0.2$, $d = 0.4$, $m_0 = 0.864$, $m_1 = 0.65$, $\beta = 0.35$ and $y_0 = -0.05$. These parameter values are exemplary but in the range considered by Courbage *et al.* (2007).

Now let us formulate the main results, which explain the behaviour of the 1D pICNV model in the invariant interval $[b, c]$. Recall that, by definition, $G(b) = qb - y_0 - am_1$ and $G(c) = qc - y_0 - am_1 - \beta$. Our first result provides the conditions for Devaney's chaos in the 1D pICNV model.

Theorem 13. (Chaos)

1. Assume that $\sqrt[3]{2} \leq q \leq 2$. Then G is chaotic in the sense of Devaney on the interval $[b, c]$ if and only if one of the following conditions is satisfied:

- (i) $\sqrt{2} \leq q \leq 2$,
- (ii) $\sqrt[3]{2} \leq q < \sqrt{2}$ and $(G(b) < b + \frac{c-b}{q(1+q)} \text{ or } c - \frac{c-b}{q(1+q)} < G(c))$.

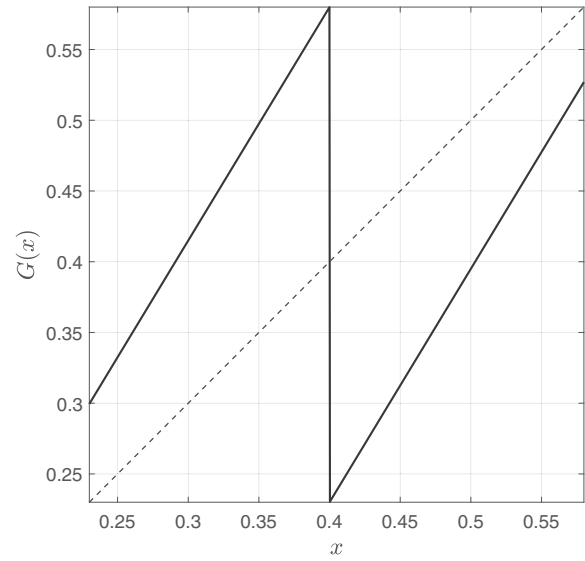


Fig. 3. Restriction of the pICNV function as a β -transformation.

2. Assume that $1 < q < \sqrt[3]{2}$. Then G is chaotic in the sense of Devaney on the interval $[b, c]$ if one of the following conditions is satisfied:

- (i) $G(b) \leq c - \frac{c-b}{q}$,
- (ii) $b + \frac{c-b}{q} \leq G(c)$.

Proof. Theorem 10 implies (1). Similarly, Theorem 11 implies (2). ■

The next result summarizes the metric properties of the restricted 1D pICNV model.

Theorem 14. (acip) *The map G has topological entropy $h(G) = \ln q$ and unique G -invariant probability measure μ with maximal entropy. The measure μ is absolutely continuous with respect to the Lebesgue measure. Moreover, the support of μ is a finite union of intervals and it is the whole interval $[b, c]$, which means that μ is equivalent to the Lebesgue measure, if*

- (i) $\sqrt{2} \leq q \leq 2$ or
- (ii) $1 < q < \sqrt{2}$ and $G(b) \leq c - \frac{c-b}{q}$ or
- (iii) $1 < q < \sqrt{2}$ and $b + \frac{c-b}{q} \leq G(c)$.

Proof. It is an immediate consequence of Theorem 8. ■

Finally, the parameter regions of the existence and stability of fixed points and chaos are depicted in Fig. 4.

9. Interpretation of orbit itineraries in terms of spiking patterns

Characterizing itineraries of periodic orbits is not only an interesting and challenging mathematical problem but it is also meaningful from the point of view of

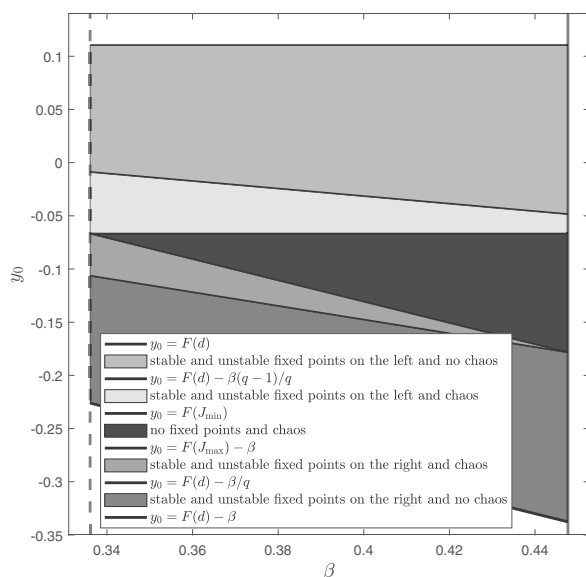


Fig. 4. Regions of different dynamics of the plCNV model.

classifying spike patterns generated by a neuron. Below we summarize some important observations that apply to both the 1D plCNV and nlCNV models. However, a similar interpretation holds also in the 2D case and can be formulated with respect to itineraries of the projection of 2D periodic orbits to their x -coordinate.

Firstly observe that, by definition, periodic orbits with rotation number $1/q$ or $(q-1)/q$ are always twist and have periodic itineraries of the form $LL \dots LR$ and $LRR \dots R$, respectively (with $q-1$ repetitions of the same corresponding symbol). Therefore, as follows from Corollary 1 (and independently from Corollary 2), if rational numbers of this form are in the rotation interval, then there are unique periodic orbits which realize them. Thus the spike trains corresponding to these rotation numbers are also unique.

Corollary 3. Suppose that the number $1/q$ is in the rotation interval of the expanding Lorenz map describing the 1D CNV model. Then there is a unique initial voltage condition x_0 (in the invariant interval) which gives rise to the periodic spiking pattern where $q-1$ time instances of the increase in the membrane voltage x are followed by one rapid decrease in the membrane voltage. The period of this periodic pattern consists of q time instances, with exactly one spike in each period.

The same holds for the rotation number $(q-1)/q$, with the difference that now an increase in the voltage per one period of length q occurs for 1 time unit and is followed by $q-1$ time instances of voltage decrease.

Note that a periodic orbit with the rotation number $1/q$ corresponds to the situation where the consecutive increase in the membrane potential (depolarization) for

$q-1$ time instances is followed by quite a rapid decrease (repolarization) which indeed reminds a spike. In this case all the spikes along the same spike train look exactly the same (in particular they have the same amplitude).

On the other hand, the spiking pattern corresponding to the rotation number $(q-1)/q$ consists of one rapid increase of the membrane voltage followed by consecutive $q-1$ time instances in repolarization. Thus in this case the decrease in the membrane voltage following a spike is milder than in the case of rotation number $1/q$.

Similarly, one can obtain easily the following result.

Corollary 4.

- A periodic orbit with rotation number $1/q$ results in a q -periodic voltage-train with $q-p$ time instances at which the membrane voltage increases and p time instances of the decrease in the voltage. Moreover, if p/q (p and q coprime) is in the rotation interval (of the expanding Lorenz map of the plCNV or nlCNV model), then there are at most $\binom{q}{p}/q$ corresponding periodic orbits, among which exactly one periodic orbit is twist but each of these orbits has a different itinerary.
- Identifying itineraries with periodic spike-trains produced by the corresponding periodic orbit, we conclude that every periodic orbit of the expanding Lorenz map of plCNV or nlCNV model gives rise to the unique spike-train.

Thus the rotation number ϱ of a given periodic orbit together with its itinerary is directly related to the periodic spiking pattern generated by this orbit. In particular, one might assume that any occurrence of the word LR in the orbit itinerary might be interpreted as a spike. However, here (except for the case $\varrho = 1/q$ and $\varrho = (q-1)/q$) the amplitude of the spike might be different for each occurrence of the word LR in the q -length periodic sequence of L and R symbols (see Example 2 and Fig. 5). Thus, hypothetically (depending on the purpose) one can consider introducing some threshold value θ such that “spikes” with the amplitude above this threshold indeed count as spikes whereas “spikes” with the amplitude below θ might be rather interpreted as subthreshold oscillations. With this interpretation, knowing the itinerary of the periodic orbit might not be enough to fully describe the resulting spiking pattern as one might need a precise location of points of the orbit, not only the continuity interval in which they appear.

Corollary 5. If p/q (p and q coprime) is in the rotation interval of the expanding Lorenz map of the 1D plCNV or nlCNV model then there exists a unique q -periodic spiking pattern of the form $(\tilde{x}_1, \tilde{x}_2, \dots, \tilde{x}_q)$ (where $\tilde{x}_i \in \{L, R\}$) such that $\tilde{x}_i = L$ if and only if $1 + (i-1)p \bmod q \leq q-p$ (with L -symbols corresponding to the increase in the neuron’s membrane potential and R with the decrease).

If the occurrence of the word LR is interpreted as a spike, then this spike train features n spikes in each q -cycle, where

$$n := \#\{1 < j < q \mid 1 + (j-1)p \bmod q \leq q-p \text{ and } 1 + jp \bmod q > q-p\}$$

(with the convention that $q \bmod q = q$).

Proof. It is not hard to guess that the spike train concerned in the above corollary corresponds in fact to a twist periodic orbit with rotation number p/q . Such a twist periodic orbit exists and is unique for the expanding Lorenz map. Thus let $\{x_1 < x_2 < \dots < x_q\}$ denote the set of points of this orbit arranged in the increasing order of their values. If (z_1, z_2, \dots, z_q) is the ordering of the orbit such that $G(z_i) = z_{i+1}$ (where G is the map of the 1D model), which corresponds to the spike train observed, then from the definition of the twist periodic orbit we have that

$$\begin{aligned} z_1 &:= x_1 \in I_L, \\ z_2 &= G(z_1) = G(x_1) = x_{1+p \bmod q}, \\ &\vdots \\ z_i &= G(z_{i-1}) = x_{1+(i-1)p \bmod q}, \\ &\vdots \\ z_q &= G(z_{q-1}) = x_{1+(q-1)p \bmod q} = x_{q-p+1} \in I_R, \end{aligned}$$

where

$$z_i \in I_L \iff (1 + (i-1)p) \bmod q \leq q-p$$

as follows from the ordering $\{x_1 < x_2 < \dots < x_q\}$ and the fact that the orbit with rotation number p/q has exactly p points in the right continuity interval I_R and $q-p$ points in the left interval I_L . The corresponding spike train $(\tilde{x}_1, \tilde{x}_2, \dots, \tilde{x}_q)$ can be encoded with the sequence of symbols $\{L, R\}^q$ where $\tilde{x}_i = L$ if and only if $1 + (j-1)p \bmod q \leq q-p$ and the rest of the statement follows. ■

Example 1. Under the assumptions of Corollary 5 assume that $p/q = 4/5$ is in the rotation interval of the corresponding 1D model. Then there is a unique 5-periodic spike train of the form $LRRRR$. The spike-train, visualized in Figs. 5(a) and (b) together with the associated periodic orbit, features one spike in each cycle of length 5. ♦

Example 2. Similarly, assume that $p/q = 7/9$. Then there is a unique 9-periodic spike train of the form $LRRRLRRRR$. The spike-train features two spikes in each cycle of length 9 and these spikes are of different amplitude, as seen in Fig. 5(d). The corresponding periodic trajectory is depicted in Fig. 5(c). ♦

10. Conclusions

Our work, although devoted to a particular neuron model, might serve also as a review of the theory of Lorenz-like maps for which we have provided a couple of noteworthy extensions. Namely, for expanding Lorenz maps we have justified the expansiveness (Proposition 1), the uniqueness of periodic orbits with a given itinerary (Proposition 4), existence and uniqueness of twist periodic orbits with a given rotation number (Corollary 1), an upper estimate of the number of periodic orbits with the same rotation number (Corollary 2), the equivalence of transitivity and Devaney chaos on the whole interval (Proposition 5) and precise conditions for Devaney chaos (Theorem 7).

All these results can be applied to both linear and nonlinear CNV models. On the other hand, we also proved more particular results on β -transformations that apply in the linear case (Theorems 10 and 11 as well as Lemmas 1 and 2).

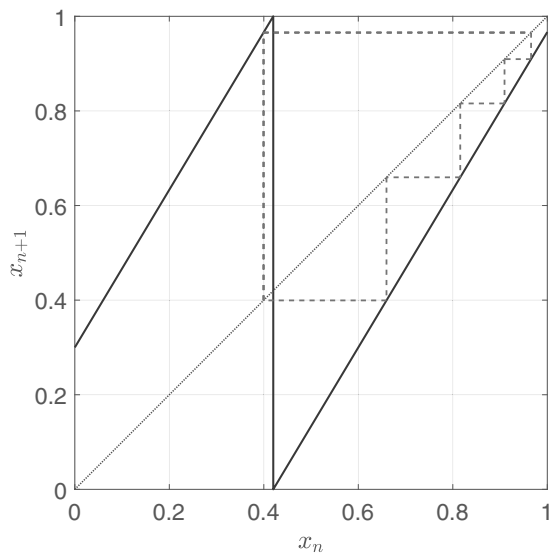
These mathematical results can be naturally applied for the study of the CNV model, mainly in its 1D reduction but partially also in its full 2D version, as we have shown in Sections 8 and 9. It has been rigorously shown how the theory of Lorenz-like maps and β transformation can be used for studying the CNV model, especially by identifying regions of chaotic and periodic behaviour in the model.

In particular, we have established the direct connection between periodic spiking patterns and periodic orbits of the voltage map in the CNV model and next, with the use of very recent findings on Farey-Lorenz permutations for Lorenz maps, we have provided a combinatorial description of the periodic spiking patterns. The rotation interval and the corresponding set of *fupos* might be viewed here as a complexity measure of the system under study.

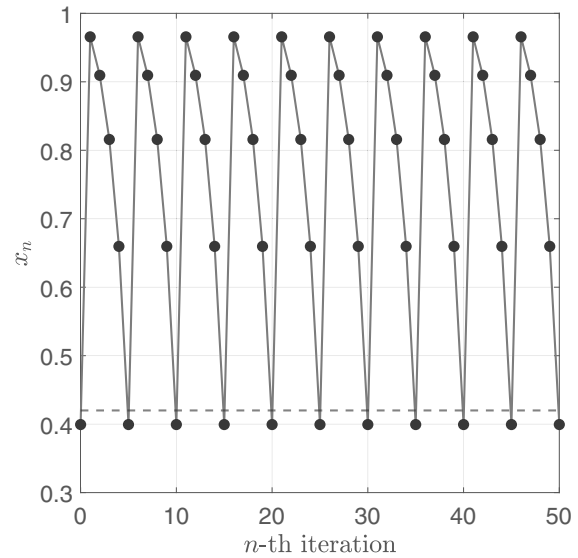
The CNV model is useful in modelling and validating results of clinical relevance as exemplified in Introduction. Furthermore, since Lorenz-like maps appear also in hybrid neural models (see, e.g., Rubin *et al.*, 2017) and in various other models of physiological and biological phenomena (see, e.g., the work of Derks *et al.* (2021) and the references therein), as well as in numerous other applications, the methods presented and developed in this work might be adapted in multiple fields.

Acknowledgment

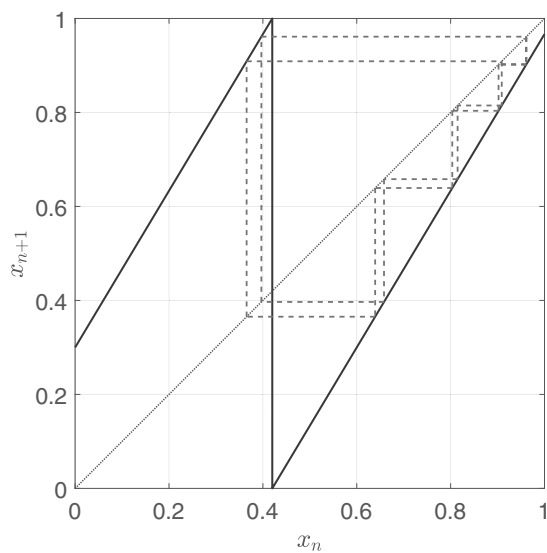
Frank Llovera Trujillo and Justyna Signerska-Rynkowska were supported by the NCN (National Science Centre, Poland), grant no. 2019/35/D/ST1/02253. Frank Llovera Trujillo was also supported by a Polonium International Doctoral Fellowships (1st edition) scholarship awarded by the Gdańsk University of Technology within the Initiative of Excellence—Research University program. Justyna



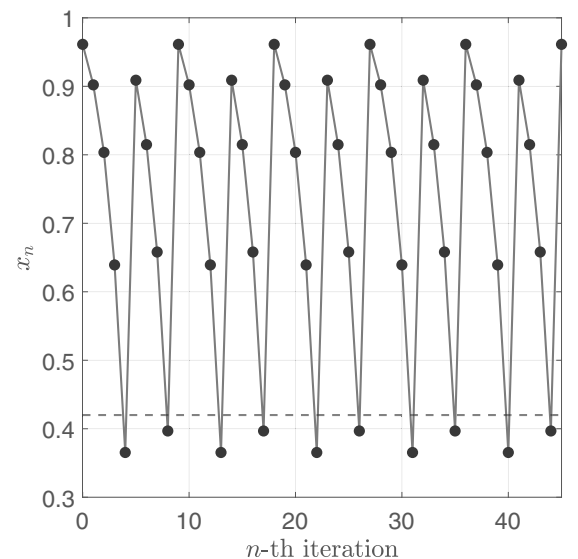
(a)



(b)



(c)



(d)

Fig. 5. Relation between the rotation number and the spike pattern: periodic orbit of the 1D model with rotation number $4/5$ (a) and the corresponding voltage trace (b), periodic orbit with rotation number $7/9$ (c) and corresponding voltage trace (d).

Signerska-Rynkowska also acknowledges the support of the Dioscuri program initiated by the Max Planck Society, jointly managed with the National Science Centre (Poland), and mutually funded by the Polish Ministry of Science and Higher Education as well as the German Federal Ministry of Education and Research.

References

- Afraimovich, V. and Hsu, S. (2002). *Lectures on Chaotic Dynamical Systems*, American Mathematical Society, Providence.
- Alsedà, L., Llibre, J., Misiurewicz, M. and Tresser, C. (1989). Periods and entropy for Lorenz-like maps, *Annales de l'Institut Fourier (Grenoble)* **39**(4): 929–952, DOI: 10.5802/aif.1195.
- Cholewa, Ł. and Oprocha, P. (2021a). On α -limit sets in Lorenz maps, *Entropy* **23**(9): 1153. DOI: 10.3390/e23091153.
- Cholewa, Ł. and Oprocha, P. (2021b). Renormalization in Lorenz maps—Completely invariant sets and periodic orbits, *arXiv*: 2104.00110[math.DS].
- Courbage, M., Maslennikov, O.V. and Nekorkin, V.I. (2012). Synchronization in time-discrete model of two electrically

- coupled spike-bursting neurons, *Chaos, Solitons, Fractals* **45**(05): 645–659, DOI: 10.1016/j.chaos.2011.12.018.
- Courbage, M. and Nekorkin, V.I. (2010). Map based models in neurodynamics, *International Journal of Bifurcation and Chaos in Applied Sciences and Engineering* **20**(06): 1631–1651, DOI: 10.1142/S0218127410026733.
- Courbage, M., Nekorkin, V.I. and Vdovin, L.V. (2007). Chaotic oscillations in a map-based model of neural activity, *Chaos* **17**(4): 043109, DOI: 10.1063/1.2795435.
- Derks, G., Glendinning, P.A. and Skeldon, A.C. (2021). Creation of discontinuities in circle maps, *Proceedings of the Royal Society A: Mathematical, Physical and Engineering Sciences* **477**(2251): 20200872, DOI: 10.1098/rspa.2020.0872.
- Ding, Y.M., Fan, A.H. and Yu, J.H. (2010). Absolutely continuous invariant measures of piecewise linear Lorenz maps. *arXiv*: 1001.3014 [math.DS].
- FitzHugh, R. (1955). Mathematical models of the threshold phenomena in the nerve membrane, *The Bulletin of Mathematical Biophysics* **17**: 257–278, DOI: 10.1007/BF02477753.
- Geller, W. and Misiurewicz, M. (2018). Farey–Lorenz permutations for interval maps, *International Journal of Bifurcation and Chaos* **28**(02): 1850021, DOI: 10.1142/S0218127418500219.
- Hess, A., Yu, L., Klein, I., Mazancourt, M.D., Jebrak, G. and Mal, H. (2013). Neural mechanisms underlying breathing complexity, *PLoS ONE* **8**(10): e75740, DOI: 10.1371/journal.pone.0075740.
- Hofbauer, F. (1979). Maximal measures for piecewise monotonically increasing transformations on $[0,1]$, in M. Denker and K. Jacobs (Eds), *Ergodic Theory*, Springer, Berlin/Heidelberg, pp. 66–77.
- Hofbauer, F. (1981). The maximal measure for linear mod. one transformations, *Journal of the London Mathematical Society* **s2–23**(1): 92–112, DOI: 10.1112/jlms/s2-23.1.92.
- Ibarz, B., Casado, J.M. and Sanjuán, M.A.F. (2011). Map-based models in neuronal dynamics, *Physics Reports* **501**(1–2): 1–74, DOI: 10.1016/j.physrep.2010.12.003.
- Kameyama, A. (2002). Topological transitivity and strong transitivity, *Acta Mathematica Universitatis Comenianae* **71**(2): 139–145.
- Korbicz, J., Patan, K. and Obuchowicz, A. (1999). Dynamic neural networks for process modelling in fault detection and isolation systems, *International Journal of Applied Mathematics and Computer Science* **9**(3): 519–546.
- Llovera-Trujillo, F., Signerska-Rynkowska, J. and Bartłomiejczyk, P. (2023). Periodic and chaotic dynamics in a map-based neuron model, *Mathematical Methods in the Applied Sciences* **46**(11): 11906–11931.
- Maslennikov, O.V. and Nekorkin, V.I. (2012). Discrete model of the olivo-cerebellar system: Structure and dynamics, *Radiophysics and Quantum Electronics* **55**(3): 198–214, DOI: 10.1007/s11141-012-9360-6.
- Maslennikov, O.V. and Nekorkin, V.I. (2013). Dynamic boundary crisis in the Lorenz-type map, *Chaos* **23**(2): 023129, DOI: 10.1063/1.4811545.
- Maslennikov, O.V., Nekorkin, V.I. and Kurths, J. (2018). Transient chaos in the Lorenz-type map with periodic forcing, *Chaos* **28**(3): 033107, DOI: 10.1063/1.5018265.
- Oprocha, P., Potorski, P. and Raith, P. (2019). Mixing properties in expanding Lorenz maps, *Advances in Mathematics* **343**: 712–755, DOI: 10.1016/j.aim.2018.11.015.
- Palmer, R. (1979). *On the Classification of Measure Preserving Transformations of Lebesgue Spaces*, PhD thesis, University of Warwick, Warwick, https://wrap.warwick.ac.uk/88796/1/WRAP_Theses_Palmer_2016.pdf
- Parry, W. (1979). The Lorenz attractor and a related population model, in M. Denker and K. Jacobs (eds), *Ergodic Theory*, Springer, Berlin/Heidelberg, pp. 169–187, DOI: 10.1007/BFb0063293.
- Patan, K., Witczak, M. and Korbicz, J. (2008). Towards robustness in neural network based fault diagnosis, *International Journal of Applied Mathematics and Computer Science* **18**(4): 443–454, DOI: 10.2478/v10006-008-0039-2.
- Rubin, J.E., Touboul, J.D., Signerska-Rynkowska, J. and Vidal, A. (2017). Wild oscillations in a nonlinear neuron model with resets. II: Mixed-mode oscillations, *Discrete and Continuous Dynamical Systems B* **22**(10): 4003–4039, DOI: 10.3934/dcdsb.2017205.
- Yu, L., Mazancourt, M.D. and Hess, A. (2016). Functional connectivity and information flow of the respiratory neural network in chronic obstructive pulmonary disease, *Human Brain Mapping* **37**(8): 2736–2754, DOI: 10.1002/hbm.23205.
- Yue, Y., Liu, Y.J., Song, Y.L., Chen, Y. and Yu, L. (2017). Information capacity and transmission in a Courbage–Nekorkin–Vdovin map-based neuron model, *Chinese Physics Letters* **34**(4): 048701, DOI: 10.1088/0256-307x/34/4/048701.



Piotr Bartłomiejczyk is a mathematician, whose research interests focus on nonlinear analysis (topological degree theory), dynamical systems (Conley index theory), homotopy theory (search for new homotopy invariants), and, recently, mathematical modelling in neuroscience. In 2000 he was awarded a PhD degree by the Institute of Mathematics of the Polish Academy of Sciences in Warsaw, and in 2016 a DSc degree by the University of Gdańsk. In 2018 he became an associate professor at the Gdańsk University of Technology.



Frank Llovera Trujillo received his MS degree in mathematics and physics from the University of L'Aquila (Italy) and the Gdańsk University of Technology (Poland) in 2019. He has been a PhD student of mathematics at the Gdańsk University of Technology since 2020. His scientific interests include dynamical systems, chaos and its applications, neuronal networks and data science.



Justyna Signerska-Rynkowska received her PhD in mathematics in 2013 from the Institute of Mathematics of the Polish Academy of Sciences (IM PAN). Then, after a postdoctoral fellowship at the INRIA Paris Research Centre, she obtained the position of an assistant professor at the Gdańsk University of Technology. Her scientific interests include mainly dynamical systems and chaos and their applications, especially in neurosciences. She has been awarded two research grants by the National Science Center in Poland and currently is a visiting assistant professor at the Dioscuri Centre in Topological Data Analysis at the IM PAN, where she works on various applications of dynamical systems theory to time-series analysis.


Received: 11 October 2022

Revised: 7 March 2023

Accepted: 13 April 2023

RESEARCH ARTICLE | APRIL 01 2024

Analysis of dynamics of a map-based neuron model via Lorenz maps **FREE**

Piotr Bartłomiejczyk ; Frank Llovera Trujillo ; Justyna Signerska-Rynkowska  



Chaos 34, 043110 (2024)

<https://doi.org/10.1063/5.0188464>





APL Quantum

Bridging fundamental quantum research with technological applications

Now Open for Submissions

No Article Processing Charges (APCs) through 2024

Submit Today



Analysis of dynamics of a map-based neuron model via Lorenz maps

Cite as: Chaos 34, 043110 (2024); doi: 10.1063/5.0188464

Submitted: 21 November 2023 · Accepted: 9 March 2024 ·

Published Online: 1 April 2024



View Online



Export Citation



CrossMark

Piotr Bartłomiejczyk,^{1,a)} Frank Llovera Trujillo,^{2,b)} and Justyna Signerska-Rynkowska^{1,3,c)}

AFFILIATIONS

¹Faculty of Applied Physics and Mathematics & BioTechMed Centre, Gdańsk University of Technology, Gabriela Narutowicza 11/12, 80-233 Gdańsk, Poland

²Doctoral School, Gdańsk University of Technology, Gabriela Narutowicza 11/12, 80-233 Gdańsk, Poland

³Dioscuri Centre in Topological Data Analysis, Institute of Mathematics of the Polish Academy of Sciences, Śniadeckich 8, 00-656 Warsaw, Poland

^{a)}Email address: piobartl@pg.edu.pl

^{b)}Email address: frank.llovera.trujillo@pg.edu.pl

^{c)}Author to whom correspondence should be addressed: justyna.signerska@pg.edu.pl

ABSTRACT

Modeling nerve cells can facilitate formulating hypotheses about their real behavior and improve understanding of their functioning. In this paper, we study a discrete neuron model introduced by Courbage *et al.* [Chaos 17, 043109 (2007)], where the originally piecewise linear function defining voltage dynamics is replaced by a cubic polynomial, with an additional parameter responsible for varying the slope. Showing that on a large subset of the multidimensional parameter space, the return map of the voltage dynamics is an expanding Lorenz map, we analyze both chaotic and periodic behavior of the system and describe the complexity of spiking patterns fired by a neuron. This is achieved by using and extending some results from the theory of Lorenz-like and expanding Lorenz mappings.

Published under an exclusive license by AIP Publishing. <https://doi.org/10.1063/5.0188464>

Map-based models form an important class of models describing the dynamics of a single nerve cell, which effectively complement earlier ODE-based ones. Although these models might seem abstract from the biological point of view, their electrophysiological relevance is in many cases more than satisfactory. Moreover, their relatively low computational complexity enables to employ them successfully in larger scale simulations of neuronal circuits motivated by biological or clinical issues. However, prior to the examination of large ensembles of coupled neurons, it is desirable to understand the dynamical mechanisms behind the phenomena observed in the chosen single neuron model. In 2007, Courbage *et al.* introduced a discrete neuron model where the membrane voltage dynamics was captured by the iterates of the piecewise linear discontinuous map. In this work, we undertake a rigorous study of its later version where, following the prominent FitzHugh–Nagumo model, the piecewise linear function is replaced by a cubic polynomial with a discontinuity point. In particular, using recent advances of the theory of Lorenz-like maps, we quantify chaotic behavior and firing patterns displayed by a reduced Courbage, Nekorkin, and Vdovin (CNV) model.

I. INTRODUCTION

Modeling neuronal behavior dates back to the beginning of previous century when Lapicque¹ formulated a simple neuron model, derived from experimental data. This model later gave rise to the famous leaky-integrate-and-fire (LIF) model (see, e.g., Ref. 2). A couple of decades later, Hodgkin and Huxley derived a much more detailed neuron model,³ consisting of four nonlinear differential equations that were able to capture many electrophysiological phenomena present in real neurons. Since this pioneering model, systems based on ODEs have become a standard in modeling of biological neurons with some later prominent examples of FitzHugh–Nagumo,^{4,5} Hindmarsh–Rose,⁶ Morris–Lecar,⁷ and other models. These models were usually significantly simpler than the original Hodgkin–Huxley model but served as a good toy model for explaining the mechanism of action potential generation and, sometimes, more complicated phenomena like *bursting* (a repetitive behavior where a series of spikes occurs in a rapid succession followed by a quiescent period).

These lower dimensional reduced models have the advantage of enabling rigorous analysis, but the continuous-time dynamics

given by systems of ODEs often requires more dimensions or separation of time scales to capture more complicated phenomena. Therefore, there appeared a need for some sort of discretization of these models. The first pronounced step in this direction was the appearance of hybrid neuron models, in which the interspike evolution of transmembrane voltage and other variables is governed by ODEs but the additional threshold-reset mechanism is introduced in order to better reproduce spike generation. The hybrid nature makes these models interesting even in one-dimensional setting,^{8–11} but one-dimensional integrate-and-fire (IF) models are too simple, e.g., to display bursting behavior. However, two-dimensional IF models^{12–14} feature both bursting and other complicated phenomena such as, e.g., spike-adding or mixed-mode oscillations^{15,16} that in ODE-systems need at least three dimensions and often separation of time scales.

Another class of deterministic neuron models are the so-called map-based models where differential equations are replaced by maps. These models might also involve some sort of resetting mechanism, which is usually incorporated in the map describing the evolution of the membrane voltage. However, many map-based models do not include directly any kind of resetting mechanism. Instead, purely discrete nature of these models can give rise to very complicated phenomena, yet their computational feasibility allows for simulating large networks consisting of map-based neurons. Some of these models arise simply as discretization of ODE-based models, whereas others rather cannot be linked with any ODE system (see, e.g., Ref. 17 for an extensive review of map-based models).

Most of the two-dimensional map-based models can be expressed in a general form

$$x_{n+1} = F(x_n, y_n), \quad (1a)$$

$$y_{n+1} = y_n + \varepsilon G(x_n, y_n), \quad (1b)$$

where often $0 < \varepsilon \ll 1$ to include separation of time scales. The main dynamical variable x stands for the membrane voltage and y is usually called *adaptation* or *recovery* variable, which replaces complicated dynamics of ion channels. Separation of time scales as $\varepsilon \rightarrow 0$ also justifies studying the first return map $x_{n+1} = F(x_n, y)$ as $y_n \equiv y$ is kept constant since this map governs the most important dynamical properties of (1a) and (1b). Similarly, this map allows us to understand intuitively such phenomena like bursting and adaptation since y can be interpreted as a slowly varying bifurcation parameters in the map $F_y(x) := F(x, y)$ and the types of bifurcations governing the onset and termination of limit cycles of map F are closely related to the classification of bursting patterns in map-based models.¹⁸

Popular 2D map-based (discrete) neuron models include, e.g., the Rulkov model,¹⁹ Chialvo model,²⁰ or Courbage, Nekorkin, and Vdovin (CNV) model.²¹ The CNV, or precisely its modification, will be the subject of our study presented in this work. However, let us first briefly mention some other properties of the above-listed models.

The *chaotic Rulkov model*¹⁹ is given as

$$x_{n+1} = \frac{\alpha}{1 + x_n^2} + y_n + I, \quad (2a)$$

$$y_{n+1} = y_n - \varepsilon(x_n - \sigma), \quad (2b)$$

where I describes external input or synaptic currents applied to the neuron and σ denotes the resting potential. In this model, the function $F(x, y) := \frac{\alpha}{1+x^2} + y + I$ is a unimodal map as a function of x for fixed y . This map can feature a stable and unstable fixed points on the left branch, which disappear under saddle-node bifurcation as I increases. Initial conditions attracted to the stable fixed point correspond to the resting state of the model. On the other hand, spiking orbits are chaotic, not periodic, which is the important property of the model, as irregular bursting is more similar to realistic bursting neurons than periodic bursting.²² In fact, chaotic dynamics in systems such as the Rulkov model is robust and can be classified with some notion of regularity,²³ which is actually consistent with the physiological function of neurons. Note that there are also other versions of the Rulkov model called *non-chaotic Rulkov model*²⁴ and *supercritical Rulkov model*.²⁵

The *Chialvo model*²⁰ is given as

$$x_{n+1} = x_n^2 \exp(y_n - x_n) + I, \quad (3a)$$

$$y_{n+1} = ay_n - bx_n + c. \quad (3b)$$

It turns out that the map $F(x, y) := x^2 \exp(y - x) + I$ defining the evolution of the voltage variable is unimodal (for fixed y) on some invariant interval, similar to the Rulkov map. However, here its dependence on the recovery variable y is not additive, but non-linear and, therefore, a small change in the value of y changes the shape of the x -nullcline in a much more complicated way than in the case of the Rulkov map. Nevertheless, this model, designed as an excitable neuron model, also reveals chaotic spiking, periodic spiking, as well as bistability and subthreshold oscillations. More detailed analysis of its 1D subsystem $x_{n+1} = F(x_n, y)$ can be done upon noticing that the map F (again for fixed y) has negative Schwarzian derivative.²⁶ Since the model does not follow exactly a typical form of the slow-fast map-based neuron models (1a) and (1b), its singular perturbation analysis also requires more general tools.²⁷

Although the Chialvo model was introduced in 1995, there is again a growing interest in this model. This is particularly due to its dependence on many parameters and the fact that small variations in these parameters can significantly change its phase portrait. Therefore, rigorous analysis of its global dynamics requires new computational and analytical tools.²⁸ On the other hand, many extensions of this model also have emerged recently (see, e.g., Ref. 29). A more detailed discussion of various discrete neuron models and how they relate to ODE-based models can be found in review articles.^{17,30}

In the current work, we undertake the study of the following two-dimensional discrete neuron model:

$$x_{n+1} = f_1(x_n, y_n) = x_n + F(x_n) - y_n - \beta H(x_n - d), \quad (4a)$$

$$y_{n+1} = f_2(x_n, y_n) = y_n + \varepsilon(x_n - J), \quad (4b)$$

introduced by Courbage *et al.*²¹ and further called the CNV model (for short). In this model, as before, x_n denotes the values of the membrane potential of the neuron at consecutive time instances $n = 1, 2, \dots$, and y_n is the values of the recovery variable. The

function $H(x)$ is the usual Heaviside step function

$$H(x) = \begin{cases} 1, & \text{if } x \geq 0, \\ 0, & \text{if } x < 0. \end{cases}$$

Parameter $\varepsilon > 0$ describes the time scale separation between variables x and y , J might stand for a constant external stimulus, whereas $\beta > 0$ and $d > 0$ control the threshold properties of oscillations. Typically, $F(x)$ is defined as follows:

$$F(x) = \begin{cases} -m_0x, & \text{if } x \leq J_{\min}, \\ m_1(x - a), & \text{if } J_{\min} \leq x \leq J_{\max}, \\ -m_0(x - 1), & \text{if } x \geq J_{\max}, \end{cases} \quad (5)$$

where

$$m_0, m_1 > 0, \quad 1 > a > 0, \quad J_{\min} = \frac{am_1}{m_0 + m_1}, \quad J_{\max} = \frac{m_0 + am_1}{m_0 + m_1}.$$

Due to the piecewise linear form of $F(x)$, the model (4a) and (4b) with F given by (5) will be referred to as the pICNV model (piecewise linear CNV model). Detailed analysis of this model, and especially its first return map, was performed in our recent paper.³¹ However, given the similarity of the CNV model with FitzHugh–Nagumo one,^{4,32} it seems natural to replace the piecewise linear function F with some cubic polynomial (see Ref. 30). Of course, introducing a nonlinear function F requires a bit different analytical tools (in particular, the theory of β -transformations, successively applied in Ref. 31, must be replaced by the general theory of Lorenz-like or expanding Lorenz maps).

The CNV model displays a range of attractors and regimes of neural activity, including phasic spiking, phasic bursts, tonic spiking, chaotic spiking, subthreshold oscillations, or chaotic bursting oscillations. General conditions in parameter spaces for these various types of qualitative behaviors have been identified in Ref. 21.

In this paper, we study the CNV model, where the function F is defined as

$$F(x) = \mu x(x - a)(1 - x), \quad (6)$$

with $\mu > 0$ and $0 < a < 1$. The model (4a) and (4b) where F is given by (6) will be called in our analysis nonlinear CNV (nICNV) model. Its simplified one dimensional version consisting of (4a), with $y_n := \alpha$ being a constant parameter, will be referred to as the 1D nICNV model.

Our study of the 1D nICNV model is motivated, among others, by the fact that it actually governs the behavior of the full model and thorough understanding of its properties such as chaos and structure of periodic orbits with respect to γ and other parameters are essential. Obviously, this one-dimensional system is also interesting from purely mathematical point of view. However, as 1D map-based models are also known in the literature (e.g., the models proposed by Aguirre *et al.*,³³ Cazelles *et al.*,³⁴ or just the fast subsystem of the chaotic Rulkov model, see the review articles Refs. 17 and 30 and references therein), we also argue later (in Sec. VIII) that it can be considered an independent neuron model.

Theoretical analysis of some aspects of Courbage–Nekorkin–Vdovin model has been done, e.g., in Refs. 35 and 36. Small networks

of interacting CNV neurons have been analyzed in Ref. 37. The model has been also used in biologically or clinically motivated studies, as, e.g., in Refs. 38–40. In particular, the work⁴¹ builds a discrete model of the olivo-cerebellar system based on the nonlinear version of the CNV model.

Note that the earlier works^{21,30} discussing chaos of the map corresponding to the fast subsystem of the CNV model did not distinguish between chaos on the whole invariant interval or only on its subinterval, and the analysis provided therein was not fully rigorous (though qualitatively describing the mechanism of many important properties of the full model such as chaotic spike-bursting oscillations, subthreshold oscillations, and phasic spiking). The work³⁰ also reported numerically (see Fig. 22 therein) that the invariant subset on which the dynamics of the 1D nICNV accumulates might be the whole invariant interval or the union of subintervals. This observation is rigorously justified by us in Theorem 5.5 about the support of the absolutely continuous invariant probability measure (ACIP). Further, none of the earlier works studied the combinatorial structure of periodic orbits, which we carried out with the use of finite unions of periodic orbit (FUPO) theory and matched these with the spiking patterns generated.

The organization of the paper is as follows. Section II describes fundamentals of rotation theory applied to Lorenz-like maps. Definitions of Lorenz-like and expanding Lorenz maps and their main properties, also related to chaos, are recalled in Appendix A. Providing extensive introduction to the theory of Lorenz maps is motivated by the fact that the map $g_\alpha(x) := x + F(x) - \alpha - \beta H(x - d)$, describing the dynamics of the voltage variable x , while the second variable $y = \alpha$ is kept constant, is the Lorenz-like map for a large range of parameter values of interest. That fact will be crucial for our further analysis of the nICNV model. In addition to the present state of the art of this theory, in Sec. II and in Appendix A, we prove a couple of contributing results in the general theory of Lorenz-like maps useful for investigating the dynamics of the model. In Sec. III, we briefly recall our results from Ref. 31 on the 1D pICNV model. Next, in Sec. IV, we state preliminary results for the 1D nICNV model and indicate regions in parameter space corresponding to the existence of invariant intervals on which model maps are expanding Lorenz. This allows us to apply the theory of (expanding) Lorenz maps to provide sufficient conditions for chaos in the model (Sec. V) and to obtain results on rotation interval (Sec. VI) and itineraries of periodic orbits (Sec. VII). These results describe quantitatively the complexity of periodic behavior and spike patterns in the 1D nICNV model. Moreover, Sec. VII contains also examples and numerical simulations in which rotation intervals and itineraries of periodic orbits are computed for some choices of parameters. The theory of FUPOs and Farey–Lorenz permutations, which we widely use in Sec. VII, is summarized in Appendix F. In Sec. VIII, we discuss the implications of our results in terms of activity patterns and the shape of the action potential under the constant stimulus. Moreover, we also go beyond the autonomous case studied in this work and include numerical examples of voltage time series generated for popular varying inputs. We also sum up the results obtained for the 1D nICNV model and debate on their connections with the full model (4a) and (4b). Longer and technical proofs of some of our theorems are included in Appendixes C–E.

II. ROTATION THEORY FOR LORENZ MAPS

We will now look at the rotation theory properties related to Lorenz maps. To this end, we mainly recall definitions and results from Ref. 42, essential for our analysis of the CNV model. Let $f: [0, 1] \rightarrow [0, 1]$ be a Lorenz-like map (see Appendix A for definition and basic properties of Lorenz-like maps).

Definition 2.1. For a point $x \in [0, 1]$ and a positive integer n , we will denote by $R(x, n)$ the number of integers $i \in \{0, \dots, n-1\}$ such that $f^i(x) \in I_R$. If the limit

$$\rho(x) = \lim_{n \rightarrow \infty} \frac{R(x, n)}{n}$$

exists, we call it the *rotation number* of x .

Obviously, if x is a periodic point of f of period q , then $\rho(x)$ exists and equals $R(x, q)/q$. We have the following result⁴³ on the uniqueness of the rotation number in the nonoverlapping setting.

Theorem 2.2 (Rhodes–Thompson). If $f(0) \geq f(1)$, then all points have the same rotation number.

In this case, we denote the rotation number simply by $\rho(f)$. Therefore, in particular, nonoverlapping Lorenz-like maps admit unique rotation number. In the special case, when $f(0) = f(1)$ and f is strictly increasing on I_L and on I_R , the map can be identified with the orientation preserving homeomorphism of the unit circle $\mathbb{S}^1 = \mathbb{R}/\mathbb{Z}$. In such a situation, the existence and uniqueness of the rotation number and the fact that it is rational if and only if f has a periodic point follows from the classical Poincaré rotation theory (see, e.g., Ref. 44).

The alternative case $f(0) < f(1)$ can be accessed by the use of so-called water maps.

Definition 2.3. Let f be a Lorenz-like map and $t \in f(I_L) \cap f(I_R)$. The *water map* of f at level t is defined by

$$f_t(x) = \begin{cases} \max(t, f(x)) & \text{if } x \in I_L, \\ \min(t, f(x)) & \text{if } x \in I_R. \end{cases}$$

Note that a water map is also Lorenz-like and that $f_t(0) = f_t(1)$. Thus, all points $x \in [0, 1]$ have the same rotation number $\rho(f_t)$ for it. It is known (see, e.g., Ref. 45 or 46, Subsec. 3.3) that $\rho(f_t)$ is a continuous nondecreasing function of t , and, in consequence, if $f(0) < f(1)$, then $\rho(f_{f(0)}) \leq \rho(f_{f(1)})$. Unfortunately, we cannot expect that in case $f(0) < f(1)$, all points in I have a well-defined rotation number. However, the following important result concerning the set of the rotation numbers of all points for which the rotation number exists holds (see Ref. 42, Sec. 2).

Theorem 2.4. Assume that f is a Lorenz-like map such that $f(0) > f(1)$. Then, the set of the rotation numbers for f of all points having rotation number is equal to the interval $\text{Rot}(f) := [\rho(f_{f(0)}), \rho(f_{f(1)})]$. In particular, for each $r \in \text{Rot}(f)$, regardless of whether r is rational or irrational, there exists $x \in I$ such that $\rho(x) = r$.

The set $\text{Rot}(f)$ will be called the *rotation interval* of f . Finally, due to the lack of the suitable reference, we present below a sufficient condition for the existence of period 2 periodic orbit of a Lorenz-like map, which also implies that the rotation interval $\text{Rot}(f)$ contains $1/2$. The proof of this result with the remark is postponed to Appendix B.

Theorem 2.5. Let $f: [0, 1] \rightarrow [0, 1]$ be Lorenz-like map with the discontinuity point $c \in (0, 1)$. Suppose that

$$f(0) < c < f(1). \quad (7)$$

Then, f has a period 2 periodic orbit. Moreover, if f is expanding, then this orbit is unstable (repelling) and is unique period 2 periodic orbit of f .

III. TWO VERSIONS OF ONE-DIMENSIONAL COURBAGE-NEKORKIN-VDOVIN MODEL

Assuming the variable $y = \alpha$ is constant, the CNV model can be reduced to a one-dimensional map $g: \mathbb{R} \rightarrow \mathbb{R}$ given by

$$g(x) = x + F(x) - \alpha - \beta H(x - d). \quad (8)$$

In general, in the above function, we will vary the parameters β and/or α keeping all other parameters fixed. We consider two main versions of the 1D CNV model:

- A *piecewise linear* case (plCNV for short), when $F(x)$ is a piecewise linear continuous function defined as follows:

$$F(x) = \begin{cases} -m_0x, & \text{if } x \leq J_{\min}, \\ m_1(x - a), & \text{if } J_{\min} \leq x \leq J_{\max}, \\ -m_0(x - 1), & \text{if } x \geq J_{\max}, \end{cases}$$

where

$$m_0, m_1 > 0, \quad 1 > a > 0, \quad J_{\min} = \frac{am_1}{m_0 + m_1},$$

$$J_{\max} = \frac{m_0 + am_1}{m_0 + m_1},$$

- a *nonlinear* case (nlCNV for short), when $F(x) = \mu x(x - a)(1 - x)$ with $0 < a < 1$ and $\mu > 0$.

Observe that in both cases, the function g is discontinuous at d and the plot of F has the shape of the upside down reversed N letter. However, the nonlinear map is formally simpler (has less parameters) and, at the same time, exhibits similar complex dynamics. Before we study in detail the nonlinear CNV model, we briefly recall our previous results on the plCNV model from Ref. 31.

A. 1D plCNV model

We studied piecewise linear case (1D plCNV) in detail in our recent work.³¹ In particular, we analyzed existence, location, and stability of fixed points giving explicit conditions with respect to all model parameters. After restricting the model to the invariant interval (the dynamics beyond thus interval is trivial), we established the conditions for Devaney chaos and described metric properties of this model (i.e., existence and form of the absolutely continuous invariant probability measure). Moreover, the itineraries of periodic orbits were linked with patterns of spike trains fired by the 1D plCNV. Some of these results were possible due to the fact that the map defining the 1D plCNV model is a β -transformation, not a general Lorenz-like map. Here, our goal is to check if and how these results transfer to the nlCNV model and identify differences between the piecewise linear and nonlinear case.

B. 1D nICNV model

In Ref. 30, the nonlinear part of the CNV model is determined by the cubic polynomial $F(x) = x(x-a)(1-x)$, whose plot has the shape of the upside down reversed *N* letter and which has three zeroes $0 < a < 1$. Unfortunately, this assumption seems to be too much restrictive. It occurs that in the piecewise linear case the parameter m_1 related to the derivative (slope) of the function F plays a crucial role in creating interesting dynamics. To obtain similar control on the slope of F , we have decided to introduce a new parameter $\mu > 0$ and define $F(x)$ as $\mu x(x-a)(1-x)$. It is worth pointing out that such a parameter appears often in some versions of the FitzHugh–Nagumo model, which was one of the main motivations for the 2D CNV model. So, finally, in our paper, the nICNV function $g: \mathbb{R} \rightarrow \mathbb{R}$ is defined as

$$g(x) = x + \mu x(x-a)(1-x) - H_{\alpha,\beta}^d(x), \quad (9)$$

where

$$H_{\alpha,\beta}^d(x) = \begin{cases} \alpha, & \text{if } x < d, \\ \alpha + \beta, & \text{if } x \geq d. \end{cases}$$

Following Ref. 30, we will also assume that $\beta > 0$ and the discontinuity point d lies between the extrema of the function F . Detailed results on the 1D nICNV model are presented in the rest of the paper.

IV. ANALYSIS OF INVARIANT INTERVALS FOR 1D nICNV MODEL

This section is devoted to the study of the basic dynamical properties of the 1D nICNV model, i.e., the function

$$\begin{aligned} g(x) &= x + \mu x(x-a)(1-x) - H_{\alpha,\beta}^d(x) \\ &= x + F(x) - H_{\alpha,\beta}^d(x) = f(x) - H_{\alpha,\beta}^d(x). \end{aligned}$$

Namely, we will examine the existence of the invariant interval, on which the 1D nICNV function is an expanding Lorenz map (see Fig. 1). The ends of this interval are given, similar to the piecewise linear case, by the formulas

$$\begin{aligned} b &= \lim_{x \rightarrow d^+} g(x) = g(d) = d + F(d) - \alpha - \beta, \\ c &= \lim_{x \rightarrow d^-} g(x) = d + F(d) - \alpha. \end{aligned}$$

Let x_{\min} and x_{\max} denote the points of local minimum and maximum of the cubic polynomial F . An immediate calculation gives

$$x_{\min} = \frac{a+1-\sqrt{a^2-a+1}}{3} \quad \text{and} \quad x_{\max} = \frac{a+1+\sqrt{a^2-a+1}}{3}.$$

We will work here with the three general assumptions

- $0 < a < 1$,
- $\mu > 0$,
- $x_{\min} < d < x_{\max}$,

which are quite natural and does not seem to be very restrictive. Now, let us assume that values of a , μ , and d are fixed and satisfy the above conditions. We will search for the values of α and β for which the restriction of g to the interval $[b, c]$ is an expanding Lorenz map. It is easy to observe that to guarantee this we need the following additional assumptions:

- $x_{\min} < b < d < c < x_{\max}$,
- $g(b) \geq b$ and $g(c) \leq c$.

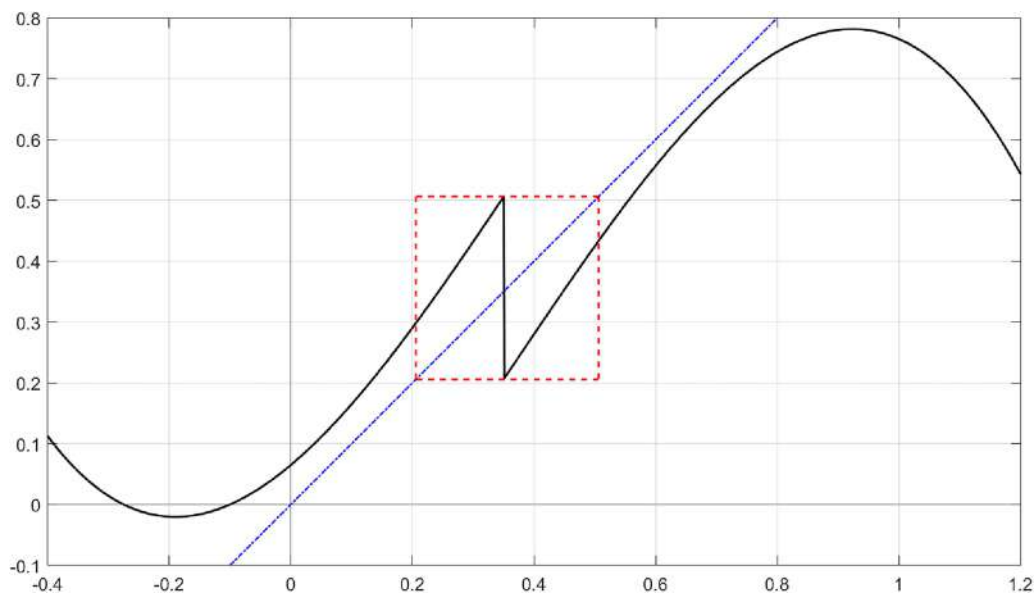


FIG. 1. Plot of the nICNV function (in black) and the invariant interval (denoted by a square of dashed lines). Parameter values: $\mu = 1.6$, $a = 0.1$, $d = 0.35$, $\alpha = -0.065$, $\beta = 0.3$.

TABLE I. Conditions for the existence of an invariant interval.

No.	Condition	Parametric form
1.	$x_{\min} < b$	$\beta < d + F(d) - x_{\min} - \alpha$
2.	$c < x_{\max}$	$\alpha > d + F(d) - x_{\max}$
3.	$b < d$	$\beta > F(d) - \alpha$
4.	$d < c$	$\alpha < F(d)$
5.	$g(b) \geq b$	$\alpha \leq F(d + F(d) - \alpha - \beta)$
6.	$g(c) \leq c$	$\beta \geq F(d + F(d) - \alpha) - \alpha$

Table I shows how the above conditions can be translated in the terms of parameters α and β . Since $[b, c] \subset (x_{\min}, x_{\max})$, we obtain immediately that $F'(x) > 0$ and, in consequence, $g'(x) > 1$ for $x \in [b, c]$, which is required in the definition of an expanding Lorenz map.

Let G denote g restricted to $[b, c]$. Let us summarize the first result concerning the 1D nLCNV model.

Theorem 4.1 (expanding Lorenz map). Assume that conditions 1–6 listed in Table I are satisfied. Then, the map $G: [b, c] \rightarrow [b, c]$ is a well-defined expanding Lorenz map.

Now, let us look for the answer to the following question. Assuming a , μ , and d are fixed, and we can always find the values of α and β for which the conditions 1–6 hold? Fortunately, the answer is positive under quite mild assumptions as we can see below. The technical proof of Theorem 4.2 is postponed to Appendix C.

Theorem 4.2 (existence of invariant interval). If $F'(d) < 1$, then the subset of the plane α – β for which the conditions 1–6 are true is nonempty (in fact, it has positive Lebesgue measure).

It remains to check when the condition $F'(d) < 1$ holds. As expected, we obtain some mild restriction on the parameter μ responsible for the slope of F .

Proposition 4.3 (conditions for invariant interval). For any arbitrary values of parameters $a \in (0, 1)$, $d \in (x_{\min}, x_{\max})$, and $\mu \in (0, 3]$, we have $F'(d) < 1$.

Proof. Since

$$F'(x) = \mu(-3x^2 + 2(a+1)x - a),$$

it is enough to show that for each $x \in (x_{\min}, x_{\max})$

$$w(x) = -3x^2 + 2(a+1)x - a < 1/\mu,$$

if $0 < a < 1$ and $0 < \mu \leq 3$. Note that $w(x)$ attains maximum at the point $x = (a+1)/3$ and the maximum value is $\frac{1}{3}(a^2 - a + 1)$. But, $a^2 - a + 1 < 1$ for $a \in (0, 1)$ and, in consequence, $w(x) < 1/3 \leq 1/\mu$, which is the desired conclusion. \square

The left panel of Fig. 2 provides an illustration of how the set of parameters from Theorem 4.2 may look like if the conditions 1–6 are satisfied. In fact, for the chosen parameter values (see the caption of Fig. 2), we have $F'(d) \approx 0.607 < 1$. Black lines on the left panel correspond to the borders of areas described by the conditions 1–6. The red area shows parameter values of α and β for which G is an expanding Lorenz map. Geometrically, this area is a subset of the parallelogram (conditions 1–4) between the two nonlinear curves (conditions 5–6). In turn, the right panel shows how the conditions for α and β can be translated into the conditions for b and c (end points of the invariant interval). We simply use the linear change of coordinates given by the formulas for b and c . In other words, the right panel presents the set of pairs (b, c) corresponding to invariant intervals for expanding Lorenz maps. Note that the red area is contained in the square $[x_{\min}, x_{\max}]^2$ between the plot of the function $x \mapsto f(d) - F(x)$ and its inverse function. Symmetry of the red area in the right panel is related to the choice of d as $(x_{\min} + x_{\max})/2$.

Remark 4.4. Even if $F'(d) \geq 1$, the set of α and β for which the conditions 1–6 hold may be nonempty as shows Fig. 3 [here $\mu = 4$ and $F'(d) \approx 1.21$]. Observe that compared to Fig. 2, the red

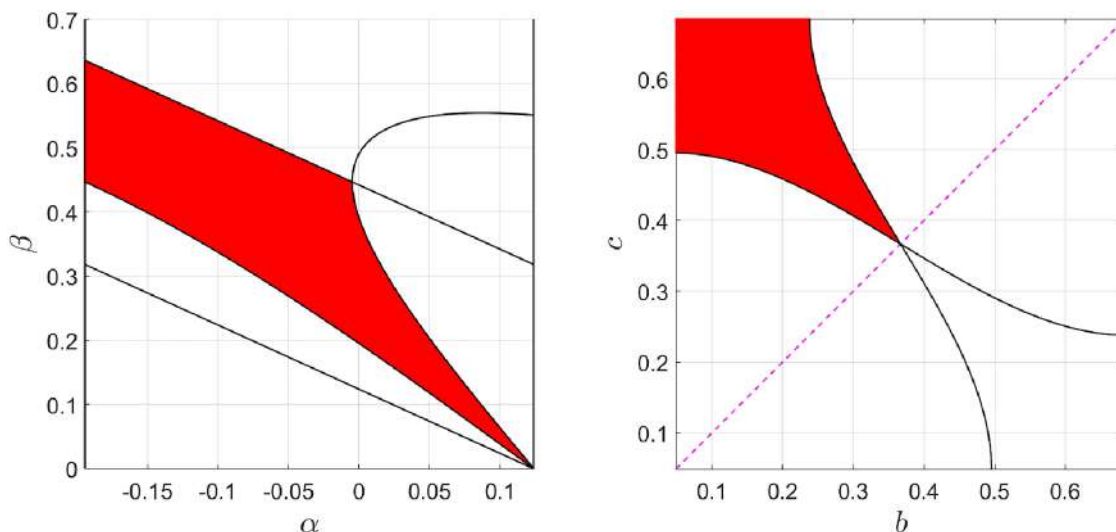


FIG. 2. Set of parameters α – β for which the conditions 1–6 hold and, in consequence, the invariant interval exists (left in red) and the respective set of possible end points (b the beginning and c the end) of invariant intervals (right in red) for parameter values: $\mu = 2$, $a = 0.1$, $d = 0.367$ (case $F'(d) < 1$ covered by Theorem 4.2).

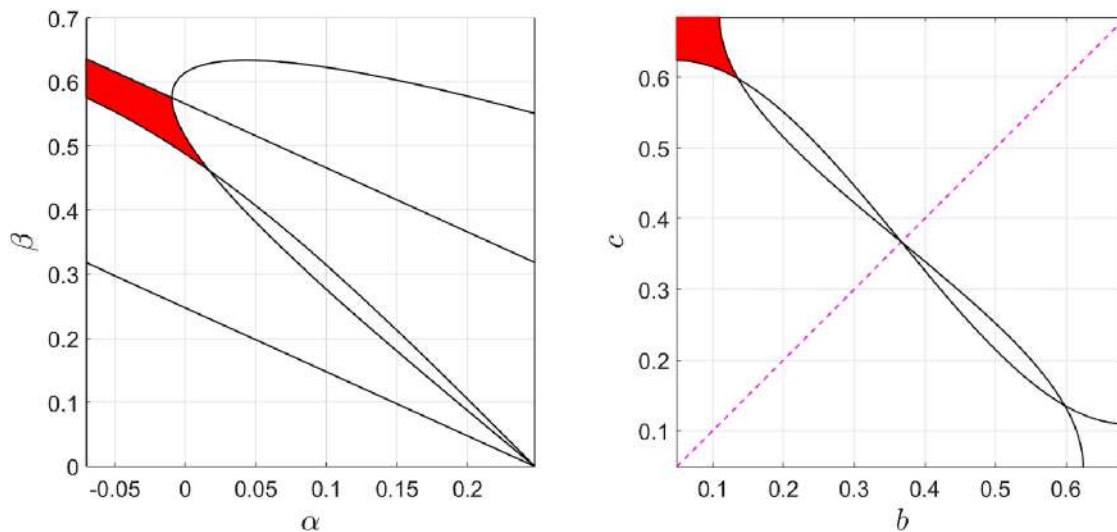


FIG. 3. Set of parameters α - β satisfying the conditions 1–6, i.e., guaranteeing the existence of the invariant interval (left in red) and the respective set of possible end points (b, c) of invariant intervals (right in red) for parameters values: $\mu = 4$, $a = 0.1$, $d = 0.367$ [case $F'(d) \geq 1$, which is not covered by Theorem 4.2].

area in Fig. 3 occupies a relatively much smaller part of the parallelogram given by the conditions 1–4. Moreover, in that case it is rather hard to formulate the nice condition for the existence of the invariant interval similar to that formulated in Theorem 4.2. However, if the parameter μ will be big enough, then the set of parameters α and β for which the conditions 1–6 are satisfied may be empty (this is the case when $\mu = 5$, $a = 0.1$, $d = 0.367$).

V. CHAOTIC BEHAVIOR IN THE 1D nICNV MODEL

This section, divided into three subsections, is devoted to examine main chaotic properties of the 1D nICNV model.

A. Conditions for chaos for a single model map

Below, we present a sufficient condition for chaotic dynamics in terms of the derivative of the model map. Let $\lambda = \inf \{G'(x) \mid x \in [b, c]\}$.

Theorem 5.1. *If one of the following conditions is satisfied:*

- $\sqrt{2} \leq \lambda \leq 2$,
- $\sqrt[3]{2} \leq \lambda < \sqrt{2}$ and $G(b) - b \geq \frac{\beta}{1+\lambda}$,
- $\sqrt[3]{2} \leq \lambda < \sqrt{2}$ and $c - G(c) \geq \frac{\beta}{1+\lambda}$,

then G is chaotic in the sense of Devaney on the interval $[b, c]$. It is also strongly transitive and mixing.

Proof. It is a consequence of Theorem A.8 after scaling the interval $[0, 1]$ to $[b, c]$, i.e., by the factor β . \square

Finally, note that expanding Lorenz map G is also expansive without any assumptions (see Appendix A). Conditions of Theorem 5.1 might be hard to verify analytically. However, Lemma 5.2 yields a bit more explicit expression for λ .

Lemma 5.2. *To determine whether the 1D nICNV model is chaotic, it suffices to estimate the value of G' at the end points of the invariant interval $[b, c]$:*

- Suppose that $b \geq \frac{1+a}{3}$. Then, $\lambda = G'(c)$.
- Suppose that $c \leq \frac{1+a}{3}$. Then, $\lambda = G'(b)$.
- If $b < \frac{1+a}{3} < c$, then $\lambda = \min\{G'(b), G'(c)\}$.

In particular, it always holds that $\lambda = \min\{G'(b), G'(c)\}$.

Proof. Differentiating G twice yields $G''(x) = 2\mu(1+a-3x)$ from which it follows that $G'(x)$ is increasing for $x < \frac{1+a}{3}$ and decreasing for $x > \frac{1+a}{3}$. \square

B. Conditions for the existence of chaos in the α - β parameter plane

In this subsection, we provide sufficient conditions for nonemptiness of the set of parameters that guarantee Devaney's chaos on the whole invariant interval. Let us begin with a brief analysis of the quadratic equation $G'(x) = \sqrt{2}$, i.e.,

$$-3\mu x^2 + 2\mu(a+1)x + 1 - \mu a = \sqrt{2}.$$

Note that this equation has two distinct real roots (denote them by $x_1 < x_2$) if and only if $\Delta = 4\mu(\mu a^2 - \mu a + \mu - 3\sqrt{2} + 3) > 0$ or, equivalently, $\mu > 3(\sqrt{2} - 1)/(a^2 - a + 1)$. An immediate computation shows that

$$x_{1,2} = \frac{\mu(a+1) \mp \sqrt{\mu(\mu a^2 - \mu a + \mu - 3\sqrt{2} + 3)}}{3\mu}.$$

Now, let A denote the set of parameters α - β for which G is an expanding Lorenz map on the invariant interval $[b, c]$. Let us formulate in the sufficient condition the existence of chaos parameters in the α - β plane.

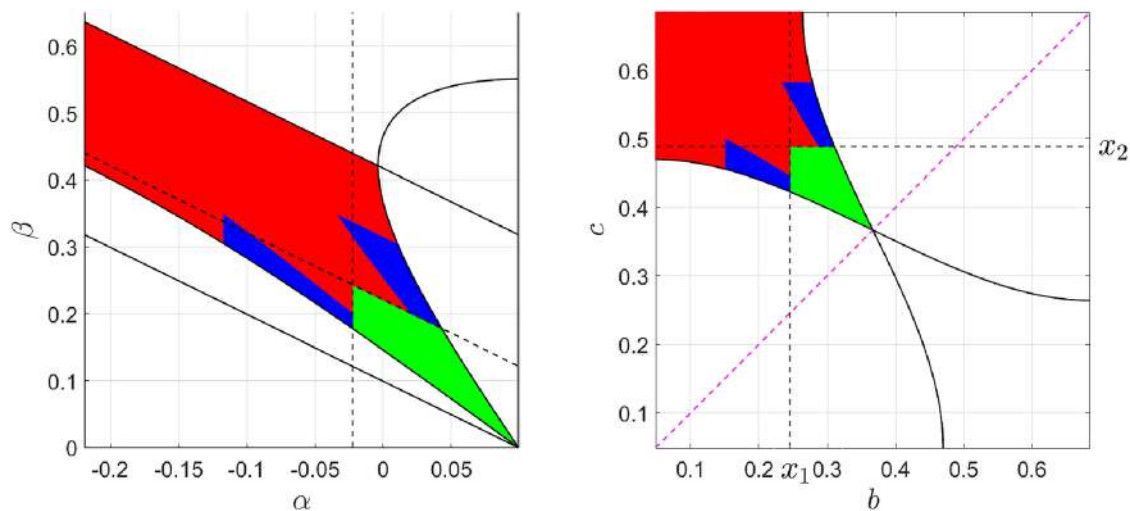


FIG. 4. Set of parameters α - β for which the conditions (from Theorem 5.1) sufficient for chaos existence hold. On the left panel in green area corresponding to Theorem 5.1 (i) and in blue area corresponding to Theorem 5.1 (ii) and (iii). On the right panel the respective sets of possible end points of “chaotic” invariant intervals (in green and blue). Other parameter values: $\mu = 1.6$, $a = 0.1$, $d = 0.367$.

Theorem 5.3. Assume that $a \in (0, 1)$, $d \in (x_{\min}, x_{\max})$ and $\mu \in (0, 3]$, which implies that A is nonempty (has positive Lebesgue measure). If, in addition,

$$\mu > \frac{3(\sqrt{2} - 1)}{a^2 - a + 1} \quad \text{and} \quad x_1 < d < x_2, \quad (10)$$

then the subset $C \subset A$ consisting of parameters α - β , for which G is chaotic on the interval $[b, c]$, is also nonempty (contains a set of positive Lebesgue measure).

The proof of Theorem 5.3 is postponed to Appendix D.

It may be interesting to compare both size and location of areas in the α - β parameter plane related to different chaos conditions from Theorem 5.1. Figure 4 presents the result of our numerical simulations: in green, we see the area corresponding to the simpler condition $\sqrt{2} \leq \lambda \leq 2$ and in blue, the area corresponding to the more complex condition $\sqrt[3]{2} \leq \lambda < \sqrt{2}$ and $(G(b) - b \geq \frac{\beta}{1+\lambda})$ or $c - G(c) \geq \frac{\beta}{1+\lambda}$.

Remark 5.4. Note that the “chaos existence condition” (10) from Theorem 5.3 can be formulated for all $a \in (0, 1)$ simultaneously (full parameter range). Since $a^2 - a + 1 \geq 3/4$, we obtain the estimation

$$\mu > 4(\sqrt{2} - 1) \approx 1.6569.$$

Alternatively, it can be calculated for the fixed value of a , which gives, in general, sharper estimations. For example, if $a = 0.1$, we obtain the condition

$$\mu > \frac{3(\sqrt{2} - 1)}{0.91} \approx 1.3655.$$

In fact, the inequality (10) provides nice functional dependence between μ and a . Namely, let $\mu_0(a) = 3(\sqrt{2} - 1)/(a^2 - a + 1)$, i.e.,

$\mu_0(a)$ is the threshold above which the values of μ (up to 3) guarantee for a given a , according to Theorem 5.3, the existence of nonempty chaos area. Then, the μ_0 as a function of a is symmetric unimodal with maximum at $a = 0.5$.

C. Ergodicity and ACIP

The hierarchy of chaos often starts from *ergodicity*, which alone is of course barely considered as real chaos. For that reason, it is worth emphasizing that the nICNV map restricted to the invariant interval is always *ergodic*, which is a natural prerequisite for chaos.

Recall first few notions of the ergodic theory. Let $f: [b, c] \rightarrow [b, c]$ be an expanding Lorenz map and λ be a measure on the interval $[b, c]$. We say that

- f preserves measure λ or that λ is f -invariant if $\lambda(f^{-1}(B)) = \lambda(B)$ for all measurable sets B ,
- a measure-preserving f is *ergodic* if for any measurable B , such that $f^{-1}(B) = B$, $\lambda(B) = 0$ or $\lambda([b, c] \setminus B) = 0$.

Since ergodicity is a property of the pair (f, λ) , we often say that f has an ergodic measure λ .

We use the standard abbreviation ACIP for an f -invariant probability measure that is absolutely continuous with respect to the Lebesgue measure of $[b, c]$. Given a measure λ , the *support* of λ [denoted by $\text{supp}(\lambda)$] is the smallest closed set of full λ -measure. Note that the following result does not require any extra assumptions apart from the existence of invariant interval.

Theorem 5.5. Under the conditions 1–6 from Table I, the map $G: [b, c] \rightarrow [b, c]$ has a unique ergodic ACIP measure, and the support of this measure is a finite union of closed intervals.

Proof. Recall that any piecewise C^1 -function f is of bounded variation and if, in addition, f is separated from 0, i.e., $|f| \geq \sigma > 0$ for some $\sigma > 0$, then the reciprocal $1/f$ is also of bounded variation.

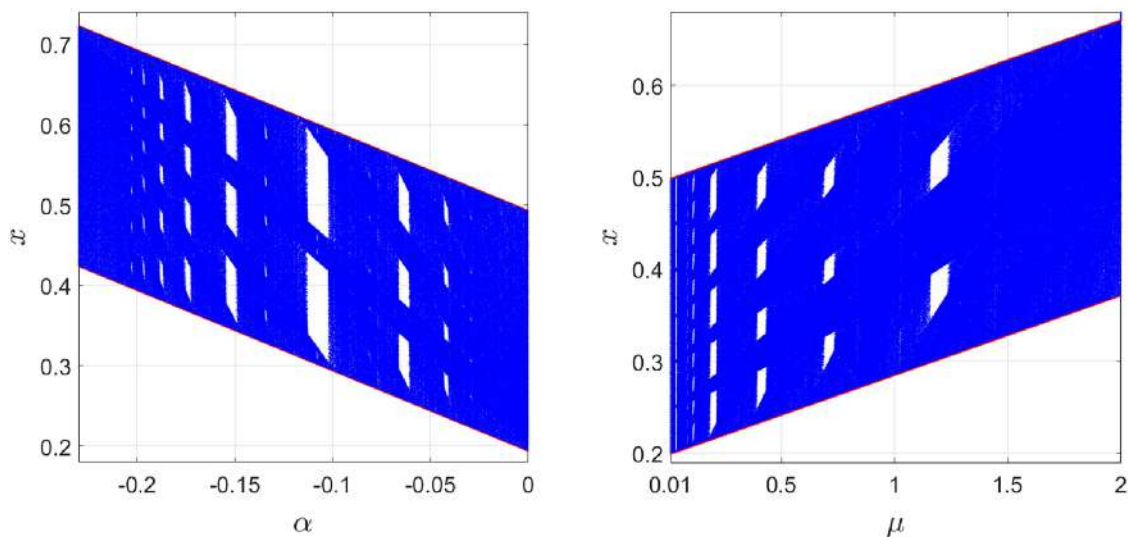


FIG. 5. Bifurcation diagrams for the family of nICNV maps with respect to α (left) and μ (right). Other parameter values: $a = 0.1$, $d = 0.45$, $\beta = 0.3$, $\mu = 0.5$ (left) and $\alpha = -0.048$ (right).

Since the map G is piecewise C^2 and $|G'| \geq \sigma > 1$, it satisfies the assumptions of Theorems 5.2.1, 8.2.1, and 8.2.2 in Ref. 47. Now, our assertion follows immediately from these three results. \square

Remark 5.6. Observe that any ergodic measure-preserving maps on the interval (more generally, on compact metric space) is topologically transitive on $\text{supp}(\lambda)$ (see, for instance, Exercise 6.15 in Ref. 48). Hence, if $\text{supp}(\lambda)$ is the whole domain $[b, c]$, then the map is transitive on $[b, c]$ and, in consequence, is chaotic in the sense of Devaney on $[b, c]$ from Theorem A.8.

Numerically, the fact that the support of the acip measure consists of a finite union of closed intervals can be clearly observed on the bifurcations diagrams for the nICNV family of maps (see Fig. 5).

Namely, notice the appearance and the location of “white gaps” in the bifurcation diagram, which corresponds to the situation when the support of acip is not the whole interval $[b, c]$ but the union of a finite number of smaller disjoint intervals. Observe that “white gaps” only appear for relatively small values of μ and, in consequence, values of $\lambda = \inf \{G'(x) \mid x \in [b, c]\}$ just above 1.

Moreover, the numerical analysis (see Fig. 6) shows that the probability density function of acip in our model is far from being uniform. However, the analysis also suggests that the probability distribution is more regular (flattened) for higher values of $\lambda = \inf \{G'(x) \mid x \in [b, c]\}$. In Fig. 6, these values are, respectively: $\lambda = 1.17$ (left), $\lambda = 1.29$ (middle), $\lambda = 1.41$ (right).

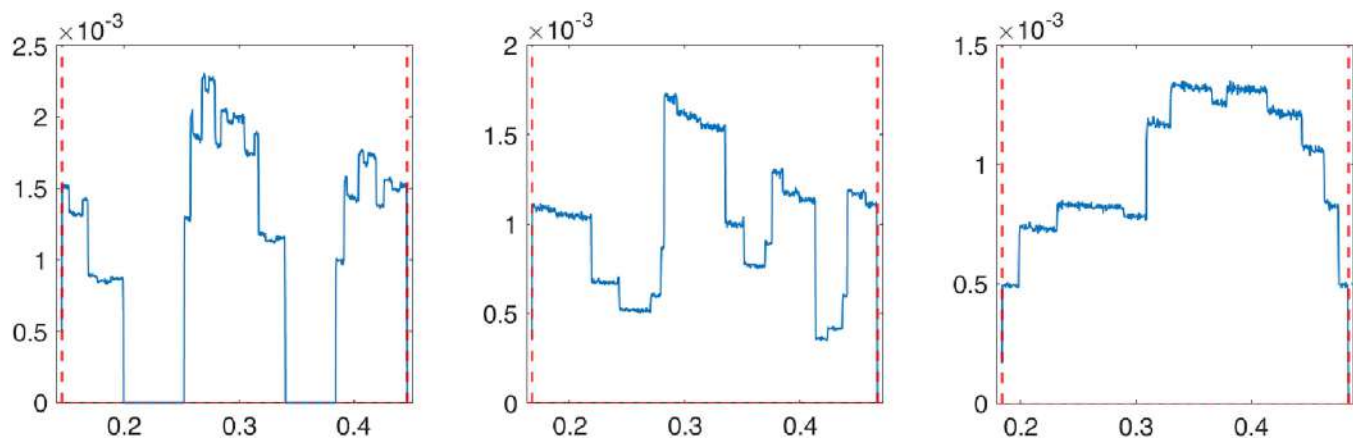


FIG. 6. Distributions of probability density functions, i.e., frequencies of visits to different parts of the invariant interval for three values of the parameter μ : $\mu = 1.1$ (left), $\mu = 1.6$ (middle), $\mu = 2$ (right). Other common parameter values: $a = 0.1$, $d = 0.3$, $\alpha = -0.1$, $\beta = 0.3$.

VI. PERIODICITY AND ROTATION INTERVAL FOR THE 1D nICNV MODEL

In this section, we discuss topics related to periodicity and rotation interval for the model map. Here, unless stated otherwise, we assume that the conditions 1–6 are satisfied, i.e., the map defining the voltage dynamics in the 1D nICNV model is an expanding Lorenz map.

A. Fixed points of the 1D nICNV map

The following observation can be easily justified by the fact that the map $G : [b, c] \rightarrow [b, c]$ is expanding:

- the only possible fixed points of G are b and c ; in particular, if $G(b) = b$ (or $G(c) = c$), then the rotation interval of G $\text{Rot}(G)$ contains 0 (respectively, 1),
- if $G(b) > b$ and $G(c) > c$, then G does not have fixed points.

B. Period-2-periodicity condition for a single model map

Below, we provide a geometric condition for the existence of period two periodic orbit in this system, which is an immediate consequence of Theorem 2.5.

Lemma 6.1. *Let $G : [b, c] \rightarrow [b, c]$ be the expanding Lorenz map describing the 1D nICNV model. Suppose that*

$$G(b) < d < G(c). \quad (11)$$

Then, G has exactly one period-2 periodic orbit and consequently $\frac{1}{2} \in \text{Rot}(G)$. This orbit is repelling.

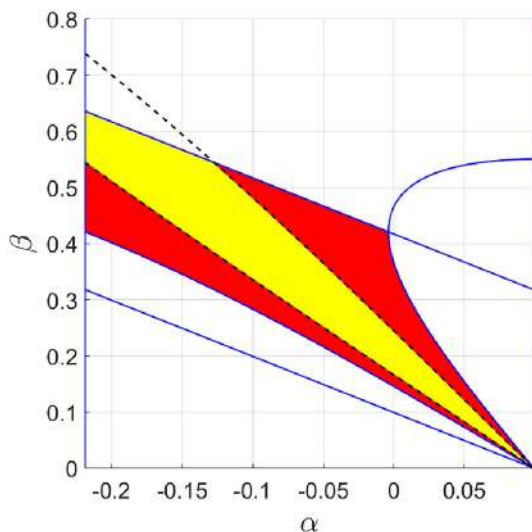


TABLE II. Conditions for the existence of a 2-periodic orbit.

No.	Condition	Parametric form
10.	$g(b) < d$	$F(d + F(d) - \alpha - \beta) + F(d) - 2\alpha - \beta < 0$
11.	$g(c) > d$	$F(d + F(d) - \alpha) + F(d) - 2\alpha - \beta > 0$

C. Conditions for the existence of a 2-periodic orbit in the α – β parameter plane

Let A denote the set of parameters α – β for which G is an expanding Lorenz map. Note that the following result does not require any new additional assumptions (compare Theorem 4.2). Its proof is postponed to [Appendix E](#).

Theorem 6.2. *Assume that $F'(d) < 1$, which implies that A is nonempty (has positive Lebesgue measure). Then, the subset $B \subset A$ consisting of parameters α – β for which G has a 2-periodic orbit is also nonempty (has positive Lebesgue measure).*

Remark 6.3. Numerical simulations in MATLAB show that for some choice of the parameter μ , the set B is a proper subset of A and for the other choice $B = A$. [Figure 7](#) presents both cases. On the left panel, the yellow area of parameters corresponding to the existence of a 2-periodic orbit lies strictly inside the red area corresponding to invariant interval parameters ($\mu = 1.6$, $a = 0.1$, $d = 0.367$). In the right panel, the yellow area covers the whole red area ($\mu = 3$, $a = 0.1$, $d = 0.367$), which means that if we have an invariant interval, we also have a 2-periodic orbit.

D. Analysis of rotation interval

Rotation numbers were defined by H. Poincaré for circle homeomorphisms and diffeomorphisms to characterize the set of periods

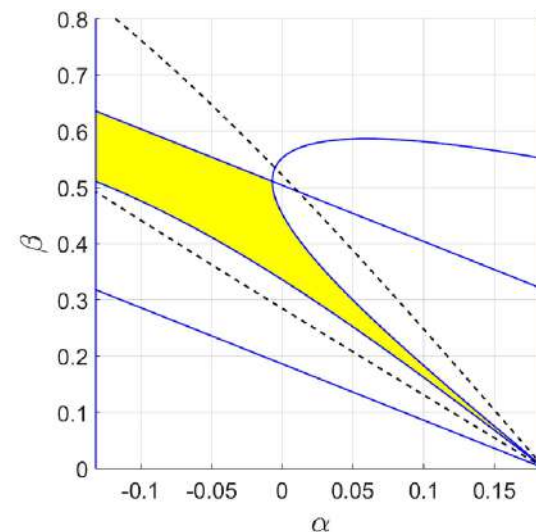


FIG. 7. Regions of parameters giving a 2-periodic orbit (in yellow) inside the areas corresponding to invariant interval (in red). On the right panel, the yellow region fully covers the red area. Main parameter: $\mu = 1.6$ (left) and $\mu = 3$ (right). Other common parameter values: $a = 0.1$, $d = 0.367$.

of these maps. These real numbers between 0 and 1 naturally generalize the usual geometric rotation angle (modulo 2π) for circle translations. Interestingly, they occurred to be quite useful in the number of applications, especially in complex dynamics. In 1983, Newhouse *et al.* (see Ref. 49) extended the notion of rotation number to continuous circle maps of degree one. Instead of a single number they got, in general, a closed interval, which they called *rotation set* or *rotation interval*. The original rotation number for homeomorphisms does not depend on the choice of the point on the circle. However, for a continuous circle map (not homeomorphism), we may obtain different rotation numbers starting from different points. Now, the collection of rotation numbers computed for all points on the circle forms the rotation interval. Finally, and maybe a bit surprisingly, the rotation theory works fine also for discontinuous circle maps⁴⁶ and Lorenz-like maps.⁴²

The notions of rotation number and rotation interval have found various applications. In particular, they appear in situations where circle maps arise naturally and are connected with phenomenon of *phase locking*. Among others, they are used in modeling of electronic oscillators, cardiac rhythms, heart arrhythmias, and other biological clocks.^{50,51} In the context of neuroscience, the rotation theory is a tool to qualify and explain firing rates and neural oscillations, both at the level of large neuronal circuits (see, e.g., Ref. 52) as well as at the level of a single cell (see, e.g., Refs. 8 and 53–55).

In our setting, roughly speaking, the meaning of the rotation interval is as follows. If a number p/q (p, q coprime) is in the rotation interval of a Lorenz-like map defined on $[0, 1]$, then this map has a periodic orbit of period q such that exactly p points of the periodic orbit are contained in the right subinterval $[c, 1]$ of the domain, where c is a discontinuity point. The precise formulation of this observation is given by Proposition F.8.

As we see, the rotation interval provides important information on the periodic behavior of a map. In a nutshell, the larger rotation interval the bigger periodic diversity. Since to all rational fractions p/q (p, q coprime) correspond some q -periodic orbits, we see that in general bigger rotation intervals admit abundance of shorter periods, but, of course, do not exclude long ones. Conversely, smaller rotation intervals yield rather mainly longer periods. Actually, the mechanism of producing periodic orbits with different periods is much more complicated and will be described in detail in Sec. VII.

It is well known (see, e.g., Ref. 46) that

- the rotation number and, in consequence, the end points of the rotation interval *depend continuously* on the map in the norm of uniform convergence,
- the rotation number is *monotonic*, i.e., $f \geq g$ implies $\rho(f) \geq \rho(g)$,
- the plot of the rotation number often contains of a version of a *devil's staircase*,

but instead of providing rigorous results of that type concerning the 1D nCNV map we present the numerical analysis of rotation interval for the model with respect to different parameters. This analysis shows that all three phenomena mentioned above occur numerically in our simulations.

In this subsection, the graphs of the rotation intervals for the 1D nCNV map are plotted as functions of three main parameters of our model: α , β and μ . Since the functional dependence in each of these three case follows different pattern, we present here three separate plots. On all figures we can observe two main effects: when one of the parameters varies the rotation interval moves up or down and it shrinks or expands. Moreover, these two processes usually occur simultaneously. Note that usually the length of the rotation interval is not monotonic as a function of a parameter. However, we

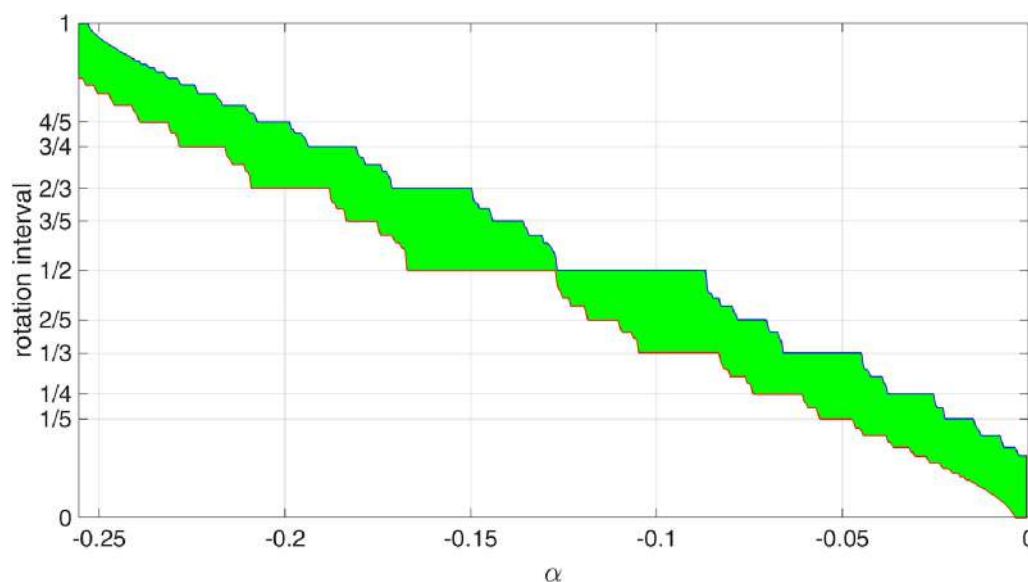


FIG. 8. Dependence of rotation interval (in green) on the parameter α for the nCNV map family. Other parameter values: $a = 0.1$, $d = 0.37$, $\beta = 0.455$, $\mu = 1.6$.

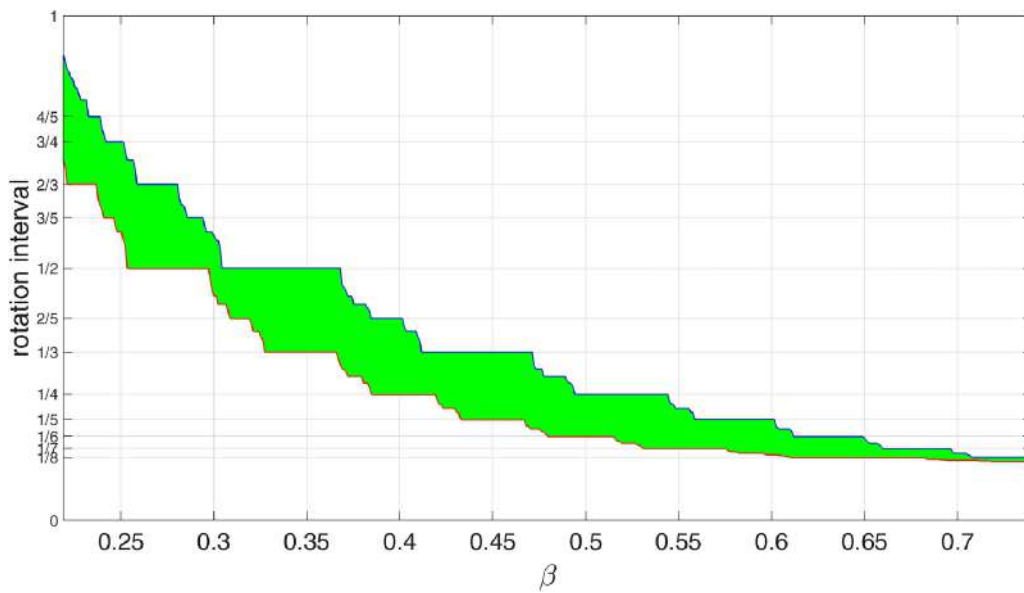


FIG. 9. Dependence of rotation interval (in green) on the parameter β for the nICNV map family. Other parameter values: $a = 0.1$, $d = 0.37$, $\alpha = -0.05$, $\mu = 1.6$.

can sometimes observe some general tendencies like shrinking and expanding of the interval.

Figure 8 shows the dependence of the rotation interval on α , which is the parameter corresponding to the second variable in the 2D CNV model. The distinguishing feature is its symmetry. In the center of symmetry, the interval seems to degenerate to a single

point. In turn, in Fig. 9, we see dependence on β (the length of invariant interval). In general, as a trend, the larger β the smaller rotation interval. However, shrinking is not monotonic, but rather oscillatory.

Finally, Fig. 10 presents dependence on μ , which controls the size of nonlinearity in our model. Here, we can observe quite rapid

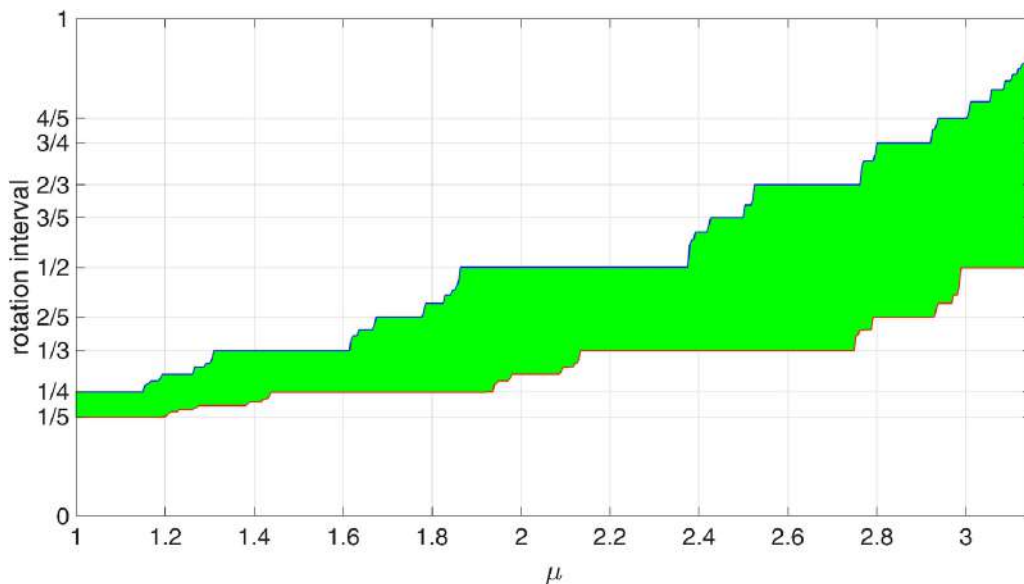


FIG. 10. Dependence of rotation interval (in green) on the parameter μ for the nICNV map family. Other parameter values: $a = 0.1$, $d = 0.37$, $\alpha = -0.065$, $\beta = 0.455$.

(but once more not entirely monotonic) expanding of the rotation interval. It is worth emphasizing that the range of rotation interval plays crucial role in the considerations of Sec. VII.

VII. ORBIT ITINERARIES AND COMPLEXITY OF SPIKE-TRAINS

This section consisting of two subsections develops and continues the analysis of periodic behavior of the model. In order to address the question of the structure of periodic orbits in the CNV model, we will rely on the notions of FUPOs and FL-permutations. This allows to derive a large subset of periodic orbit itineraries which then can be linked with patterns of spike trains fired by a neuron.

Theory of periodic orbits and their finite concatenations (FUPOs) is presented in Appendix F, relying on the results from Ref. 42 (most of them are also summarized in Ref. 31). An example of a FUPO in the 1D nCNV model is shown in Fig. 11.

A. Complexity of spiking patterns

In our previous work,³¹ we have identified the itineraries of periodic orbits with spike patterns fired by the 1D CNV model. In particular, basing on Corollaries 3–5, therein we can formulate the following useful observation for the 1D nCNV model.

Proposition 7.1. Assume that the conditions 1–6 listed in Table I hold. If $p/q \in \text{Rot}(G)$ (p and q coprime), where G defines the 1D nCNV model, then there is a q -periodic voltage-train (with $q - p$ time instances at which the membrane voltage increases and

p time instances of the decrease in the voltage). Moreover, there are at most $\binom{q}{p}/q$ such periodic spike trains, each of different itineraries. Among them, there exists a unique q -periodic spiking pattern with the itinerary of the form $(\tilde{x}_1, \tilde{x}_2, \dots, \tilde{x}_q)$ (where $\tilde{x}_i \in \{L, R\}$) such that $\tilde{x}_i = L$ if and only if $1 + (i - 1)p \bmod q \leq q - p$ (with L -symbols corresponding to the increase in the neuron's membrane potential and R with the decrease). If the occurrence of the word LR is interpreted as a spike, then this spike train features n spikes in each q -cycle, where

$$n := \# \{1 < j < q \mid 1 + (j - 1)p \bmod q \leq q - p \text{ and } 1 + jp \bmod q > q - p\}$$

(with the convention that $q \bmod q = q$).

Moreover, from Theorem F.10, we immediately obtain the following fact.

Proposition 7.2. Assume that the conditions 1–6 listed in Table I hold. If $[a/p, b/q] \subset \text{Rot}(G)$, where $a/p < b/q$ are Farey neighbors and $p < q$, then there exist twist periodic orbits P and Q , with rotation numbers a/p and b/q , respectively, and each itinerary, which is a concatenation of finitely many periodic itineraries of P and Q , corresponds to the exactly one periodic spike train fired by the 1D nCNV model.

Figure 12 presents three types of periodic spiking behavior (lower panel) of the 1D nCNV model together with related orbits of the Lorenz map G (upper panel). In particular, we see twist periodic orbits corresponding to Farey neighbors $2/3$ and $3/4$ (left and center, respectively) and the FUPO of $2/3 < 3/4$ type, obtained as a concatenation of one copy of the $2/3$ -twist periodic orbit and two copies of the $3/4$ -twist periodic orbit, as described by Proposition 7.1. The periodic orbit obtained in this way has rotation number equal to $8/11$ and itinerary $LRRLRRRLRR$.

Note that Propositions 7.1 and 7.2 do not cover the whole complexity of attainable spike patterns since there might be other periodic orbits which are not necessarily a concatenation of periodic itineraries of this form as well as many nonperiodic orbits. These propositions also do not imply how a “typical” spike pattern observed looks like since the periodic orbits cannot be stable as the map g is expanding under conditions 1–6. Therefore, a firing pattern highly depends on the initial condition and one can mostly expect “irregular” spiking trains, as the one depicted in Fig. 13, which was obtained for the same parameter values as Fig. 12 presenting periodic-like behavior. The fact that a randomly chosen orbit looks chaotic and that it is practically impossible to find numerically purely periodic orbits is also confirmed by the results of the so-called 0–1 chaos test (see Ref. 56) carried by us, which returned values very close to 1 (see Fig. 14).

Observe that the periodic orbit with given itinerary is always unique (and unstable), as the map G is expanding and, therefore, finding numerically such a periodic is very challenging. Thus, the method of FUPOs, as described by Propositions 7.1 and 7.2, enables to deduce the existence of infinitely many periodic spiking patterns of the 1D CNV model, which, due to the above mentioned reasons, would be rather impossible to find numerically and often, especially in case of long periods, also analytically. On the other hand, the knowledge on the existence of such periodic patterns implies that we can expect transient spiking behaviors which look like periodic ones (corresponding to initial conditions close to periodic orbits

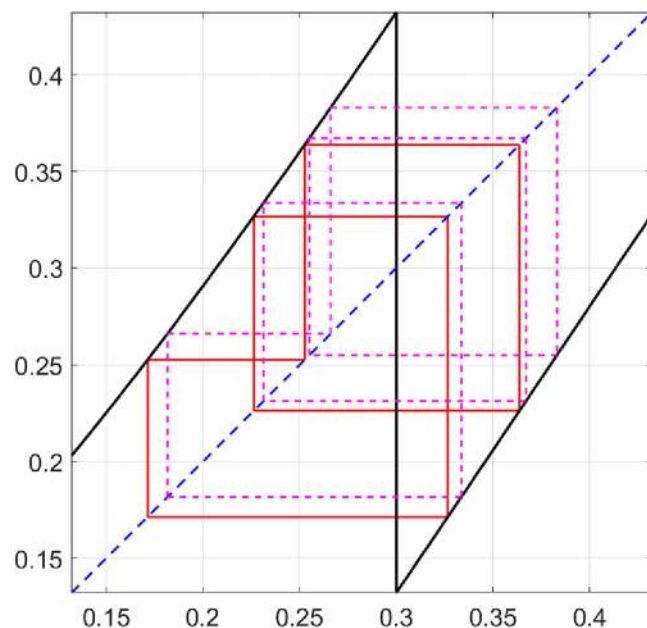


FIG. 11. FUPO (two periodic orbits of periods 5 and 7) of FL type corresponding to rotation numbers being Farey neighbors: $2/5 < 3/7$. This FUPO appears in the nCNV model with parameter values: $\mu = 1.6$, $a = 0.1$, $d = 0.35$, $\beta = 0.3$, $\alpha = -0.065$.

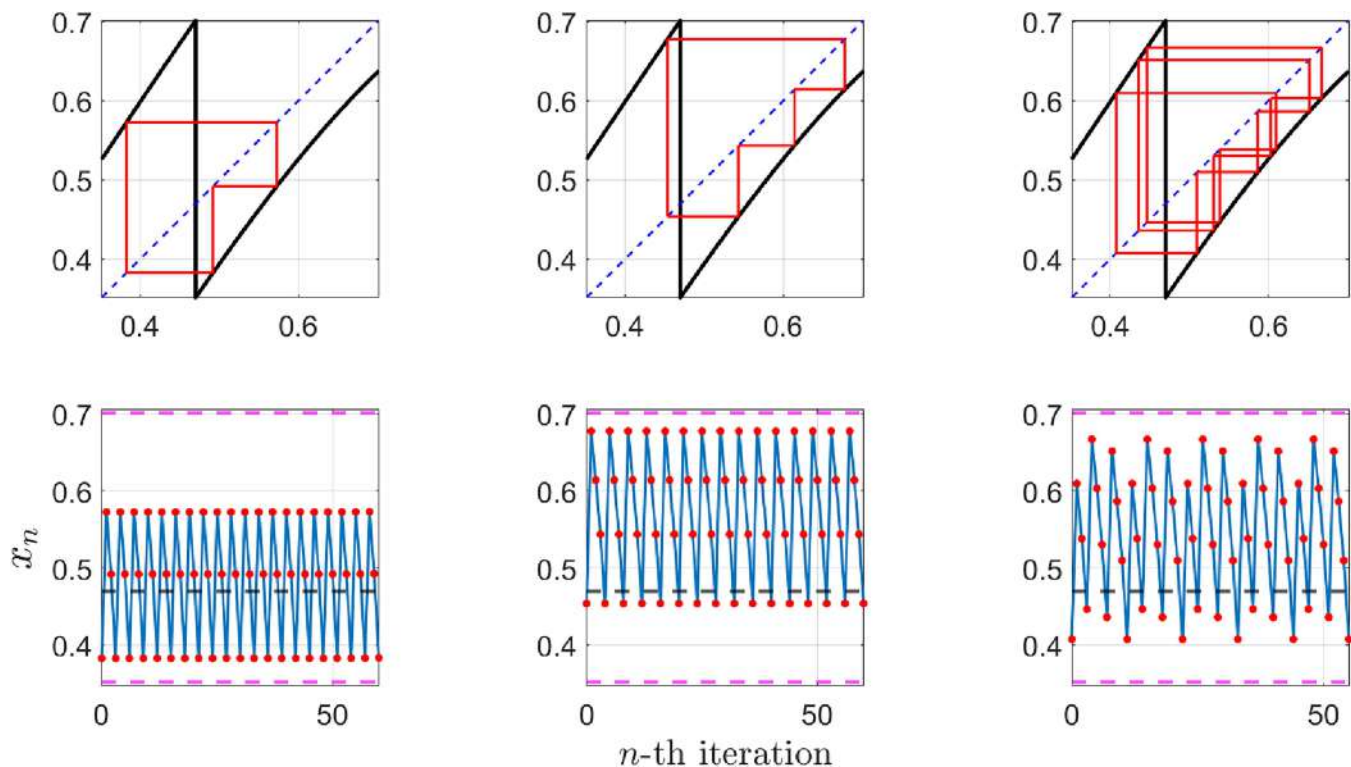


FIG. 12. The FUPU effect in the nCNV system: creation of a periodic orbit of period $11 = 3 + 4 + 4$ (right panel) from two periodic orbits of periods 3 and 4 (left and middle panels). The respective rotation numbers are Farey neighbors: $2/3 < 3/4$. Parameter values: $a = 0.1$, $d = 0.47$, $\alpha = -0.082$, $\beta = 0.35$, $\mu = 1.62$.

with given itineraries). Of course, numerically every such a “periodic orbit” will eventually “desynchronize” and the asymptotic behavior observed will be irregular, but long transient periodic spiking patterns can be observed (as depicted in Fig. 12).

B. Examples and simulations

In the last subsection, we present results of numerical simulations related to the existence of periodic orbits with the specific periods in the 1D nCNV model. They are conducted using MATLAB

scripts, implementing FUPU- and rotation theory of Lorenz-like maps and available in open repositories.^{57,58} For convenience, we denote here itineraries of periodic orbits by 0–1 sequences, instead of L – R sequences (i.e., 0 and 1 replace, respectively, L and R in encoding periodic orbits). Moreover, let a^i denote the repetition of the symbol or string a for i times.

Tables III and IV depict the output of our MATLAB scripts for several parameters settings. We restrict ourselves to presenting only second and third order concatenations, because higher order concatenations become much longer. Let us describe briefly how

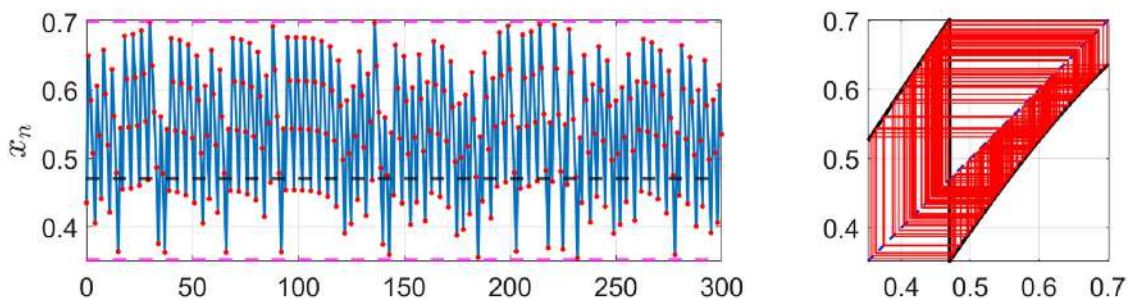


FIG. 13. Chaotic spiking typical for the 1D nCNV model: time series (left) and cobweb (right). Parameter values as in Fig. 12. Initial point: $x_0 = 0.435$.

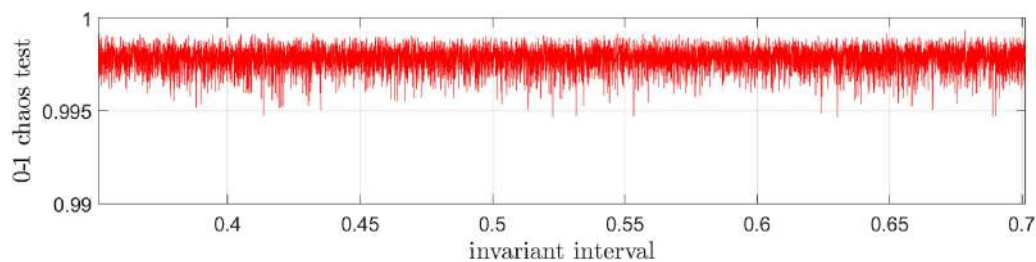


FIG. 14. Results of the 0–1 chaos test on the whole invariant interval $[b, c] = [0.35, 0.7]$ for 10^4 uniformly distributed initial points. The value of chaos test is very close to 1, which confirms chaotic behavior of a randomly selected point in $[b, c]$. Parameter values of the model as in Fig. 12.

our program works. First, we compute the rotation interval of a given 1D nCNV map. Then, we find inside the rotation interval the longest subinterval which end points are Farey neighbors. Note that the longest subinterval provides Farey neighbors with the smallest denominators and, in consequence, FUPO with the shortest periods of periodic orbits. Finally, we construct

- (1) finite periodic parts of the itineraries corresponding to these Farey neighbors according to the formula from Remark F.4) [denote these parts (blocks) by A and B],
- (2) all concatenations of A and B of a given order n , i.e., formed by taking n blocks (each of them is A or B) concatenating all of them (see Theorem F.10).

Recall that the main idea behind FUPO is that each Farey neighbors pair in the rotation interval guarantees the existence of infinitely many periodic orbits with itineraries being finite concatenations of itineraries corresponding to Farey neighbors. In other words, some distinguished pairs of periodic orbits (FUPOs) act as a machine producing infinitely many new periodic orbits with periods being the sum of multiples of the periods of the original pair. Moreover, each of such produced periodic orbits has unique itinerary determined by itineraries of FUPO.

A quick analysis of the tables shows that, as could be expected,

- shorter rotation intervals produce longer periods and vice versa,
- the length of periods (related to the length of rotation intervals) does not change monotonically as the parameter increases.

Finally, observe that finite concatenations of itineraries represent a quite regular (although usually nonperiodic) type of finite binary sequences. For example, their Lempel–Ziv complexity (known as a good measure of the repetitiveness of binary sequences, see Ref. 59) is low in comparison with random finite sequences, but we will not prove that fact here.

VIII. ACTIVITY PATTERNS IN THE MODEL

Our study of the 1D nCNV model revealed that as a discrete dynamical system it certainly possesses very interesting dynamics that depends on a couple of parameters. However, since it originated from a neuron model, it is tempting to ask whether it can be viewed as a simple independent neuron model. For this purpose, let us consider the system

$$x_{n+1} = \begin{cases} f(x_n) - y_n, & \text{if } x_n < d, \\ f(x_n) - y_n - \beta, & \text{if } x_n \geq d, \end{cases} \quad (12)$$

where y_n can be treated as an external input current, constant or time-dependent. To emphasize that y can vary with time we write $y_n := \alpha(n)$, where $\alpha(n)$ is some function of time step n , independent of the value of x_n . This is partially in accordance with the original CNV model (4a) and (4b), where the external stimulus J is included only in the equation for the recovery variable y and changes the membrane voltage x indirectly through y . As previously, we refer to the system (12) as the 1D nCNV. Note that in (12) the variable y enters the system with negative sign, i.e., the input current $y > 0$ acts

TABLE III. Concatenations of Farey neighbors itineraries with respect to α (other parameters: $\mu = 1.6$, $\beta = 0.455$, $a = 0.1$, $d = 0.37$).

α	rotation interval	Farey neighbors itineraries	Concatenations of second and third order
−0.25	[0.888, 1]	8/9: 01 ⁸ 9/10: 01 ⁹	2nd: 01 ⁸ 01 ⁹ 3rd: 01 ⁸ 01 ⁸ 01 ⁹ , 01 ⁸ 01 ⁹ 01 ⁹
−0.2	[0.666, 0.8]	2/3: 01 ² 3/4: 01 ³	2nd: 01 ² 01 ³ 3rd: 01 ² 01 ² 01 ³ , 01 ² 01 ³ 01 ³
−0.15	[0.5, 0.666]	1/2: 01 3/5: (01) ² 1	2nd: (01) ³ 1 3rd: (01) ⁴ 1, (01) ³ 1(01) ² 1
−0.13	[0.5, 0.555]	1/2: 01 6/11: (01) ⁵ 1	2nd: (01) ⁶ 1 3rd: (01) ⁷ 1, (01) ⁶ 1(01) ⁵ 1

TABLE IV. Concatenations of Farey neighbors itineraries with respect to μ (other parameters: $\alpha = -0.065$, $\beta = 0.455$, $a = 0.1$, $d = 0.37$).

μ	Rotation interval	Farey neighbors itineraries	Concatenations of 2nd and 3rd order
1.1	[0.2, 0.25]	1/5: 10^4 1/4: 10^3	2nd: $10^3 10^4$ 3rd: $10^3 10^3 10^4$, $10^3 10^4 10^4$
2.2	[0.333, 0.5]	1/3: 10^2 1/2: 10	2nd: $10 10^2$ 3rd: $(10)^2 10^2$, $10 10^2 10^2$
2.75	[0.357, 0.666]	2/5: $(10)^2 0$ 1/2: 10	2nd: $(10)^3 0$ 3rd: $(10)^4 0$, $(10)^3 0 (10)^2 0$
3.1	[0.5, 0.875]	1/2: 01 2/3: 011	2nd: $(01)^2 1$ 3rd: $(01)^3 1$, $(01)^2 10 11$

as an inhibitory current, whereas $\gamma < 0$ would have an excitatory effect (we used this convention in our simulations below).

A. Autonomous 1D nICNV model

Although studying the 1D nICNV map $g(x)$ is mainly motivated by the need to explain the behavior of the whole slow-fast 2D system (4a) and (4b), it appears that the 1D nICNV model has surprisingly rich dynamics, even in the autonomous case when the input current $\gamma = \alpha$ is constant. For example, in previous section we showed how the combinatorial structure of periodic orbits of the 1D nICNV map can be matched with the spiking patterns generated. The real strength of the FUPO-method used for this purpose is that it allows one to rigorously prove the existence of infinitely many periodic firing patterns of the 1D CNV model, which otherwise would be very hard to find numerically. In numerical simulations, these patterns are not likely to persist asymptotically (due to the instability of periodic orbits) but, being aware of their existence, one can find initial conditions with long transient behavior of the particular period and itinerary type. This also reveals a special feature of the 1D CNV model, where (unless the map g has an attracting fixed point as in Fig. 3 in Ref. 21) for wide range of parameters, we are in the expanding Lorenz map regime and asymptotic behavior is always chaotic. Note that this makes the CNV model different than, for example, Chialvo model where in both 1D and 2D cases (see Refs. 20, 26, and 28), asymptotically periodic behavior could be observed due to the existence of attracting periodic orbits.

The 1D nICNV model can display a great variety of behaviors under the constant stimulus current. Some of them are depicted in Fig. 15, where we see chaotic bursting (top), tonic spiking (middle), or oscillatory spiking (bottom), which (depending on how one defines spikes) could be also interpreted as subthreshold oscillations alternating with spikes (sort of mixed-mode oscillations). The corresponding value α of the external current and the values of other parameters are given in the caption of the figure. We also include the value of the initial point. However, as we examined numerically, the qualitative behavior rather did not depend on the initial point. Corresponding trajectories in the form of the cobweb plot are presented in Fig. 16. We see clear matching between the orbit itineraries and distribution of points with the type of voltage trace in Fig. 15 (for picture clarity, we include only parts of corresponding trajectories in the cobweb plots).

Note that stable periodic orbits might exist in the 1D nICNV model beyond the expanding regime, studied by us herein. However, the absence of stable periodic behavior and the presence of chaos in the expanding case are not necessarily the disadvantage of the model as there are many map-based models especially designed to display chaotic behavior such, e.g., famous chaotic Rulkov model.¹⁹ On the other hand, chaotic spike trains appear commonly in experimental data, especially at the level of single cells (see, e.g., Ref. 22 and references therein).

B. Dynamics for varying input currents

As we mentioned, the 2D CNV model can be seen as a slow-fast system with γ as a slow variable which also depends on the external input J . However, the way at which the slow parameter γ changes with time steps n has important implications. In particular, the works (Refs. 35 and 36) numerically studied the one-dimensional map (4a) with cubic function $F(x)$ when parameter $\gamma = \alpha_n$ changes linearly and, respectively, sinusoidally with consecutive time instances $n = 1, 2, \dots$. Their results on the transient chaotic dynamics in the 1D system (4a) with varying control parameter α_n suggest that even numerical analysis of chaotic dynamics in the 2D system (4a) and (4b) can be quite challenging. This is in correspondence with our results from Sec. VII showing that even with constant input γ the dynamics of trajectories shows variety of transiently periodic behavior, prior to the irregular, chaotic asymptotic behavior. Similarly, numerical simulations presented in Fig. 15 reveal that 1D model displays wide repertoire of different voltage traces that might be interpreted in terms of biological neurons behaviors, indicating that the intrinsic dynamics of such a neuron is very rich.

Motivated by this and the observations of other authors mentioned above, we now investigate the dynamics of the 1D nICNV model under varying external input γ since the way a neuron responds to a certain input is its most important property. For this purpose, we consider two quite typical types of inputs: a periodic piecewise constant current with alternating stimulus amplitudes $\gamma = \alpha_1$ and $\gamma = \alpha_2$ and a constant stimulus with a short impulse of a larger amplitude. The results are presented, respectively, in Figs. 17 and 18.

We see that periodically changing the value of the input current can cause switching between tonic spiking and bursting, whereas

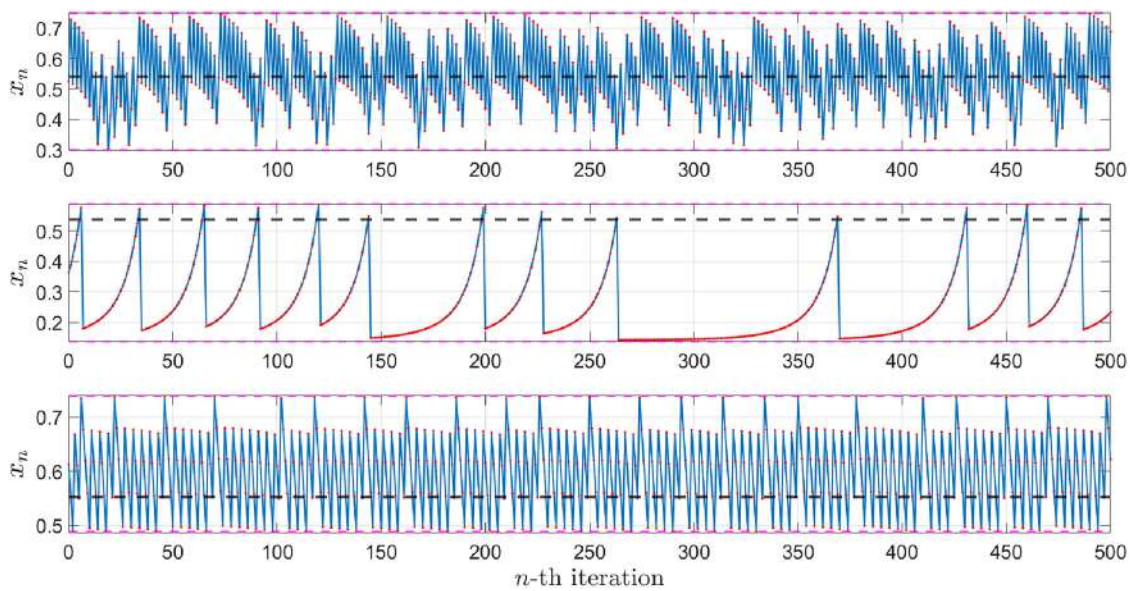


FIG. 15. Three different patterns of time series reproducing consecutively from the top: bursting, tonic spiking, and oscillatory spiking. Parameter values TOP: $\mu = 1.5$, $a = 0.15$, $d = 0.539$, $\alpha = -0.065$, $\beta = 0.45$, $x_0 = 0.524$; MIDDLE: $\mu = 0.5$, $a = 0.15$, $d = 0.539$, $\alpha = -0.0005$, $\beta = 0.45$, $x_0 = 0.363$; BOTTOM: $\mu = 0.405$, $a = 0.2$, $d = 0.553$, $\alpha = -0.15$, $\beta = 0.25$, $x_0 = 0.613$ (x_0 initial point). The horizontal dashed black line shows the discontinuity level.

the short impulse of higher amplitude changes temporarily the amplitude and frequency of oscillations. In fact, even after removing the short impulse returning to the steady-behavior might not be immediate and takes significant time. Note that as in our convention the current y has an inhibitory role, applying current with greater (or less negative) amplitude in general results in smaller potential values and lower frequency of oscillations.

C. Multistability

Figure 18 depicts a situation when a short impulse of a different amplitude has only temporal effect on the neuron's voltage trace

since after removing the impulse the system returns to its previous behavior, but this is not always the case. In particular, in Fig. 19, the neuron is first subjected to a constant input with amplitude of α_1 under which it converges to a resting state. However, applying an inhibitory current of the amplitude α_2 (for some duration time) causes first a rapid increase in voltage and small oscillations (bursting). Next, the input level returns back to α_1 but the neuron does not return to its previous resting state. Instead, it generates chaotic spiking oscillations. This phenomena can be explained by looking at the left panel of Fig. 20, which shows the map g obtained for $y = \alpha_1$ and the same values of other parameters. The map features two fixed points, stable and unstable, with stable fixed point corresponding

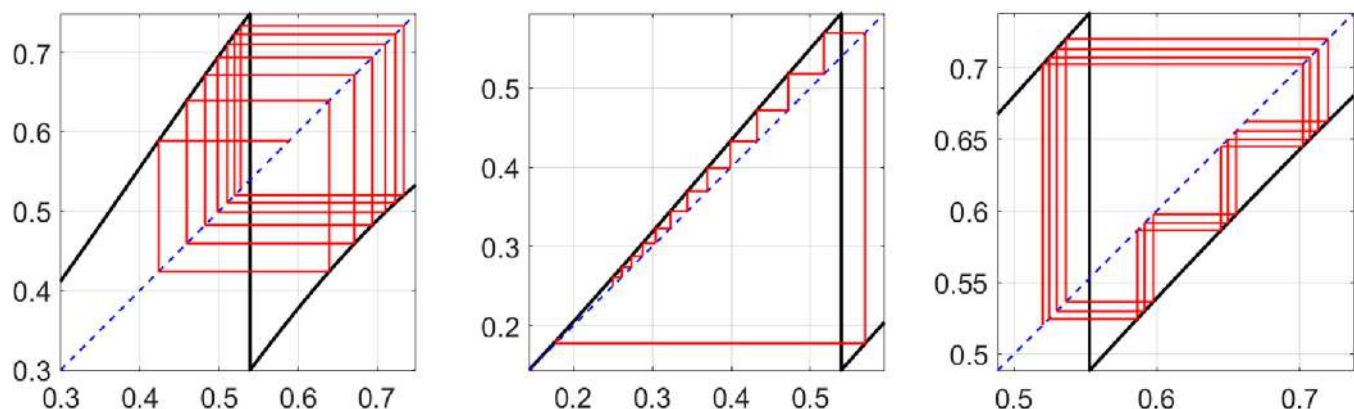


FIG. 16. Three cobwebs for plots of the nICNV maps corresponding (from the left) to the time series (from the top) presented in Fig. 15. Parameter values as on this figure.

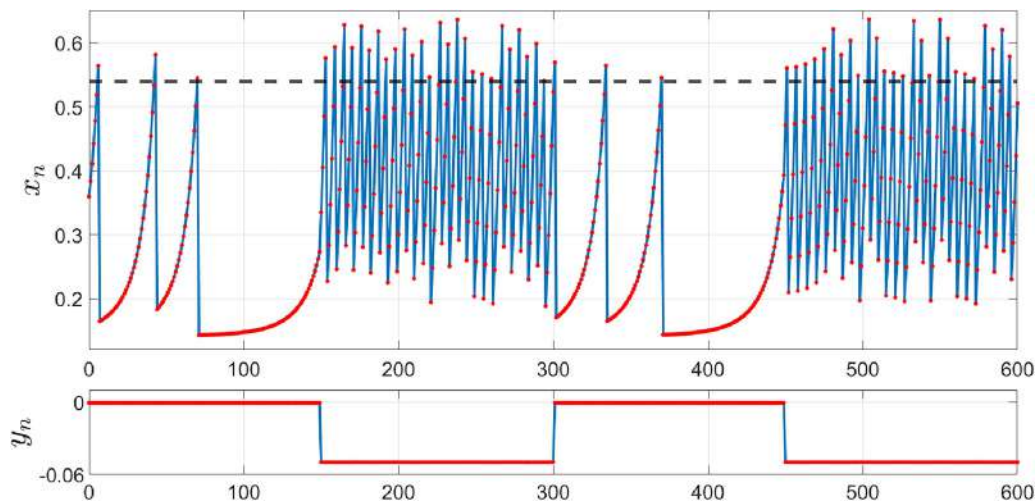


FIG. 17. Alternate spiking and bursting as an effect of switching the values of $y = \alpha$ between y_1 and y_2 . Other common parameter values of the 1D nICNV model: $\mu = 0.49$, $a = 0.15$, $d = 0.539$, $\beta = 0.45$, $\alpha_1 = -0.0005$, $\alpha_2 = -0.05$. Initial point $x_0 = 0.359$. Each switchover takes place after 150 time units. The horizontal dashed black line shows the discontinuity level.

to the resting state. Initial conditions to the right of the unstable fixed point get trapped within the invariant interval (marked as a red square). Therefore, applying additional inhibition to the neuron converging to its resting state shifts the graph of g up and enables “escaping” from the basin of attraction of the stable fixed point (or disappearance of the fixed points as a result of saddle-node bifurcation). If that inhibition is within a proper range of amplitudes and its duration is not too short nor too long, then after removing the inhibitory pulse, the graph of g returns to its initial configuration

but the trajectory stays constrained in the invariant interval exhibiting chaotic spiking (or chaotic subthreshold oscillations, depending on the interpretation). Therefore, even a transient input current can control switching between various oscillatory modes and detailed explanation of these effects can be a subject of further studies.

For completeness, we also notify that fixed points can appear to the right of the discontinuity point, with a particular example in the right panel of Fig. 20.

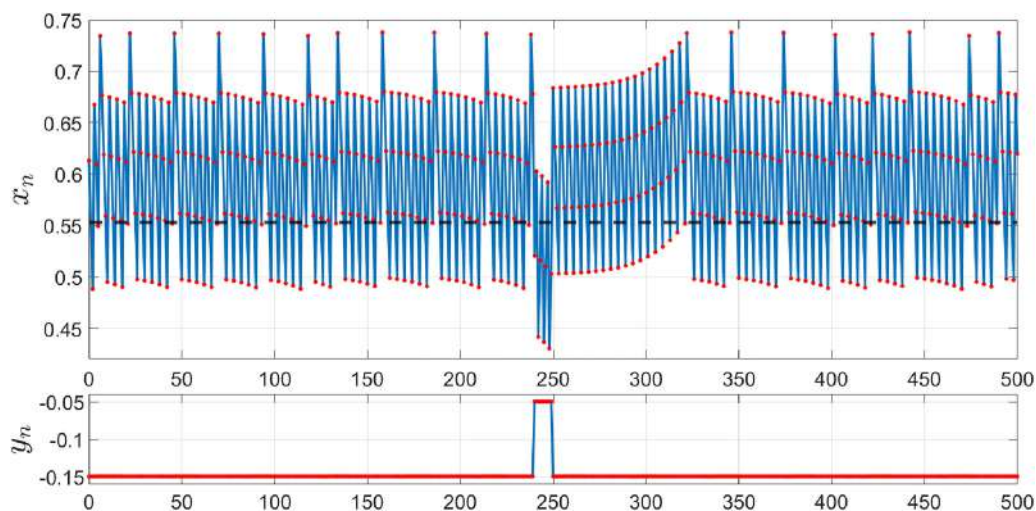


FIG. 18. Transient adaptation of a spiking pattern as an effect of a short impulse of $y = \alpha$ in the 1D nICNV model. Parameter values: $\mu = 0.405$, $a = 0.2$, $d = 0.55$, $\beta = 0.25$, $\alpha_1 = -0.15$, $\alpha_2 = -0.05$. Initial point $x_0 = 0.6131$. The horizontal dashed black line shows the discontinuity level.

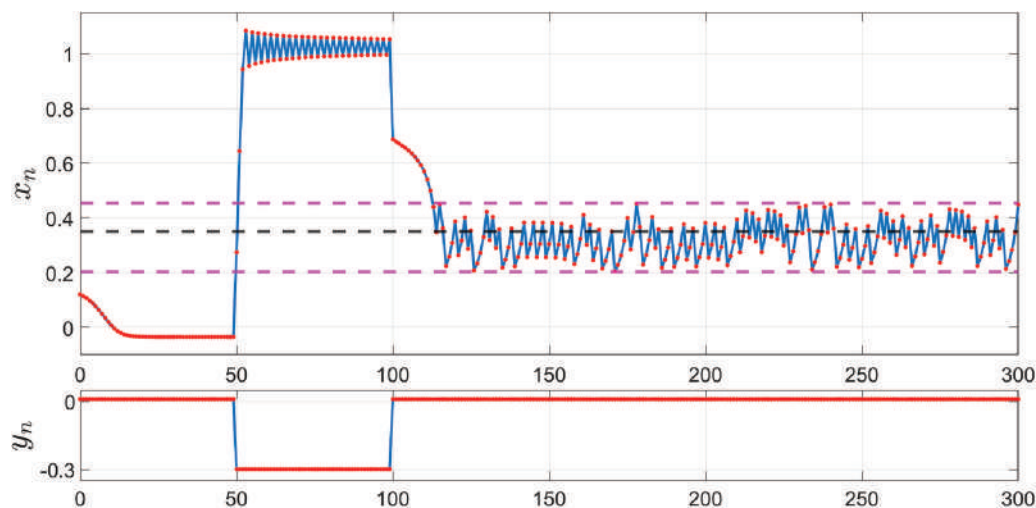


FIG. 19. Switching between various stable modes as an effect of an impulse of $y = \alpha$ in the 1D nICNV model. Parameter values: $\mu = 0.2, a = 0.1, d = 0.35, \beta = 0.25, \alpha_1 = 0.01, \alpha_2 = -0.3$. Initial point $x_0 = 0.12$. The horizontal dashed black line shows the discontinuity level and horizontal dashed maroon lines range of invariant interval corresponding to α_1 .

D. Shape of an action potential

Obviously, in case of a simple 1D map-based model, we do not aim at reproducing real time-continuous voltage recordings of biological neurons. However, expecting such a good matching with the real data is usually also not possible with higher dimensional discrete models or often even for their ODE- or hybrid counterparts. Rather, for map-based models, we are interested in reproducing the general spike train pattern (such as, e.g., tonic spiking, subthreshold oscillations, chaotic bursting, etc.) and sometimes just the information on whether in a given interval there was a spike or what is the

average firing rate. From that point of view the 1D nICNV model shows quite surprising ability to mimic various neuronal behaviors, some of them presented above. The reason for that is twofold: first, in the discrete setting complex dynamics (e.g., chaos) can arise even in one dimension and, second, the discontinuity present in the system allows for new types of behaviors not present in continuous maps, yet maintaining the complexity of, e.g., unimodal continuous maps.

An interesting feature of the 1D nICNV model is that, even under constant stimulus, it is possible to reconstruct various shapes of action potential. One shape of an action potential is visible in

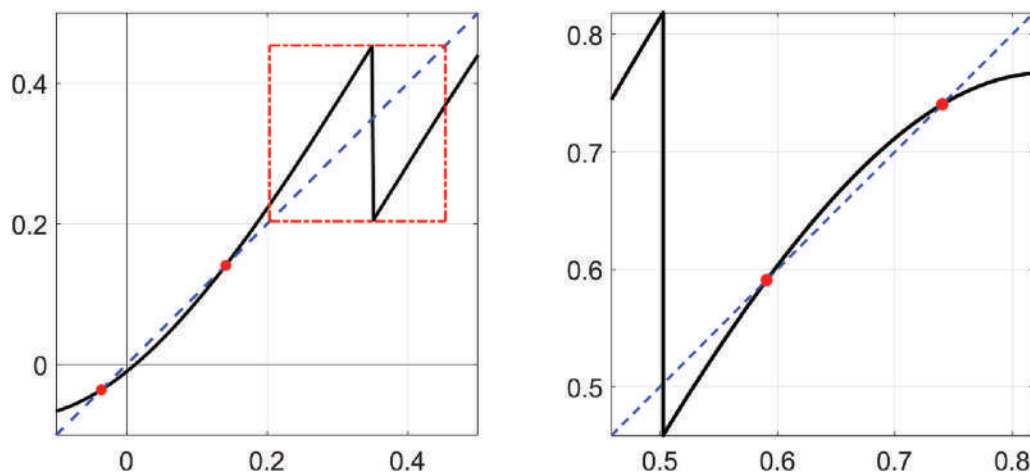


FIG. 20. Stable and unstable fixed points (red dots) of two 1D nICNV maps. On the left panel, both points are outside the invariant interval (red square). On the right panel, they are inside the invariant interval. Parameter values: LEFT: $\mu = 2, a = 0.1, d = 0.35, \alpha = 0.01, \beta = 0.25$; RIGHT: $\mu = 2.55, a = 0.01, d = 0.5025, \alpha = -0.002, \beta = 0.36$.

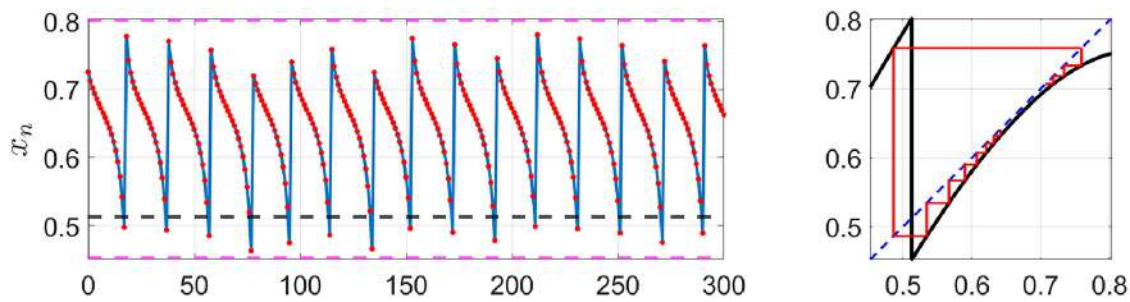


FIG. 21. Cardiac spiking in the 1D nICNV model (time series left, cobweb right). Parameter values: $\mu = 2.5$, $a = 0.05$, $d = 0.5127$, $\alpha = -0.0005$, $\beta = 0.35$. Initial point: $x_0 = 0.6271$.

the middle panel of Fig. 15, where the voltage first slowly increases, then depolarization accelerates and finally the voltage rapidly drops down. This is in correspondence with the trajectory that features many consecutive iterates on the left of the discontinuity point, followed by a point on the right and then turning to the left side again, as visible in the middle panel of Fig. 16. This configuration is likely among trajectories with rotation numbers of the form $1/q$, where q is large, as follows from the definition of the rotation number. On the other hand, Fig. 21 presents an action potential where depolarization of the membrane voltage is very rapid whereas repolarization (decrease in the membrane voltage) takes many time instances and has a different shape. Such a shape corresponds to the so-called cardiac action potential which has been recently reported in the Hindmarsh-Rose model as well as in the logistic KTz model in autonomous regime.⁶⁰ Therefore, the KTz model is another example of a map-based model which can successfully reconstruct dynamical behavior present in more complicated higher dimensional continuous-time models. Interestingly, cardiac spikes are also present in the 1D nICNV model and are realized by trajectories featuring a point to the left of the discontinuity, as depicted in the right panel of Fig. 21, which presents a couple of initial points on such a trajectory. This, in turn, is likely to occur for trajectories with rotation numbers of the form $(q - 1)/q$, where q is relatively large. It also seems that it is the discontinuity and, in particular, Lorenz-like nature of the 1D nICNV map that enables generating cardiac-like and “typical” spikes.

Remark 8.1. The voltage trace of cardiac-like spikes depicted in Fig. 21 has been obtained for the 1D nICNV model beyond the expanding Lorenz map regime (since the infimum of the derivative g' is slightly less than 1). However, the map is still Lorenz-like.

The above remark suggests that studying the nICNV model beyond the expanding case is also of interest. Nevertheless, we also expect that it is possible to obtain a similar shape of spikes for expanding Lorenz maps, e.g., with infimum of derivative slightly greater than 1. In addition, it is worth pointing out the following two observations.

Remark 8.2. If the map g in the 1D nICNV model is expanding (in the invariant interval of interest), then all the orbits (with initial condition in this interval) are unstable. However, for non-expanding maps (such as in Fig. 21), it makes sense to study stability of the periodic orbits.

Remark 8.3. In both situations of various types of action potentials, such as in the middle panel of Fig. 15 and in Fig. 21, we are in the vicinity of the “ghost” of the fixed point (see corresponding cobwebs), which makes the trajectories move slowly and very close to the diagonal. In purely expanding Lorenz map setting (i.e., under conditions listed in Table I), fixed points are not possible in the invariant interval but adjusting parameters beyond this regime enables this as well as non-overlapping setting where stable periodic behavior exists.

In the current work, we focus mainly on the expanding case (motivated by the presence of clear chaotic behavior) but the above remarks, results of simulations and observations suggest that obtaining comprehensive picture of the dynamics in the whole multidimensional parameter space of the 1D nICNV map could be a subject for further research. Certainly, the behavior of this, apparently simple, one dimensional discrete model is richer than, for example, for one-dimensional IF models.

IX. DISCUSSION AND CONCLUSIONS

Let us briefly summarize the presented results and discuss some possibilities of further developments.

First, we have showed how chaos theory and rotation theory of Lorenz-like and expanding Lorenz maps, which main results we reviewed in the first section and in Appendix A, can be effectively applied to the study of the 1D nICNV model. In particular, we have rigorously established sufficient conditions for the 1D nICNV map to be an expanding Lorenz map on an appropriate invariant interval (Theorem 4.1) and showed that the set of parameters where these conditions are satisfied is “not small” (Theorem 4.2 and Proposition 4.3). Next, we directed our interests towards chaotic properties of the model by providing theoretical and more explicit conditions under which the 1D model exhibits chaos in the sense of Devaney on the whole invariant interval (Theorem 5.1 and Lemma 5.2, respectively). Then, we investigated the range of chaotic behavior in the α - β parameter plane (Theorem 5.3, Table V and plots in Fig. 4). The even more fundamental properties of the model are its ergodicity and acip, which are related to the distribution of orbits. Depending on parameters (see Fig. 5), a typical orbit can asymptotically accumulate on the whole invariant interval or on the union of its disjoint subintervals. Further, explicit conditions for the existence of period 2 orbit have been provided (Lemma 6.1 and Theorem 2.5) and numerical

investigation of the behavior of the rotation interval with respect to the various parameters have yield that, as expected, the end points of this interval typically depend monotonically on a given parameter but, interestingly, its length (which might be identified with a sort of complexity measure) might change in a far more complicated way. Finally, using the notion of FUPOs, we have matched the itineraries of periodic orbits and their concatenations with spike patterns fired for the 1D nLCNV model (Propositions 7.1 and 7.2). We also included further numerically obtained examples depicting the behavior of the model established by some of our results, especially in terms of concatenations of periodic itineraries obtained from “most prominent” twist periodic orbits. However, as we have showed, the voltage traces produced by the 1D nLCNV model can be both irregular (i.e., non-periodic, “chaotic”) or (transiently) periodic which might depend on the initial voltage value and be quite fragile to the small variation in parameters. The last section discusses biological relevance of the findings on the 1D nLCNV model and shows that even with constant external stimulus the 1D model can present variety of behaviors.

There arises though a natural question on the implications of these results for the original 2D nLCNV model. Note that due to the discrete, and discontinuous, nature of this model obtaining rigorous mathematical results (formal theorems and proofs) seems quite challenging and is an interesting topic for further research. However, since the 1D nLCNV model, which can be seen as a Poincaré section of the full model, already shows significant complexity (e.g., in terms of spiking patterns fired as established by Propositions 7.1 and 7.2), we can expect that the level of complexity of the full 2D model is not less than that of its 1D reduction and thus providing the results on the 2D system, maintaining the same level of analytical rigorousness, is very challenging. In fact, the first steps in the direction of rigorous examination of the 2D model are the results concerning behavior of the 1D reduction with respect to the α -parameter (since this parameter corresponds to the y -variable in the 2D model), in particular our Theorems 4.2, 2.5, and 5.3 since, as also pointed out in Ref. 21, the dynamical mechanism of chaotic behavior in the 2D model is induced by the 1D nLCNV map.

Another idea comes by applying elements of fast-slow analysis since with $\varepsilon \rightarrow 0$ the 2D model shows a natural separation of time scales in which case y becomes a slow parameter controlling the evolution of the voltage x . Observations in this vein were included in the main works on the CNV model.^{21,30} Nevertheless, the rigorous approach would require applying the tools of discrete geometric singular perturbation theory as recently developed in Ref. 27 and illustrated therein, among others, with the example of the Chialvo model,²⁰ where some parameter sets corresponding to various types of spiking dynamics could be identified. Unfortunately, the 1D CNV map is not continuous, contrary to the map describing the evolution of the voltage variable x in the Chialvo model, which seems to be a technical obstacle in such analysis.

ACKNOWLEDGMENTS

Frank Llovera Trujillo and Justyna Signerska-Rynkowska were supported by NCN (National Science Centre, Poland) Grant No. 2019/35/D/ST1/02253. Justyna Signerska-Rynkowska also acknowledges the support of Dioscuri program initiated by the Max Planck

Society, jointly managed with the National Science Centre (Poland), and mutually funded by the Polish Ministry of Science and Higher Education and the German Federal Ministry of Education and Research.

AUTHOR DECLARATIONS

Conflict of Interest

The authors have no conflicts to disclose.

Author Contributions

Piotr Bartłomiejczyk: Conceptualization (equal); Data curation (lead); Formal analysis (equal); Investigation (equal); Methodology (equal); Resources (equal); Software (equal); Supervision (equal); Validation (equal); Visualization (equal); Writing – original draft (equal); Writing – review & editing (equal). **Frank Llovera Trujillo:** Data curation (equal); Formal analysis (equal); Investigation (equal); Software (lead); Validation (equal); Visualization (equal); Writing – original draft (equal). **Justyna Signerska-Rynkowska:** Conceptualization (equal); Formal analysis (equal); Funding acquisition (lead); Investigation (equal); Methodology (equal); Supervision (equal); Validation (equal); Writing – original draft (equal); Writing – review & editing (equal).

DATA AVAILABILITY

The data (software) upon which our numerical computations are based are publicly and freely available at Refs. 57 and 58.

APPENDIX A: THEORY OF LORENZ-LIKE MAPS

1. Basic definitions

Let (X, d) be a compact metric space and $f: X \rightarrow X$ a map (not necessarily continuous). Recall that a nonempty and open set $U \subset X$ is called *opene*.

We start with the following general notions.

Definition A.1. The map f is called

- *transitive* if for every two opene sets $U, V \subset X$ there is $n \in \mathbb{N}$ such that $f^n(U) \cap V \neq \emptyset$,
- *mixing* if for every two opene sets $U, V \subset X$ there is $N \in \mathbb{N}$ such that for every $n \geq N$, we have $f^n(U) \cap V \neq \emptyset$,
- *sensitive* if there exists a $\delta > 0$ such that for every $x \in X$ and every neighborhood U of x , there exists $y \in U$ and $n \in \mathbb{N}$ such that $d(f^n(x), f^n(y)) > \delta$,
- *expansive* if there exists a $\delta > 0$ such that for any $x, y \in X, x \neq y$, there exists $n \in \mathbb{N}$ such that $d(f^n(x), f^n(y)) > \delta$.

We remark that

- mixing implies transitivity,
- expansiveness implies sensitivity.

One of the most classical definitions of chaos is due to R. L. Devaney.

Definition A.2. A map $f: X \rightarrow X$ is called *chaotic in the sense of Devaney* on X if

- (1) f is transitive,
- (2) the set of periodic points of f is dense in X ,
- (3) f is sensitive.

An interesting class of maps are Lorenz-like and expanding Lorenz maps, which are special type of maps defined on the subinterval of the real line, i.e., $X = [a, b] \subset \mathbb{R}$. Therefore, next definitions and results will be formulated for $f: [0, 1] \mapsto [0, 1]$ (which naturally extends to the case $f: [a, b] \mapsto [a, b]$).

Definition A.3. We say that a map $f: [0, 1] \rightarrow [0, 1]$ is *strongly transitive* if for every nonempty open subinterval $J \subset (0, 1)$, there exists $n \in \mathbb{N}$ such that $\bigcup_{i=0}^n f^i(J) \supset (0, 1)$.

Note that strong transitivity implies transitivity. The opposite is, in general, not true, but the following essential result holds (see Ref. 61, Theorem 3).

Theorem A.4. Assume that $f: [0, 1] \rightarrow [0, 1]$ is piecewise continuous piecewise strictly monotone. If f is transitive, then it is strongly transitive.

Definition A.5. A Lorenz-like map is a map f of an interval $[0, 1]$ to itself, for which there exists a point $c \in (0, 1)$ such that

- f is continuous and increasing (not necessarily strictly) on $[0, c]$ and on $(c, 1]$,
- $\lim_{x \rightarrow c^-} f(x) = 1$ and $\lim_{x \rightarrow c^+} f(x) = f(c) = 0$.

The intervals of continuity in the domain of the Lorenz map play a crucial role in its analysis. Therefore, denote $I_L = [0, c]$ and $I_R = [c, 1]$.

Definition A.6. The Lorenz-like map f is called *nonoverlapping* if $f(0) > f(1)$ (i.e., when $f(I_L) \cap f(I_R) = \emptyset$). Otherwise, (i.e., when $f(0) \leq f(1)$ implying $f(I_L) \cap f(I_R) \neq \emptyset$), the map is called *overlapping*.

It turns out that nonoverlapping and overlapping Lorenz-like maps have completely distinct properties (see, e.g., Refs. 62 and 43), especially in terms of their rotation sets as mentioned in Sec. II.

Definition A.7. An *expanding Lorenz map* is a map $f: [0, 1] \rightarrow [0, 1]$ satisfying the following three conditions:

- there is a *critical point* $c \in (0, 1)$ such that f is continuous and strictly increasing on $[0, c]$ and $(c, 1]$,
- $\lim_{x \rightarrow c^-} f(x) = 1$ and $\lim_{x \rightarrow c^+} f(x) = f(c) = 0$,
- f is differentiable for all points not belonging to a finite set $F \subset [0, 1]$ and such that $\inf \{f'(x) \mid x \in [0, 1] \setminus F\} > 1$.

Observe that expanding Lorenz maps are overlapping Lorenz-like maps. Moreover, every expanding Lorenz map is expansive (see Ref. 31, Proposition 1).

2. Chaos in Lorenz maps

Let

$$\begin{aligned} f_1(x) &= \sqrt{2}x + \frac{2 - \sqrt{2}}{2} \pmod{1}, \\ f_2(x) &= \sqrt[3]{2}x + \frac{2 + \sqrt[3]{4} - 2\sqrt[3]{2}}{2} \pmod{1}, \\ f_3(x) &= \sqrt[3]{2}x + \frac{2 - \sqrt[3]{4}}{2} \pmod{1}, \end{aligned}$$

for $x \in [0, 1]$.

The results for the occurrence of chaos and related phenomena in expanding Lorenz maps, important from the point of view of further analysis of the nlCNV model, can be summarized in the following:

Theorem A.8. Let $f: [0, 1] \rightarrow [0, 1]$ be an expanding Lorenz map. Then, the following conditions are equivalent:

- f is transitive,
- f is strongly transitive,
- f is chaotic in the sense of Devaney.

Now, let $\lambda := \inf \{f'(x) \mid x \in [0, 1] \setminus F\}$. If one of the following conditions is satisfied:

- (i) $\sqrt{2} \leq \lambda \leq 2$,
- (ii) $\sqrt[3]{2} \leq \lambda < \sqrt{2}$ and $f(0) \geq \frac{1}{1+\lambda}$,
- (iii) $\sqrt[3]{2} \leq \lambda < \sqrt{2}$ and $f(1) \leq 1 - \frac{1}{1+\lambda}$,

then f is chaotic in the sense of Devaney.

Moreover, if $f \neq f_1$, $f \neq f_2$, and $f \neq f_3$, then f is also mixing.

Proof. It is obvious that strong transitivity implies transitivity. On the other hand, the opposite is also true in this case, as f is piecewise continuous piecewise strictly (see Theorem A.4). However, an expanding Lorenz map is transitive if and only if it is chaotic in the sense of Devaney (see, e.g., Proposition 5 in Ref. 31 and references therein). The second part of Theorem A.8 follows from Theorems 4.5–4.8 in Ref. 63 and above observations (see also Theorem 7 in Ref. 31). \square

Corollary A.9. An expanding Lorenz map $f: [0, 1] \rightarrow [0, 1]$ is chaotic in the sense of Devaney (on $[0, 1]$) if and only if it has a dense orbit.

Proof. It is easy to justify that the existence of a dense orbit implies transitivity. The opposite implication holds for Lorenz-like maps (not necessarily expanding) in the view of Proposition 1 in Ref. 64. Now, the equivalence with chaos in the sense of Devaney for expanding Lorenz maps follows from Theorem A.8. \square

APPENDIX B. PROOF OF THEOREM 2.5

Proof of Theorem 2.5. First, let us assume that f is strictly increasing in each of the continuity intervals $[0, c]$ and $(c, 1]$. Suppose that (7) holds and consider $g: [0, 1] \rightarrow [0, 1]$ defined as $g(x) = f^2(x)$. Then, g has precisely three discontinuity points c_1 , c , and c_2 such that $0 < c_1 \in f^{-1}(c) \cap (0, c)$ and $c < c_2 \in f^{-1}(c) \cap (c, 1)$. Let us investigate the limits of g at these discontinuity points. We have

$$\begin{aligned} \lim_{x \rightarrow c_1^-} g(x) &= \lim_{x \rightarrow c_2^-} g(x) = 1, \\ \lim_{x \rightarrow c_1^+} g(x) &= \lim_{x \rightarrow c_2^+} g(x) = 0, \\ \lim_{x \rightarrow c^-} g(x) &= f(1), \quad \lim_{x \rightarrow c^+} g(x) = f(0). \end{aligned}$$

Between the discontinuity points, the graph of g is continuous and increasing. Thus, by analyzing these limits, we see that g has (at least) two fixed points: $x_1 \in (c_1, c)$ and $x_2 \in (c, c_2)$. On the other hand, f cannot have fixed points in the intervals (c_1, c) and (c, c_2) . Indeed, suppose that $x_* \in (c_1, c)$ is a fixed point of f , i.e., $f(x_*) = x_*$. Then, $f(c_1) = c$ since $c_1 \in f^{-1}(c)$. As f is increasing, we

have $f(c_1) < f(x_*)$, which means $c < x_*$, contradicting the assumption that $x_* \in (c_1, c)$. Similarly, f cannot have fixed points in (c, c_2) . Thus, the points x_1 and x_2 are not fixed points and must be points of period 2, and we have proved the existence of period 2 periodic orbit.

The above reasoning also applies if f is not strictly increasing in its continuity intervals but is strictly increasing at all those arguments x such that $f(x) = c$. Now, let us see what changes if there are intervals $[c_{1,1}, c_{1,2}] \subset (0, c)$ and/or $[c_{2,1}, c_{2,2}] \subset (c, 1)$ such that $f(x) = c$ for each $x \in [c_{1,1}, c_{1,2}] \cup [c_{2,1}, c_{2,2}]$. Then, for the map $g = f^2$, we have

$$\lim_{x \rightarrow c_{1,1}^-} g(x) = \lim_{x \rightarrow c_{2,1}^-} g(x) = 1,$$

$$\lim_{x \rightarrow c_{1,2}^+} g(x) = \lim_{x \rightarrow c_{2,2}^+} g(x) = 0,$$

and $g(x) = f(c) = 0$ for $x \in [c_{1,1}, c_{1,2}] \cup [c_{2,1}, c_{2,2}]$. Similarly, as before g has at least two fixed points: $x_1 \in (c_{1,2}, c)$ and $x_2 \in (c, c_{2,1})$, which simultaneously cannot be fixed points of f since f cannot have fixed points in these intervals. Thus, x_1 and x_2 are period 2 periodic points.

For the expanding case, uniqueness of this orbit, as a period 2 periodic orbit, follows from the forthcoming Proposition F.8. The fact that it is unstable is also an immediate consequence of the expansiveness. \square

Remark B.1. It is worth pointing out that there is also a natural geometric method for both justification of Theorem 2.5 and graphical locating of 2-periodic points. Namely, let us consider the square $S = [0, 1] \times [0, 1]$ on the plane and the two curves in S : $\gamma_1: [0, c] \rightarrow S$ given by $\gamma_1(t) = (t, f(t))$ [assume for simplicity that $\gamma_1(c) = (c, 1)$] and $\gamma_2: [c, 1] \rightarrow S$ given by $\gamma_2(t) = (f(t), t)$. Observe that the curve γ_1 is a part of the plot of f (between 0 and c) and the curve γ_2 is the reflection of the other part of the plot of f (between c and 1) in axial symmetry with respect to the diagonal of the square.

Moreover, the points of intersection of these curves correspond exactly to 2-periodic points for f . Namely, if there are $t_1 \in [0, c)$ and $t_2 \in [0, c)$ such that $\gamma_1(t_1) = \gamma_2(t_2)$, then $t_1 = f(t_2)$ and $t_2 = f(t_1)$, which gives $t_1 = f^2(t_1)$, i.e., $\{t_1, t_2\}$ is a 2-periodic orbit.

Why do these curves have to intersect? Consider four points on the boundary of S : $A = \gamma_1(0) = (0, f(0))$, $B = \gamma_1(c) = (c, 1)$, $A = \gamma_2(c) = (0, c)$, and $A = \gamma_2(1) = (f(1), 1)$. By the assumption $f(0) < c < f(1)$, C is above A on the left side of the square S and B is to the left of D on the upper side of the square. Hence, the curves γ_1 and γ_2 have to intersect at least once from Jordan curve theorem (see Fig. 22). Finally, if f is an expanding Lorenz map, then the slope of γ_1 at each point is greater than 1 and the slope of γ_2 at each point is less than 1. In consequence, the curves cannot intersect more than once.

APPENDIX C. Proof of Theorem 4.2

Proof of Theorem 4.2. Note that five curves go through the point $(F(d), 0)$ in the α - β plane (see Table I and Fig. 23). Namely, the vertical line $\alpha = F(d)$, the horizontal line $\beta = 0$, the slant line $\beta = F(d) - \alpha$, and two nonlinear curves: $\beta = p(\alpha) = F(d + F(d) - \alpha) - \alpha$ and $\beta = q(\alpha)$. The last one given by the implicit formula

$$L(\alpha, \beta) = F(d + F(d) - \alpha - \beta) - \alpha = 0.$$

Since, by our assumptions, the area (parallelogram) between lines $\alpha = F(d + F(d) - \alpha - \beta)$, $\alpha = F(d)$, $\beta = F(d) - \alpha$, and $\beta = d + F(d) - x_{\min} - \alpha$ is always nonempty and the plot of $\beta = p(\alpha)$ is above the line $\beta = F(d) - \alpha$ for $\alpha < F(d)$ [compare the derivatives at $\alpha = F(d)$], to complete the proof, it is enough to show that in the small neighborhood of the point $\alpha = F(d)$ the plot of $\beta = q(\alpha)$ is above the plot $\beta = p(\alpha)$, which is equivalent to $p'(\alpha) > q'(\alpha)$ [see Fig. 23 and compare the slopes of $p(\alpha)$ and $q(\alpha)$ at $\alpha = F(d)$]. An easy computation gives

$$\bullet \quad p'(\alpha) = -F'(d + F(d) - \alpha - \beta) - 1 \quad \text{and} \quad p'(F(d)) = -F'(d) - 1,$$

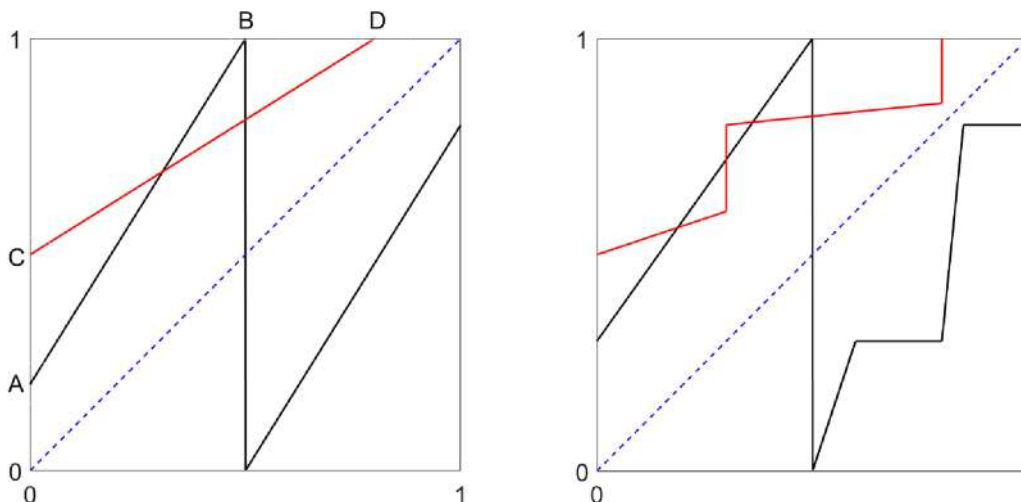


FIG. 22. Geometric method for finding 2-periodic points. Expanding Lorenz maps with a unique 2-periodic point (left) and Lorenz-like map with 3 such points (right).

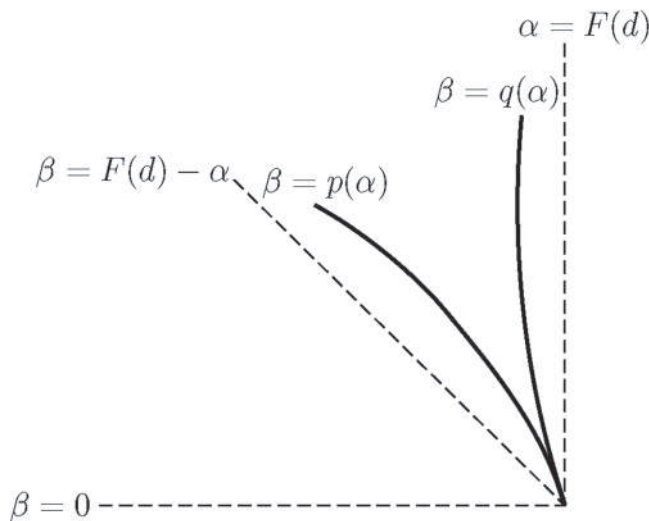


FIG. 23. Five curves from the proof of Theorem 4.2.

$$\bullet \quad q'(\alpha) = -\frac{\partial L}{\partial \alpha} / \frac{\partial L}{\partial \beta} = \frac{-F'(d+F(d)-\alpha-\beta)-1}{F'(d+F(d)-\alpha-\beta)} \text{ and } q'(F(d)) = \frac{-F'(d)-1}{F'(d)}.$$

Hence, finally, $p'(\alpha) > q'(\alpha)$ if and only if $F'(d) < 1$, which completes the proof. \square

APPENDIX D. PROOF OF THEOREM 5.3

Proof of Theorem 5.3. Note that due to Theorem 5.1(i), it is enough to show that under Assumption (10) inside the area A , there is a nonempty subarea C on which

$$\sqrt{2} \leq \lambda = \inf \{G'(x) \mid x \in [b, c]\} \leq 2.$$

It is easy to check that the condition $\lambda \leq 2$ is satisfied even without Assumption (10). Namely, since $a \in (0, 1)$, $\mu \in (0, 3]$, and $G'(x) = -3\mu x^2 + 2\mu(a+1)x + 1 - \mu a$ attains maximum at $\frac{a+1}{2}$, we have

$$\lambda \leq \sup \{G'(x) \mid x \in [b, c]\} = \frac{\mu(a^2 - a + 1) + 3}{3} \leq \frac{3 \cdot 1 + 3}{3} = 2.$$

Now, let us check when the condition $\lambda \geq \sqrt{2}$ is satisfied. Observe that λ obviously depends on α and β because we calculate λ on $[b, c]$. Recall that in Sec. IV, we searched for invariant intervals inside the interval (x_{\min}, x_{\max}) defined by the condition $\lambda > 1$. Now, we want to strengthen our condition to $\lambda \geq \sqrt{2}$ and see when parameters α and β for which this condition holds exist. It turns out that this is the case exactly if

- the quadratic equation $G'(x) = \sqrt{2}$ has two distinct real roots or, equivalently as we have seen, $\mu > 3(\sqrt{2}-1)/(a^2-a+1)$,
- the end points of the invariant interval lie inside the interval (x_1, x_2) , i.e., $x_1 < b < c < x_2$.

TABLE V. Conditions for the existence of chaos.

No.	Condition	Parametric form
7.	$\Delta > 0$	$\mu > 3(\sqrt{2}-1)/(a^2-a+1)$
8.	$x_1 < b$	$d+F(d)-x_1-\alpha-\beta > 0$
9.	$x_2 > c$	$d+F(d)-x_2-\alpha < 0$

However, since the discontinuity point d lies in the interval (x_1, x_2) , i.e., $x_1 < d < x_2$, the straight line $\beta = d + F(d) - x_1 - \alpha$ is parallelly above $\beta = d + F(d) - x_1 - \alpha$ and the vertical line $\alpha = d + F(d) - x_2$ is on the left of $\alpha = F(d)$ (see Fig. 4). In consequence, if (10) holds, then the conditions 8 and 9 from Table V always cut by rectilinear cuts from the area A the subarea of positive Lebesgue measure. Since this subarea is obviously contained in C , the proof is complete. \square

APPENDIX E. PROOF OF THEOREM 6.2

Proof of Theorem 6.2. The reasoning is similar to that in the proof of Theorem 4.2. Let us consider four nonlinear curves (see Fig. 24), which intersect at the point $\alpha = \alpha_0 = F(d)$. Two of them $\beta = p(\alpha)$ and $\beta = q(\alpha)$ correspond to the borders of the set A (see the proof of Theorem 4.2). The other two $\beta = r(\alpha)$ and $\beta = s(\alpha)$ correspond to the borders of the set B . Namely, $\beta = r(\alpha)$ is given by the implicit formula $F(d+F(d)-\alpha-\beta) + F(d) - 2\alpha - \beta = 0$, which corresponds to condition 10 (see Table II), and $\beta = s(\alpha)$ is given by the explicit formula $\beta = F(d+F(d)-\alpha) + F(d) - 2\alpha$, which corresponds to condition 11. Since all four curves are smooth and have a common point $(\alpha_0, 0)$, the proof will be completed by showing that the derivatives at α_0 satisfy the following three conditions: (a) $r'(\alpha_0) > s'(\alpha_0)$, (b) $r'(\alpha_0) > q'(\alpha_0)$, and (c) $p'(\alpha_0) > s'(\alpha_0)$. Note that we do not assume any relations between $s'(\alpha_0)$ and $q'(\alpha_0)$.

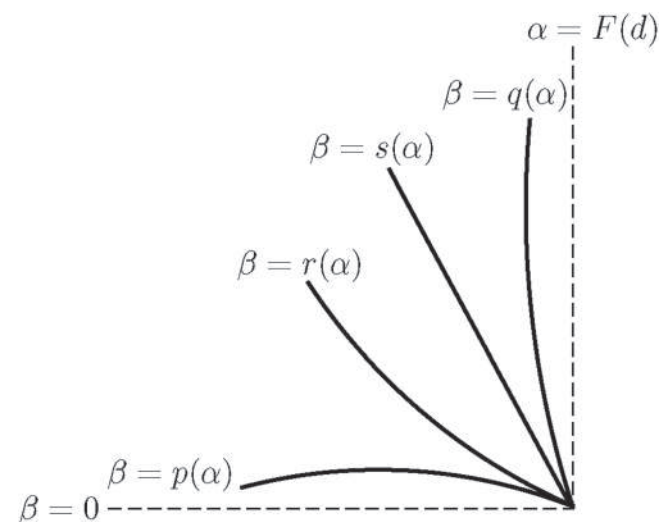


FIG. 24. Four nonlinear curves from the proof of Theorem 6.2.

and between $r'(\alpha_0)$ and $p'(\alpha_0)$. For abbreviation, let ζ stands for $F'(d)$. An easy calculation similar to that in the proof of Theorem 4.2 shows that

$p'(\alpha_0)$	$q'(\alpha_0)$	$r'(\alpha_0)$	$s'(\alpha_0)$
$-\zeta - 1$	$\frac{-\zeta - 1}{\zeta}$	$\frac{-\zeta - 2}{\zeta + 1}$	$-\zeta - 2$

Now, since $\zeta = F'(d) > 0$, we check at once that the conditions (a)–(c) are satisfied, which completes the proof. \square

APPENDIX F. FINITE UNIONS OF PERIODIC ORBITS AND FAREY-LORENZ PERMUTATIONS

Let f be a Lorenz-like map. If $P := \{x, f(x), \dots, f^{q-1}(x)\}$ is a periodic orbit of f , then the itinerary of P is the sequence (a_1, a_2, \dots, a_q) of symbols L and R such that for $i = 1, \dots, q$,

$$a_i = \begin{cases} L, & \text{if } f^i(x) \in I_L, \\ R, & \text{if } f^i(x) \in I_R. \end{cases}$$

The sequence is given up to a cyclic permutation.

Definition F.1. A finite union of periodic orbits of f is called a FUPO.

FUPOs are characterized by their permutations, i.e., a permutation of a FUPO P consisting of points $x_1 < \dots < x_n$, is a mapping $\sigma : \{1, 2, \dots, n\} \rightarrow \{1, 2, \dots, n\}$ such that $f(x_i) = x_{\sigma(i)}$.

The following observation applies to FUPOs of Lorenz-like maps.

Proposition F.2. If a FUPO P has $n > 1$ elements, then there exists $k \in \{1, \dots, n-1\}$ such that σ is increasing on $\{1, \dots, k\}$ and on $\{k+1, \dots, n\}$. Such permutations (and the permutation of $\{1\}$) are called *L-permutations*. Moreover, for every L-permutation σ there exists a Lorenz-like map f with the FUPO P such that P has permutation σ .

Note that if FUPO is a periodic orbit, then its rotation number is $(n-k)/n$.

Definition F.3. A cyclic L-permutation σ of $\{1, \dots, n\}$ is called a *twist permutation* if $\sigma(1) > \sigma(n)$.

Correspondingly, a periodic orbit with such a permutation is called a *twist periodic orbit*.

Remark F.4. Note that a twist permutation of $\{1, \dots, n\}$ with rotation number j/n has a form

$$\sigma(i) = i + j \pmod n.$$

In consequence, the k th term of the twist periodic itinerary is L if and only $(kp \pmod q) < q - p$.

Definition F.5. An L-permutation σ of $\{1, \dots, p+q\}$ is called a *Farey-Lorenz permutation* (or *FL-permutation*) if σ consists of two twist cycles, of period p and q , with rotation numbers $a/p < b/q$, respectively, such that $bp = aq + 1$.

Recall that in this case, we say that a/p and b/q are *Farey neighbors*. The ordering of point on FUPOs with FL permutations are specified by the following rule (cf. Ref. 42).

Proposition F.6. Assume that σ is an FL-permutation with cycles of rotation numbers a/p and b/q , where $a/p < b/q$ are Farey

neighbors and $p < q$. Let the points of P be $x_1 < x_2 < \dots < x_p$ and the points of Q , $y_1 < y_2 < \dots < y_q$. Then,

$$f(x_i) = x_{i+a \pmod p} \quad \text{and} \quad f(y_j) = y_{j+b \pmod q}$$

and

- $x_1 < y_1$,
- for $i = 1, \dots, p-1$, if $j = 1 + ia \pmod p$ and $l = ib \pmod q$, then $y_{l-1} < x_j < y_l$.

An example of a FUPO of FL type in the 1D nLCNV model is illustrated in Fig. 11.

The following result (see, e.g., Ref. 42, Sec. 5 or 45) states that Lorenz-like maps admit twist periodic orbits for each rational number in their rotation interval.

Theorem F.7. Let g be a Lorenz-like map. If a number p/q is in the rotation interval of g , and p, q are coprime, then g has a twist periodic orbit of period q and rotation number p/q .

If the map is also expanding, then we obtain the uniqueness of periodic orbits with given itinerary (see Ref. 31, Proposition 1) for justification).

Proposition F.8. If g is an expanding Lorenz map and p/q is in the rotation interval of g (p and q coprime), then there is exactly one twist periodic orbit with rotation number p/q . Moreover, there is at most $\binom{q}{p}/q$ periodic orbits with rotation number p/q .

Remark F.9. In fact, we show in Ref. 31 that given any periodic L - R sequence, there is at most one periodic orbit with this itinerary.

Next theorem, proved in Ref. 42 applies for Lorenz-like maps (not necessarily expanding).

Theorem F.10. Let g be a Lorenz-like map. Assume that the rotation interval of g contains the interval $[a/p, b/q]$, where $a/p < b/q$ are Farey neighbors, and $p < q$. Then, g has a twist periodic P orbit of period p and rotation number a/p and a twist periodic orbit Q of period q and rotation number b/q . If these periodic orbits are disjoint, then their union forms a FUPO with the FL-permutation. Moreover, there exist periodic orbits with itineraries being concatenation of finitely many periodic itineraries (starting at x_1 or y_1) of P and Q .

Remark F.11. If $a/p < b/q$, but $p > q$, then we replace a/p by $(p-a)/p$ and b/q by $(q-b)/q$. Then, in the itineraries, we replace symbols L by R and vice versa.

REFERENCES

- ¹L. Lapique, "Recherches quantitatives sur l'excitation électrique des nerfs traitée comme une polarisation," *J. Physiol. Pathol. Gen.* **9**, 567–578 (1907).
- ²N. Brunel and M. C. van Rossum, "Lapique's 1907 paper: From frogs to integrate-and-fire," *Biol. Cybern.* **97**, 337–339 (2007).
- ³A. L. Hodgkin and A. F. Huxley, "A quantitative description of membrane current and its application to conduction and excitation in nerve," *J. Physiol.* **117**, sp004764 (1952).
- ⁴R. FitzHugh, "Impulses and physiological states in theoretical models of nerve membrane," *Biophys. J.* **1**, 445–466 (1961).
- ⁵J. Nagumo, S. Arimoto, and S. Yoshizawa, "An active pulse transmission line simulating nerve axon," *Proc. IRE* **50**, 2061–2070 (1962).
- ⁶J. L. Hindmarsh and R. M. Rose, "A model of neuronal bursting using three coupled first order differential equations," *Proc. R. Soc. Lond. B.* **221**, 87–102 (1984).

- ⁷C. Morris and H. Lécarré, "Voltage oscillations in the barnacle giant muscle fiber," *Biophys. J.* **35**, 193–213 (1981).
- ⁸R. Brette, "Dynamics of one-dimensional spiking neuron models," *J. Math. Biol.* **48**, 38–56 (2004).
- ⁹H. Carrillo and F. Hoppensteadt, "Unfolding an electronic integrate-and-fire circuit," *Biol. Cybern.* **102**, 1–8 (2010).
- ¹⁰S. Coombes and P. Bressloff, "Mode locking and Arnold tongues in integrate-and-fire oscillators," *Phys. Rev. E* **60**, 2086–2096 (1999).
- ¹¹J. P. Keener, F. C. Hoppensteadt, and J. Rinzel, "Integrate-and-fire models of nerve membrane response to oscillatory input," *SIAM J. Appl. Math.* **41**, 503–517 (1981).
- ¹²R. Brette and W. Gerstner, "Adaptive exponential integrate-and-fire model as an effective description of neuronal activity," *J. Neurophysiol.* **94**, 3637–3642 (2005).
- ¹³E. M. Izhikevich, "Simple model of spiking neurons," *IEEE Trans. Neural Netw.* **14**, 1569–1572 (2003).
- ¹⁴J. Touboul and R. Brette, "Spiking dynamics of bidimensional integrate-and-fire neurons," *SIAM J. Appl. Dyn. Syst.* **8**, 1462–1506 (2009).
- ¹⁵J. E. Rubin, J. Signerska-Rynkowska, J. D. Touboul, and A. Vidal, "Wild oscillations in a nonlinear neuron model with resets: (I) Bursting, spike-adding and chaos," *Discrete Contin. Dyn. Syst. - B* **22**, 3967–4002 (2017).
- ¹⁶J. E. Rubin, J. Signerska-Rynkowska, J. D. Touboul, and A. Vidal, "Wild oscillations in a nonlinear neuron model with resets: (II) Mixed-mode oscillations," *Discrete Contin. Dyn. Syst. - B* **22**, 4003–4039 (2017).
- ¹⁷B. Ibarz, J. M. Casado, and M. A. F. Sanjuán, "Map-based models in neuronal dynamics," *Phys. Rep.* **501**(1–2), 1–74 (2001).
- ¹⁸E. M. Izhikevich and F. Hoppensteadt, "Classification of bursting mappings," *Int. J. Bifurcat. Chaos* **14**, 3847–3854 (2004).
- ¹⁹N. F. Rulkov, "Regularization of synchronized chaotic bursts," *Phys. Rev. Lett.* **86**, 183–186 (2001).
- ²⁰D. R. Chialvo, "Generic excitable dynamics on a two-dimensional map," *Chaos Solitons Fractals* **5**(3–4), 461–479 (1995).
- ²¹M. Courbage, V. I. Nekorkin, and L. V. Vdovin, "Chaotic oscillations in a map-based model of neural activity," *Chaos* **17**, 043109 (2007).
- ²²H. Korn and P. Faure, "Is there chaos in the brain? II. Experimental evidence and related models," *C. R. Biol.* **326**, 787–840 (2003).
- ²³J. Jaquette, S. Kedia, E. Sander, and J. D. Touboul, "Reliability and robustness of oscillations in some slow-fast chaotic systems," *Chaos* **33**, 103135 (2023).
- ²⁴N. F. Rulkov, "Modelling of spiking-bursting neural behaviour using two-dimensional map," *Phys. Rev. E* **65**, 041922 (2002).
- ²⁵A. L. Shilnikov and N. F. Rulkov, "Subthreshold oscillations in a map-based neuron model," *Phys. Lett. A* **328**, 177–184 (2004).
- ²⁶F. Llovera-Trujillo, J. Signerska-Rynkowska, and P. Bartłomiejczyk, "Periodic and chaotic dynamics in a map-based neuron model," *Math. Meth. Appl. Sci.* **46**, 11906–11931 (2023).
- ²⁷S. Jelbart and C. Kuehn, "Discrete geometric singular perturbation theory," *Discrete Contin. Dyn. Syst. Ser. A* **43**(1), 57–120 (2023).
- ²⁸P. Pilarczyk, J. Signerska-Rynkowska, and G. Graff, "Topological-numerical analysis of a two-dimensional discrete neuron model," *Chaos* **33**, 043110 (2023).
- ²⁹R. Smidtaite and M. Ragulskis, "Finite-time divergence in Chialvo hyperneuron model of nilpotent matrices," *Chaos, Solitons Fractals* **179**, 114482 (2024).
- ³⁰M. Courbage and V. I. Nekorkin, "Map based models in neurodynamics," *Int. J. Bifurcat. Chaos* **20**(6), 1631–1651 (2010).
- ³¹P. Bartłomiejczyk, F. Llovera-Trujillo, and J. Signerska-Rynkowska, "Spike patterns and chaos in a map-based neuron model," *Int. J. Appl. Math. Comput. Sci.* **33**, 395–408 (2023).
- ³²R. FitzHugh, "Mathematical models of the threshold phenomena in the nerve membrane," *Bull. Math. Biophys.* **17**, 257–278 (1955).
- ³³C. Aguirre, D. Campos, P. Pascual, and E. Serrano, "Neuronal behaviour with sub-threshold oscillations and spiking/bursting activity using a piecewise linear two-dimensional map," in *Artificial Neural Networks: Biological Inspirations ICANN 2005* (Springer, Berlin, 2005), pp. 103–108.
- ³⁴B. Cazelles, M. Courbage, and M. Rabinovich, "Anti-phase regularization of coupled chaotic maps modelling bursting neurons," *Europhys. Lett.* **56**, 504 (2001).
- ³⁵O. V. Maslennikov and V. I. Nekorkin, "Dynamic boundary crisis in the Lorenz-type map," *Chaos* **23**, 023129 (2013).
- ³⁶O. V. Maslennikov, V. I. Nekorkin, and J. Kurths, "Transient chaos in the Lorenz-type map with periodic forcing," *Chaos* **28**(3), 033107 (2018).
- ³⁷M. Courbage, O. V. Maslennikov, and V. I. Nekorkin, "Synchronization in time-discrete model of two electrically coupled spike-bursting neurons," *Chaos Solitons Fractals* **45**(5), 645–659 (2012).
- ³⁸A. Hess, L. Yu, I. Klein, M. De Mazancourt, G. Jebrak, H. Mal, O. Brugière, M. Fournier, M. Courbage, G. Dauriat, and E. Schouman-Clayes, "Neural mechanisms underlying breathing complexity," *PLoS One* **8**(10), e75740 (2013).
- ³⁹L. Yu, M. De Mazancourt, and A. Hess, "Functional connectivity and information flow of the respiratory neural network in chronic obstructive pulmonary disease," *Hum. Brain Mapp.* **37**, 2736–2754 (2016).
- ⁴⁰Y. Yue, Y. J. Liu, Y. L. Song, Y. Chen, and L. C. Yu, "Information capacity and transmission in a Courbage-Nekorkin-Vdovin map-based neuron model," *Chin. Phys. Lett.* **34**, 048701 (2017).
- ⁴¹O. V. Maslennikov and V. I. Nekorkin, "Discrete model of the olivo-cerebellar system: structure and dynamics," *Radiophys. Quantum El.* **55**(3), 198–214 (2012).
- ⁴²W. Geller and M. Misiurewicz, "Farey-Lorenz permutations for interval maps," *Int. J. Bifurcat. Chaos* **28**, 1850021 (2018).
- ⁴³F. Rhodes and C. L. Thompson, "Rotation numbers for monotone functions on the circle," *J. Lond. Math. Soc.* **34**(2), 360–368 (1986).
- ⁴⁴A. Katok and B. Hasselblatt, "Introduction to the modern theory of dynamical systems," in *Encyclopedia of Mathematics and its Applications* (Cambridge University Press, Cambridge, 1995).
- ⁴⁵L. Alsedà, J. Llibre, M. Misiurewicz, and C. Tresser, "Periods and entropy for Lorenz-like maps," *Ann. Inst. Fourier (Grenoble)* **39**, 929–952 (1989).
- ⁴⁶A. Granados, L. Alsedà, and M. Krupa, "The period adding and incrementing bifurcations: From rotation theory to applications," *SIAM Rev.* **59**(2), 225–292 (2017).
- ⁴⁷A. Boyarsky and P. Góra, "Laws of chaos. Invariant measures and dynamical systems in one dimension," in *Probability and its Applications* (Birkhäuser Boston, Inc., Boston, MA, 1997).
- ⁴⁸H. Bruin, *Topological and Ergodic Theory of Symbolic Dynamics* (American Mathematical Society, 2023).
- ⁴⁹S. Newhouse, J. Palis, and F. Takens, "Bifurcations and stability of families of diffeomorphisms," *Inst. Hautes Études Sci. Publ. Math.* **57**, 5–71 (1983).
- ⁵⁰V. I. Arnold, "Cardiac arrhythmias and circle mappings," *Chaos* **1**, 20–24 (1991).
- ⁵¹L. Glass, "Synchronization and rhythmic processes in physiology," *Nature* **410**, 277–284 (2001).
- ⁵²D. Reyner-Parra and G. Huguet, "Phase-locking patterns underlying effective communication in exact firing rate models of neural networks," *PLoS Comput. Biol.* **18**, e1009342 (2022).
- ⁵³T. Gedeon and M. Holzer, "Phase locking in integrate-and-fire models with refractory periods and modulation," *J. Math. Biol.* **49**, 577–603 (2004).
- ⁵⁴P. Kasprzak, A. Nawrocki, and J. Signerska-Rynkowska, "Integrate-and-fire models with an almost periodic input function," *J. Differ. Equ.* **264**, 2495–2537 (2018).
- ⁵⁵K. Pakdaman, "Periodically forced leaky integrate-and-fire model," *Phys. Rev. E Stat. Nonlin. Soft Matter Phys.* **63**, 041907 (2001).
- ⁵⁶G. A. Gottwald and I. Melbourne, "The 0-1 test for chaos: A review," in *Chaos Detection and Predictability. Lecture Notes in Physics*, edited by C. Skokos, G. Gottwald, and J. Laskar (Springer, Berlin, 2016), Vol. 915.
- ⁵⁷P. Bartłomiejczyk, F. Llovera Trujillo, and J. Signerska-Rynkowska, *FUPOLibrary*, <https://www.mathworks.com/matlabcentral/fileexchange/135937-fupo-library>, MATLAB Central File Exchange, 2023. Retrieved September 27, 2023.
- ⁵⁸P. Bartłomiejczyk, F. Llovera Trujillo, and J. Signerska-Rynkowska, *FUPOLibrary*, <https://github.com/bartlomiejczyk/FUPOLibrary>, GitHub repository, 2023. Retrieved September 27, 2023.
- ⁵⁹A. Lempel and J. Ziv, "On the complexity of finite sequences," *IEEE Trans. Inf. Theory* **22**(1), 75–81 (1976).

⁶⁰G. S. Bortolotto, R. V. Stenzinger, and M. H. R. Tragtenberg, “Electromagnetic induction on a map-based action potential model,” *Nonlinear Dyn.* **95**, 433–444 (2019).

⁶¹A. Kameyama, “Topological transitivity and strong transitivity,” *Acta Math. Univ. Comenianae (N.S.)* **71**(2), 139–145 (2002), see http://www.iam.fmph.uniba.sk/amuc/_vol-71/_no_2/_kameyama/kameyama.pdf.

⁶²M. Misiurewicz, “Rotation intervals for a class of maps of the real line into itself,” *Ergod. Theory Dyn. Syst.* **6**(1), 117–132 (1986).

⁶³P. Oprocha, P. Potorski, and P. Raith, “Mixing properties in expanding Lorenz maps,” *Adv. Math.* **343**, 712–755 (2019).

⁶⁴A. Peris, “Transitivity, dense orbit and discontinuous functions,” *Bull. Belg. Math. Soc. Simon Stevin* **6**, 391–394 (1999).

FRANK FERNANDO LLOVERA TRUJILLO  * (Gdańsk)

On computing periodic orbits itineraries for Lorenz-like maps

Abstract Existence and structure of periodic orbits is an important part of the investigation of dynamical systems. However, analytical calculations are possible only in very few cases and numerical identification of periodic orbits is possible only when these are attracting for a large set of initial conditions. This in particular constitutes a challenge especially in chaotic systems. In this work, following theoretical findings of W. Geller and M. Misiurewicz(2018), we outline a procedure that allows for determining the itineraries of vast majority of periodic orbits of Lorenz-like maps. We provide explicit algorithms with ready-to-use computational tools available in open repositories. Since Lorenz-like maps arise as subsystems of many complex models and are prevalent in various applications, our results open a way of investigation of their periodic structure

2010 2020 Mathematics Subject Classification: Primary: 37E05, 37-04; Secondary: 37E45, 37E15.

Key words and phrases: Lorenz-like maps, periodic orbits, itinerary, rotation interval, Farey-Lorenz permutations, random binary sequences..

1. Introduction

The following work aims at providing a tool that may help studying the structure of itineraries of periodic orbits for Lorenz-like maps and their complexity. Lorenz-like maps have received a lot of attention from the mathematical community in recent decades ([8], [1], [11]) but they also appear commonly in various applications. In particular, they appeared as the Poincare map of the geometric Lorenz model ([6]). One of other examples is the Courbage-Nekorkin-Vdovin (CNV for short) neuron model ([7]) where the dynamics of the membrane voltage variable is described by means of a Lorenz-like map.

Although there is a well-developed theory with applications regarding Lorenz-like maps and their periodic orbits, there is still the need to develop an user friendly software that could be applied by other mathematicians and for modeling various phenomena, for example, spike patterns in CNV model ([2, 3]) or mixed-mode oscillations in hybrid neuron models ([13]), where Lorenz-like maps appear as a sort of reduction of higher-dimensional models.

* The presented work was supported by NCN (National Science Centre, Poland) grant no. 2019/35/D/ST1/02253.

This work is primarily motivated by a previous research of the CNV model [2, 3] in which we address the importance and possible influence of identifying itineraries of periodic orbits for the model. This paper introduces the algorithms that allow to find itineraries of periodic orbits that can be applied not only to the CNV model but to any Lorenz-like map.

The organization of the paper is as follows. Section 2 contains some preliminaries of Lorenz-like maps, rotation theory, and Farey sequences. In Section 3 we recall definitions and results of fupos and Farey-Lorenz permutations. Our proposed algorithms are introduced in Section 4 along with some examples of their use in Section 5. Finally in section 6 we discuss the LZ-Complexity of sequences generated by one of our main algorithms and make a complexity comparison with other type of sequences (random and periodic.)

2. Preliminaries Below we present basic definitions and tools that are used throughout the paper.

2.1. Lorenz-like maps A *Lorenz-like map* is a map f of an interval $[0, 1]$ to itself, for which there exists a point $c \in (0, 1)$ such that

- f is continuous and increasing (not necessarily strictly) on $[0, c)$ and on $(c, 1]$,
- $\lim_{x \rightarrow c^-} f(x) = 1$ and $\lim_{x \rightarrow c^+} f(x) = f(c) = 0$.

Set $I_L = [0, c)$ and $I_R = [c, 1]$. If $f(0) \geq f(1)$, the Lorenz-like map f is called *non-overlapping*. Otherwise, i.e., if $f(0) < f(1)$, the map is called *overlapping*. See Figure 1 for examples of both types of maps.

The *itinerary* of $x \in [0, 1]$ under f is the sequence $s(x) = (s_0 s_1 s_2 \dots)$ where

$$s_j = \begin{cases} 0 & \text{if } f^j(x) \in I_L, \\ 1 & \text{if } f^j(x) \in I_R. \end{cases}$$

and $f^j(x) = f \circ \dots \circ f(x)$ denotes the j -fold composition of f with itself.

An important sub-class of Lorenz-like maps are expanding Lorenz maps: An *expanding Lorenz map* is a map $f: [0, 1] \rightarrow [0, 1]$ satisfying the following three conditions:

- there is a *critical point* $c \in (0, 1)$ such that f is continuous and strictly increasing on $[0, c)$ and $(c, 1]$,
- $\lim_{x \rightarrow c^-} f(x) = 1$ and $\lim_{x \rightarrow c^+} f(x) = f(c) = 0$,
- f is differentiable for all points not belonging to a finite set $\Omega \subset [0, 1]$ and such that

$$\inf \{f'(x) \mid x \in [0, 1] \setminus \Omega\} > 1.$$

However, our results herein hold for Lorenz-like maps in general (i.e. not necessarily expanding).

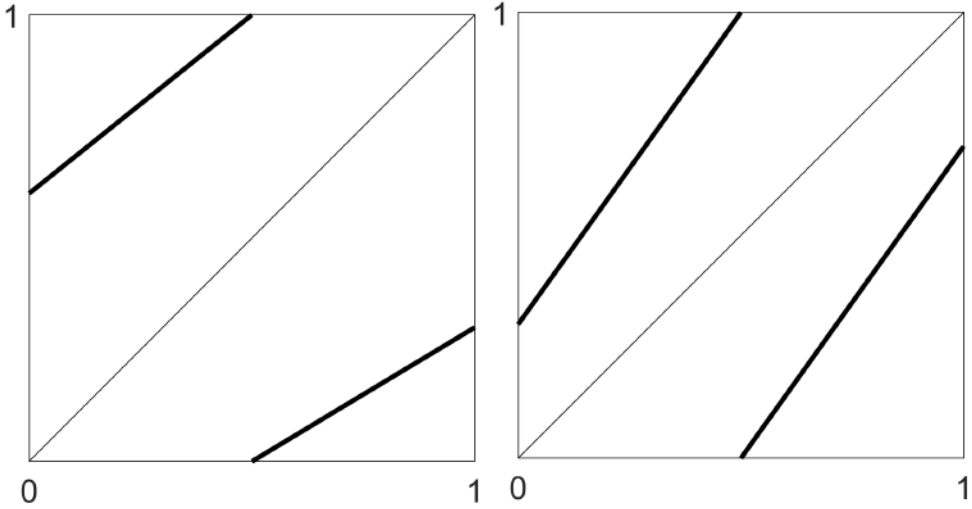


Figure 1: A non-overlapping map (left) and an overlapping map (right)

2.2. Rotation number

Unless otherwise stated we assume that f is a Lorenz-like map.

DEFINITION 2.1 For a point $x \in [0, 1]$ and a positive integer n we will denote by $R(x, n)$ the number of integers $i \in \{0, \dots, n-1\}$ such that $f^i(x) \in I_R$. If the limit

$$\rho(x) = \lim_{n \rightarrow \infty} \frac{R(x, n)}{n}$$

exists, we will call it the *rotation number* of x .

Immediately from the definition we obtain the following result.

PROPOSITION 2.2 *If x is a periodic point of f of period p then $\rho(x)$ exists and is equal to $R(x, p)/p$.*

2.3. Rotation number of non-overlapping Lorenz like maps

The following theorem is a well known result from [12].

THEOREM 2.3 (RHODES-THOMPSON) *If $f(0) \geq f(1)$, i.e., if the map is nonoverlapping, then all points have the same rotation number.*

In that case we will denote it by $\rho(f)$.

2.4. Rotation interval of an overlapping Lorenz like map

Let f be a Lorenz-like map. If $t \in f(I_L) \cap f(I_R)$, then we define the *water map* at level t by

$$f_t(x) = \begin{cases} \max(t, f(x)) & \text{if } x \in I_L, \\ \min(t, f(x)) & \text{if } x \in I_R. \end{cases}$$

The water map is indeed a Lorenz-like map and $f_t(0) = f_t(1)$ (see Figure 2). Consequently, for fixed t , all points have the same rotation number $\rho(f_t)$ for it. It is known that $\rho(f_t)$ is an increasing continuous function of t , and if $f(0) \leq f(1)$, then the set of the rotation numbers for f of all points having rotation number is equal to the interval $[\rho(f_{f(0)}), \rho(f_{f(1)})]$ (see, e.g. [1, 8] for details). We will call it the *rotation interval* of f and denote it by $\text{Rot}(f)$.

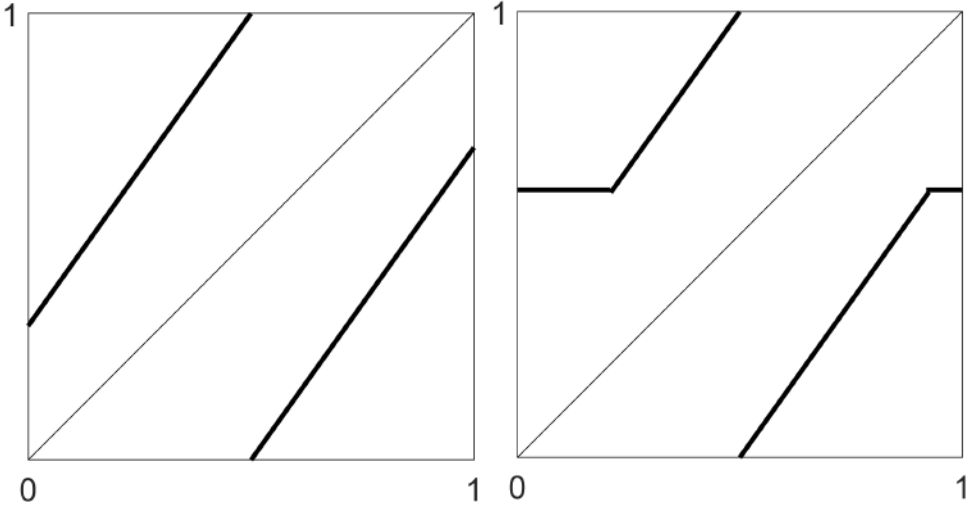


Figure 2: An overlapping map and its water map when $t = f(0)$.

2.5. Farey sequence In this section we recall several results on Farey sequences, mainly from [9, Ch. 4], that will be used in our algorithms to produce Farey sequences of an specific order.

DEFINITION 2.4 Let $\frac{m}{n}$ and $\frac{m'}{n'}$ be two adjacent fractions. The fraction $\frac{m+m'}{n+n'}$ is called the *mediant* of $\frac{m}{n}$ and $\frac{m'}{n'}$.

For example, if we start with $\frac{1}{2}$ and $\frac{1}{1}$ we can produce the following sequences by inserting in each step the mediant of every pair of adjacent fractions:

$$\frac{1}{2}, \frac{2}{3}, \frac{1}{1}$$

$$\frac{1}{2}, \frac{3}{5}, \frac{2}{3}, \frac{3}{4}, \frac{1}{1}.$$

Notice that if we start this process with the pair $\frac{0}{1}$ and $\frac{1}{1}$, we can construct the set of all non-negative irreducible fractions.

DEFINITION 2.5 The *Farey sequence* of order N , F_N , is the set of all fractions in lowest terms and in increasing order, with denominators less or equal than N . F_N can be obtained by starting with $\frac{0}{1}$ and $\frac{1}{1}$, and inserting mediant whenever possible, considering the restriction of denominators. Two consecutive elements of the Farey sequence of a given order are called *Farey neighbours*.

For example,

$$F_4 = \frac{0}{1}, \frac{1}{4}, \frac{1}{3}, \frac{1}{2}, \frac{2}{3}, \frac{3}{4}, \frac{1}{1}.$$

It follows that $m'n - mn' = 1$ whenever $\frac{m}{n}$ and $\frac{m'}{n'}$ are consecutive terms of a Farey sequence.

It is simple to observe that F_N can be obtained from F_{N-1} by inserting $\frac{m+m'}{N}$ between two consecutive fractions $\frac{m}{n}$ and $\frac{m'}{n'}$ of F_{N-1} whose denominators sum to N . When N is prime, exactly new $N - 1$ fractions will appear, otherwise the number new fractions will be less, because only new fractions with numerators that are co-prime with N are generated.

For example, starting with

$$F_4 = \frac{0}{1}, \frac{1}{4}, \frac{1}{3}, \frac{1}{2}, \frac{2}{3}, \frac{3}{4}, \frac{1}{1}.$$

F_5 can be obtained by inserting $\frac{1}{5}, \frac{2}{5}, \frac{3}{5}$ and $\frac{4}{5}$:

$$F_5 = \frac{0}{1}, \frac{1}{5}, \frac{1}{4}, \frac{1}{3}, \frac{2}{5}, \frac{1}{2}, \frac{3}{5}, \frac{2}{3}, \frac{3}{4}, \frac{4}{5}, \frac{1}{1}.$$

The following result is formulated as Exercise 61 in Section 4 of [9]. It forms a base for an easy inductive construction of the Farey sequence of the order N and will be used in our algorithms.

PROPOSITION 2.6 Let $\frac{m}{n}$, $\frac{m'}{n'}$ and $\frac{m''}{n''}$ be three consecutive elements of the Farey sequence of order N , then:

$$m'' = \lfloor (n + N)/n' \rfloor m' - m$$

$$n'' = \lfloor (n + N)/n' \rfloor n' - n$$

2.6. Periodic, aperiodic and essential binary sequences and essential classes This subsection deals with finite binary sequence, which play crucial role in our study of itineraries of Lorenz-like maps.

Recall that a finite binary sequence is called *periodic* if it can be written as a repetition of a binary sequence of smaller length. For example: 010101 is

periodic because it can be obtained by repeated appending of 01 to itself. A finite binary sequence is called *aperiodic* if it is not periodic.

The set of all aperiodic binary sequences of the fixed length n can be divided into classes in a such way that each class consists of all shifts of a given sequence. These classes will be called *essential*. Now let us find formulas for the number of all aperiodic binary sequences of the length n and the number of corresponding essential classes.

Recall that the *Möbius function* $\mu: \mathbb{N} \rightarrow \{-1, 0, 1\}$ is given by:

$$\mu(n) = \begin{cases} 0 & \text{if } n \text{ has one or more repeated prime factors,} \\ 1 & \text{if } n = 1, \\ (-1)^k & \text{if } n \text{ is a product of } k \text{ distinct primes.} \end{cases}$$

The Möbius function appears in the famous *Möbius inversion formula*, which gives a relation between pairs of arithmetic functions in terms of sums over divisors. The notation $a \setminus b$ means that a divides b and $\sum_{d \setminus n}$ is the sum over all divisors of n .

THEOREM 2.7 (INVERSION MÖBIUS THEOREM) Assume that f and g are functions from \mathbb{N} to \mathbb{C} . If $g(n) = \sum_{d \setminus n} f(d)$, then

$$f(n) = \sum_{d \setminus n} \mu(d) g\left(\frac{n}{d}\right).$$

COROLLARY 2.8 Let $f(n)$ be the number of aperiodic binary sequences of length n . Then

$$f(n) = \sum_{d \setminus n} \mu(d) 2^{\frac{n}{d}}$$

PROOF Note that the set of all binary sequences of the length n is a pairwise disjoint union of the set aperiodic sequences of the length n and the sets of periodic sequences with prime periods d dividing n (corresponding bijectively to aperiodic sequences of the length d). Thus

$$\sum_{d \setminus n} f(d) = 2^n,$$

which, by Theorem 2.7, immediately gives our assertion. ■

Let us emphasize two important consequences of Corollary 2.8. Firstly, if n is prime then $f(n) = 2^n - 2$. Secondly, the number of essential classes is given by

$$\frac{\sum_{d \setminus n} \mu(d) 2^{\frac{n}{d}}}{n},$$

because each essential class contains exactly n shifts of some aperiodic sequences of the length n .

3. Fupo theory

In this section we recall important definitions and results on fupos based on [8].

A finite union of periodic orbits of f is called a *fupo*. For each fupo we will consider its permutation, that is, if a fupo P consists of points $x_1 < \dots < x_n$, and $f(x_i) = x_{\sigma(i)}$ for $i = 1, \dots, n$, then σ is the permutation of P .

Permutations of fupos of Lorenz-like maps have a specific form. Namely, if a fupo has $n > 1$ elements, then there exists $k \in \{1, \dots, n-1\}$ such that σ is increasing on $\{1, \dots, k\}$ and on $\{k+1, \dots, n\}$. We will call such permutations (and the permutation of $\{1\}$) *L-permutations*. If our fupo is a periodic orbit, then its rotation number is $(n-k)/n$.

Among L-permutations there are some special ones, which look like cyclic permutations for circle rotations. A cyclic L-permutation σ of $\{1, \dots, n\}$ will be called a *twist* permutation if $\sigma(1) > \sigma(n)$. Similarly, a periodic orbit with such a permutation will be called a *twist* orbit. It is easy to describe explicitly a twist permutation of $\{1, \dots, n\}$ with rotation number j/n . Note that a twist permutation of $\{1, \dots, n\}$ with rotation number j/n has a form

$$\sigma(i) = i + j \pmod n.$$

In consequence, the k th term of the twist periodic itinerary is L if and only

$$(kp \pmod q) < q - p.$$

An L-permutation σ of $\{1, \dots, p+q\}$ will be called a *Farey-Lorenz permutation* (or *FL-permutation*) if σ consists of two cycles, both of them twist, of period p and q , with rotation numbers a/p and b/q respectively, and $a/p < b/q$ are Farey neighbours, that is, $bp = aq + 1$.

Let us assume that σ is an FL-permutation with cycles of rotation numbers a/p and b/q , where $a/p < b/q$ are Farey neighbours and $p < q$. We will call those cycles *slow* and *fast*, respectively. Note that:

- the slow cycle contains 1, and the fast cycle contains $p+q$,
- the fast cycle contains 2.

We will refer to P as the slow orbit and Q as the fast orbit. Let the points of P be $x_1 < x_2 < \dots < x_p$ and the points of Q , $y_1 < y_2 < \dots < y_q$. Denote $J_1 = [x_1, y_1]$ and $J_j = [y_{j-1}, y_j]$ for $j = 2, \dots, q$.

PROPOSITION 3.1 *With the notation we adopted,*

$$f(x_i) = x_{i+a \pmod p} \quad \text{and} \quad f(y_j) = y_{j+b \pmod q}.$$

The relative order of the points of the orbits P and Q is given by the following rule: $x_1 < y_1$; then for $i = 1, \dots, p-1$, if $j = 1 + ia \pmod p$ and $l = ib \pmod q$, then $y_{l-1} < x_j < y_l$.

The following result describes the so-called *fupo effect*, i.e., the way, in which a pair of special periodic orbits (fupo with FL) “produce” infinitely many new periodic orbits with itineraries being concatenations of itineraries of starting two periodic orbits (see Figures 3 and 4).

THEOREM 3.2 *Let f be a Lorenz-like map. Assume that the rotation interval of g contains the interval $[a/p, b/q]$, where $a/p < b/q$ are Farey neighbours, and $p < q$. Then*

1. *there exist periodic orbits P and Q , with rotation numbers a/p and b/q respectively,*
2. *for each finite binary sequence being a finite concatenation of finitely many itineraries of P and Q , there is a unique periodic orbit, which itinerary corresponds to this sequence.*

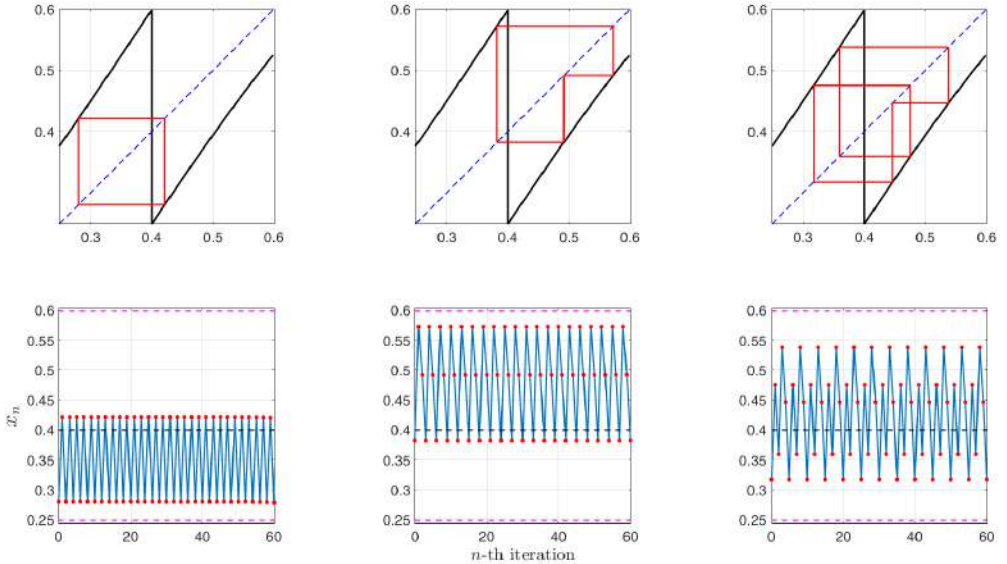


Figure 3: Fupo effect from Theorem 3.2 for periodic orbits with rotation numbers being Farey neighbours $1/2 < 2/3$. The new periodic orbit has rotation number $3/5$.

REMARK 3.3 If $a/p < b/q$, but $p > q$, then we replace a/p by $(p - a)/p$ and b/q by $(q - b)/q$. Then, in the itineraries we replace symbols L by R and vice versa.

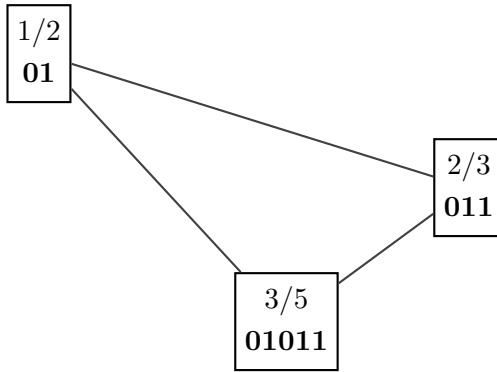


Figure 4: Concatenation of itineraries for the Farey neighbours $1/2 < 2/3$.

Theorem 3.2 is the main subject of interest of this paper and in what follows we will study it from computational point of view. We provide algorithms enabling the construction of periodic orbit itineraries as concatenations of fupo provided by this theorem.

4. Algorithms In this section we present pseudo-codes of algorithms implementing the theory included in previous theoretical sections, in particular allowing to calculate the rotation interval, its inner approximation by an interval with endpoints being Farey neighbors and concatenations of corresponding periodic orbits itineraries. Detailed algorithms have been coded in MATLAB scripts and are freely available in open repositories [4] and [5].

4.1. Algorithms on rotation interval The definition of *rotation interval* requires previous definitions of *water maps* and *rotation number* (see Subsection 2.4 for details). The same order must be followed when listing the algorithms. So let us start with the algorithm describing the construction of water map. In fact, we define the whole family of water maps associated to a given Lorenz-like map and parametrized by real parameter t .

Algorithm 1 Construction of the water map for a given Lorenz-like map

Input: a Lorenz-like map f and a real number t **Output:** the water map f_t

```

1: procedure WATERMAP( $f, t$ )
2:   if  $x < d$  then                                      $\triangleright d$  is a discontinuity point of  $f$ 
3:      $f_t(x) \leftarrow \max(t, f(x))$ 
4:   else
5:      $f_t(x) \leftarrow \min(t, f(x))$ 
6:   end if
7:   return the map  $f_t$ 
8: end procedure

```

According to Subsection 2.2 for non-overlapping Lorenz-like maps we can define rotation number as a limit (see Definition 2.1), but the approximate value of rotation number can be calculated using the following simple algorithm. The larger number of iteration we take, the better approximation we obtain, but the result will be always rational. Observe that the choice of a non-overlapping Lorenz-like map determines the invariant interval (the domain) and the discontinuity point.

Algorithm 2 Computation of the rotation number of a non-overlapping Lorenz-like map

Input: a non-overlapping Lorenz-like map f , a discontinuity point d , an initial point of iterations z and a total number of iterations n **Output:** the rotation number r $\triangleright r$ is a rational number from the interval $[0, 1]$

```

1: procedure ROTATIONNUMBER( $f, d, z, n$ )
2:    $k \leftarrow 0$ 
3:   for  $i \leftarrow 1$  to  $n$  do
4:     if  $d \leq z$  then                                      $\triangleright d$  is a discontinuity point of  $f$ 
5:        $k \leftarrow k + 1$ 
6:     end if
7:      $z \leftarrow f(z)$                                       $\triangleright$  take the next iteration of  $f$ 
8:   end for
9:    $r \leftarrow k/n$ 
10:  return the number  $r$ 
11: end procedure

```

Now, using two previous algorithms we can construct rotation interval for an overlapping Lorenz-like map. Rotation interval is determined by its endpoints, which are rotation numbers of two water-maps being in turn a non-overlapping Lorenz maps.

Algorithm 3 Computation of the rotation interval of an overlapping Lorenz-like map

Input: an overlapping Lorenz-like map f , a discontinuity point d , an initial point of iterations z and a total number of iterations n

Output: the endpoints of rotation interval $[r_0, r_1]$.

```

1: procedure ROTATIONINTERVAL( $f, d, z, n$ )
2:    $f_{\text{down}} \leftarrow \text{WATERMAP}(f, f(0))$ 
3:    $f_{\text{up}} \leftarrow \text{WATERMAP}(f, f(1))$ 
4:    $r_0 \leftarrow \text{ROTATIONNUMBER}(f_{\text{down}}, d, z, n)$ 
5:    $r_1 \leftarrow \text{ROTATIONNUMBER}(f_{\text{up}}, d, z, n)$ 
6:   return two numbers  $r_0, r_1 \triangleright r_0, r_1$  are rational and  $0 \leq r_0 \leq r_1 \leq 1$ 
7: end procedure
```

4.2. Three auxiliary algorithms on finite sequences In what follows we will use three simple auxiliary algorithms related to finite sequences. Two first ones work with finite increasing sequences of real numbers. The third one concerns finite binary sequences.

Algorithm 4 Searching for the longest subinterval $B = [a, b]$ of an increasing finite sequence A such that a, b are consecutive elements in A

Input: an increasing list of real numbers A

Output: the longest subinterval B \triangleright ends of B must be consecutive elements of A

```

1: procedure LONGESTSUBINTERVAL( $A$ )
2:    $B \leftarrow []$   $\triangleright B$  is an empty list
3:    $n \leftarrow \text{LENGTH}(A)$   $\triangleright \text{LENGTH}(A)$  returns the number of elements of
     the sequence  $A$ 
4:   if  $n \leq 1$  then
5:     return  $B$ 
6:   else
7:      $a \leftarrow A[1]; b \leftarrow A[2]$ 
8:   end if
9:   for  $i \leftarrow 3$  to  $n$  do
10:    if  $A[i] - A[i-1] > b - a$  then
11:       $a \leftarrow A[i-1]; b \leftarrow A[i]$ 
12:    end if
13:  end for
14:   $B \leftarrow [a \ b]$ 
15:  return the two-element list  $B$   $\triangleright$  elements of  $B$  are real and
     increasing
16: end procedure

```

The algorithm below produces a sub sequence B of a finite increasing sequence A , which is contained in a fixed interval $[a, b]$.

Algorithm 5 Searching for subsequence contained in a fixed interval

Input: an increasing list of real numbers A and $a < b$ endpoints of the interval

Output: the subsequence B of A contained in $[a, b]$

```

1: procedure SEQINSIDEINTERVAL( $A, a, b$ )
2:    $B \leftarrow []$   $\triangleright B$  is an empty list
3:    $n \leftarrow \text{LENGTH}(A)$ 
4:   for  $i \leftarrow 1$  to  $n$  do
5:     if  $a \leq A(i) \leq b$  then
6:        $B \leftarrow [B \ A(i)]$ 
7:     end if
8:   end for
9:   return the sequence  $B$   $\triangleright B$  is an increasing list of real numbers
10: end procedure

```

The following algorithm allows to produce a binary sequence T , starting

from three binary sequences S , A and B , by taking sequence S and replacing each 0 element in S by sequence A and each 1 by sequence B .

Algorithm 6 Replacing all occurrences of 0 with A and 1 with B in a given binary sequence S

Input: three finite binary sequences S , A , B

Output: the finite binary sequence T

```

1: procedure SUBSTITUTION( $S, A, B$ )
2:    $T \leftarrow []$  ▷  $T$  is an empty array
3:    $n \leftarrow \text{LENGTH}(S)$ 
4:   for  $i \leftarrow 1$  to  $n$  do
5:     if  $S(i) = 0$  then
6:        $T \leftarrow [T \ A]$ 
7:     else
8:        $T \leftarrow [T \ B]$ 
9:     end if
10:  end for
11:  return the sequence  $T$ 
12: end procedure

```

4.3. Algorithms on Farey numbers and sequences

The following algorithm allows to generate the Farey sequence of order n , based on the formula given in Proposition 2.6.

Algorithm 7 Generating the Farey sequence of order n

Input: a natural number n

Output: the Farey sequence A of n -th order.

```

1: procedure FAREYSEQUENCE( $n$ )
2:    $A \leftarrow [0]$  ▷ one-element list containing 0
3:    $a \leftarrow 0; b \leftarrow 1; c \leftarrow 1; d \leftarrow n$ 
4:   while  $c \leq n$  do
5:      $k \leftarrow \lfloor (n + b)/d \rfloor$ 
6:      $a_{\text{new}} \leftarrow c; b_{\text{new}} \leftarrow d; c_{\text{new}} \leftarrow k \cdot c - a; d_{\text{new}} \leftarrow k \cdot d - b$ 
7:      $a \leftarrow a_{\text{new}}; b \leftarrow b_{\text{new}}; c \leftarrow c_{\text{new}}; d \leftarrow d_{\text{new}}$ 
8:      $A \leftarrow [A \ a/b]$ 
9:   end while
10:  return the Farey sequence  $A$ 
11: end procedure

```

The algorithm below produces the best approximation of a given interval $[a, b] \subset [0, 1]$ by a subinterval $[a', b'] \subset [a, b]$ with endpoints a' and b' being Farey neighbours in a Farey tree of depth n , where by the best approximation we mean the longest subinterval among such subintervals.

Algorithm 8 Approximation of a given interval from inside by Farey neighbours

Input: a natural number n and ends of the interval $[a, b] \triangleright n$ corresponds to the deepest examined Farey level

Output: the two-element list C of Farey neighbours approximating the interval $[a, b]$ from inside

```

1: procedure OPTIMALFAREYNGHBS( $n, a, b$ )
2:   for  $i \leftarrow 1$  to  $n$  do
3:      $A \leftarrow \text{FAREYSEQUENCE}(i)$ 
4:      $B \leftarrow \text{SEQINSIDEINTERVAL}(A, a, b)$ 
5:      $C \leftarrow \text{LONGESTSUBINTERVAL}(B)$   $\triangleright C$  may be empty
6:     if  $C$  is non-empty then
7:       break  $\triangleright$  use first non-empty  $C$  found and do not go deeper
8:     end if
9:   end for
10:  return the two-element list  $C$ 
11: end procedure

```

The next algorithm allows to compute the itinerary of a q -periodic orbit with rotation number p/q , according to the formula in Proposition 3.1. The itinerary will be a chain of 0 and 1, representing positions to the left or right hand side of the discontinuity point of the Lorenz-like map as stated directly in Subsection 2.1.

Algorithm 9 Creating the itinerary of a periodic orbit with rotation number p/q

Input: two natural coprime numbers $p < q$

Output: the itinerary A $\triangleright A$ is a binary sequence of the length q

```

1: procedure ROTATIONSEQUENCE( $p, q$ )
2:   for  $i \leftarrow 1$  to  $q$  do
3:     if  $\text{REM}((i-1)p, q) < q-p$  then  $\triangleright \text{REM}(a, b)$  is the remainder
       after division of  $a$  by  $b$ 
4:        $A(i) \leftarrow 0$ 
5:     else
6:        $A(i) \leftarrow 1$ 
7:     end if
8:   end for
9:   return the binary sequence  $A$ 
10: end procedure

```

4.4. Algorithms on essential patterns and general concatenations

The following algorithm produces all essential patterns. Recall that essential patterns form a subset of all binary sequences of a given length. Roughly speaking essential means here: not being of a smaller period and not being a shift of other pattern.

Algorithm 10 Generating the sequence of all essential patterns of length n .

Input: a natural number n

Output: the finite sequence A of all essential sequences \triangleright terms of A are binary sequences of length the n

```

1: procedure ESSENTIALSEQ( $n$ )
2:    $A \leftarrow \text{BINARY}(n) \triangleright \text{BINARY}(n)$  is the sequence of all binary sequences
   of the length  $n$ 
3:    $j \leftarrow 1$ 
4:   while  $j \leq \text{LENGTH}(A)$  do  $\triangleright$  remove all smaller periods
5:     if  $A[j]$  is periodic of period smaller than  $n$  then
6:       REMOVE( $A, A[j]$ )  $\triangleright$  REMOVE( $A, A[j]$ ) removes  $A[j]$  from  $A$ 
       and reduces LENGTH( $A$ ) by 1
7:     end if
8:      $j \leftarrow j + 1$ 
9:   end while
10:   $m \leftarrow 1$ 
11:  while LENGTH( $A$ )  $- m > 0$  do  $\triangleright$  remove all shifts of  $A[m]$ 
12:     $i \leftarrow m + 1$ 
13:    while  $i \leq \text{LENGTH}(A)$  do
14:      if  $A[i]$  is a shift of  $A[m]$  then
15:        REMOVE( $A, A[i]$ )
16:      end if
17:    end while
18:     $m \leftarrow m + 1$ 
19:  end while
20:  return the finite sequence  $A$  of finite binary sequences  $\triangleright$  each term
   of  $A$  has the length  $n$ 
21: end procedure

```

In turn, the algorithm ESSENTIALCONCAT produces all possible concatenations of two sequences A and B , generated on the base of all essential patterns of a given length n . Roughly speaking, we just replace 0 by A and 1 by B in all essential patterns produced by the previous algorithm ESSENTIALSEQ.

Algorithm 11 Generating essential concatenations of two finite binary sequences

Input: a natural number n , two finite binary sequences A and B

Output: the sequence C of concatenation of A and B according to all essential patterns of length n

```

1: procedure ESSENTIALCONCAT( $n, A, B$ )
2:    $P \leftarrow \text{ESSENTIALSEQ}(n)$        $\triangleright P$  is a finite sequence of finite binary
      sequences of length  $n$ 
3:    $m \leftarrow \text{LENGTH}(P)$        $\triangleright m$  is the number of all essential sequences of
      length  $n$ 
4:   for  $i \leftarrow 1$  to  $m$  do
5:      $C[j] \leftarrow \text{SUBSTITUTE}(P[j], A, B)$    $\triangleright$  both  $P[j]$  and  $C[j]$  are finite
      binary sequences
6:   end for
7:   return the finite sequence  $C$  of concatenations  $\triangleright$  the terms of  $C$  are
      of different length
8: end procedure

```

4.5. Main algorithm

The final effect of our construction is the following complex algorithm FUPOCONCAT, that resembles a script combining the main previous algorithms. Let us discuss briefly how it works:

1. firstly we compute the rotation interval corresponding to an overlapping Lorenz-like map (procedure ROTATIONINTERVAL),
2. then we find optimal Farey neighbours $a/p < b/q$ inside this rotation interval (procedure OPTIMALFAREYNGHBS),
3. next we generate finite itineraries A and B corresponding to this Farey neighbours (procedure ROTATIONSEQUENCE),
4. finally we generate all essential concatenations of A and B following the set of essential patterns (procedure ESSENTIALCONCAT).

Algorithm 12 Main procedure — generating concatenation of itineraries of fupo

Input: an overlapping Lorenz-like map f , the discontinuity point c , the initial point x , the total number of iterations n , the Farey level m and the length of concatenation pattern k

Output: the finite sequence C of concatenations of itineraries of fupo

```

1: procedure FUPONCAT( $f, c, x, n, m, k$ )
2:    $[r \ s] \leftarrow \text{ROTATIONINTERVAL}(f, c, x, n)$   $\triangleright r < s$  are real numbers
3:    $X \leftarrow \text{OPTIMALFAREYNGHBS}(m, r, s)$ 
4:   if  $X$  is empty then  $\triangleright X$  is empty if we are not deep enough in the
     Farey tree
5:      $C \leftarrow []$   $\triangleright$  procedure terminated unsuccessfully; assign an empty
     list to the output
6:   else
7:      $[u \ v] \leftarrow X$   $\triangleright$  success;  $u < v$  are Farey neighbours in the form of
     irreducible fractions
8:   end if
9:    $[a \ p] \leftarrow \text{NUMDEN}(u)$   $\triangleright \text{NUMDEN}(u)$  returns the numerator and
     denominator of the fraction  $u$ 
10:   $[b \ q] \leftarrow \text{NUMDEN}(v)$ 
11:  if  $p > q$  then  $\triangleright$  the basic case is  $p < q$ ; the case  $p > q$  requires
     technical adjustments (some swaps)
12:     $olda \leftarrow a$ ;  $oldp \leftarrow p$ 
13:     $a \leftarrow q - b$ ;  $p \leftarrow q$ 
14:     $b \leftarrow oldp - olda$ ;  $q \leftarrow oldp$ 
15:  end if
16:   $A \leftarrow \text{ROTATIONSEQUENCE}(a, p)$ 
17:   $B \leftarrow \text{ROTATIONSEQUENCE}(b, q)$ 
18:  if  $p > q$  then  $\triangleright$  one more adjustment in the non-basic case  $p > q$ 
19:     $A \leftarrow 1 - A$   $\triangleright$  replacing in  $A$  all 0 by 1 and vice versa
20:     $B \leftarrow 1 - B$   $\triangleright$  the same for  $B$ 
21:  end if
22:   $C \leftarrow \text{ESSENTIALCONCAT}(k, A, B)$ 
23:  return the finite sequence  $C$  of finite binary sequences  $\triangleright$  the terms
     of  $C$  have different lengths
24: end procedure

```

The tree from Figure 5 depicts the relation between all twelve algorithms from Section 4 using the abbreviations from Table 1.

5. Examples

We use MATLAB programs, implementing the algorithms developed in previous sections, and included in open repositories [4] and [5] to show some

Table 1: Abbreviations of names the algorithms.

abbreviation	Algorithm Name
FC	FupoConcat
EC	EssentialConcat
ES	EssentialSeq
RS	RotationSequence
OFN	OptimalFareyNghbs
FS	FareySequence
S	Substitution
SII	SeqInsideInterval
LS	LongestSubinterval
RI	RotationInterval
RN	RotationNumber
WM	WaterMap

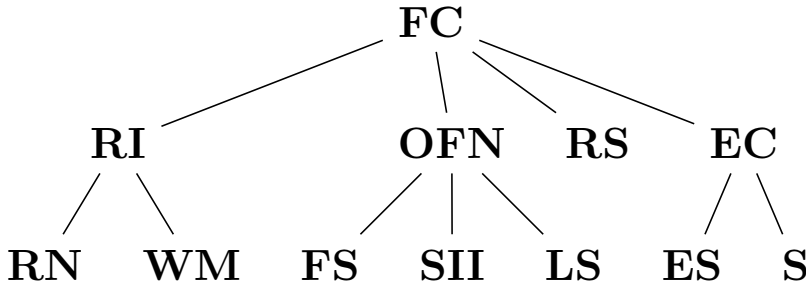


Figure 5: The relation between the algorithms.

particular numerical examples. The first two examples of Lorenz-like maps are beta transformations $T = \beta x + \alpha$ where the discontinuity point is $d = \frac{1-\alpha}{\beta}$, while the example 3 depicts a quadratic Lorenz-Like map with discontinuity point in $d = \frac{1}{2}$.

For convenience we denote itineraries of periodic orbits by 0-1 sequences, instead of L - R sequences (i.e. 0 and 1 replace, respectively, L and R in encoding periodic orbits). Moreover, let a^i denote the repetition of the symbol or string a for i times.

Let us now describe the course of our simulations. First, we compute the rotation interval of a given Lorenz-like map (see Algorithms 2 and 3). Then we find inside the rotation interval the longest subinterval which endpoints are Farey neighbours (Algorithms 8). Finally, we produce

- finite periodic parts of the itineraries corresponding to these Farey neighbours according to the formula from Algorithm 9 (denote these parts by X and Y),

- all concatenations of X and Y of a given *order* n , i.e., formed by taking n blocks (each of them is X or Y) concatenating all of them (see Algorithms 11 and 12 for details).

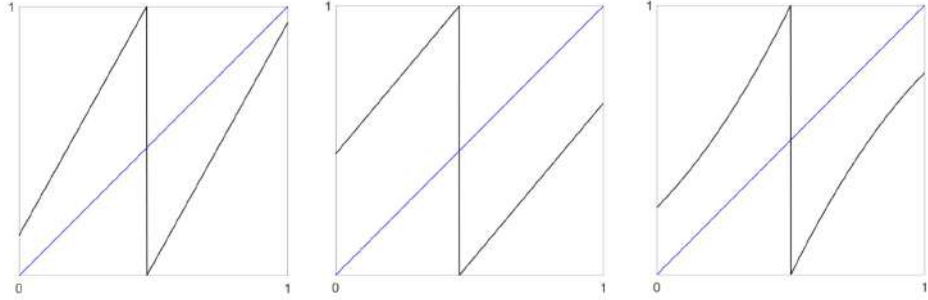


Figure 6: Plots of the maps from Examples 5.1, 5.2 and 5.3 (from the left to the right)

EXAMPLE 5.1 Our first example is a beta transformation: $T(x) = 1.79x + 0.15$ with a relatively large slope (see left panel of Figure 6). This is in turn reflected in the relatively large rotation interval, which is equal to $[0.333, 0.75]$. Now we approximate the rotation interval from inside with Farey neighbours: $1/2 < 2/3$ (see Algorithm 8 for details) and produce the corresponding concatenation of order 7, which are presented in the last column of Table 2.

EXAMPLE 5.2 In this example we consider beta transformation $T(x) = 1.19x + 0.45$ with a slope closer to the identity map. It is depicted in Figure 6 (middle panel). Its rotation interval obtained is $[0.5; 0.555]$. The respective Farey neighbours are $1/2 < 5/9$ and the concatenations of order 7 are included in Table 3.

EXAMPLE 5.3 For this example, we consider the following nonlinear Lorenz map:

$$T(x) = \begin{cases} x^2 + x + \frac{1}{4} & \text{if } 0 \leq x < \frac{1}{2}, \\ -x^2 + 3x - \frac{5}{4} & \text{if } \frac{1}{2} \leq x \leq 1, \end{cases}$$

with graph depicted in Figure 6 (right panel). Here rotation interval obtained is $[0.4, 0.6]$ and Farey neighbours are $2/5 < 1/2$. Table 4 presents the concatenations of order 6.

Table 2: Concatenations for Example 5.1

rotation interval	Farey Neighbours	Concatenations of order $k = 7$
$[0.333, 0.75]$	$1/2$ $2/3$	$(01)^7 1$ $(01)^6 1011$ $(01)^5 (10)^2 11$ $(01)^5 101^2 01^2$ $(01)^4 (10)^3 1^2$ $(01)^4 (10)^2 1^2 01^2$ $(01)^4 101^2 (01)^2 1$ $(01)^4 101^2 0^2 01^2$ $(01)^3 (10)^3 1^2 01^2$ $(01)^3 (10)^2 1^2 (01)^2 1$ $(01)^3 (10)^2 1^2 01^2 01^2$ $(01)^3 101^2 (01)^2 101^2$ $(01)^3 101^2 01^2 (01)^2 1$ $(01)^3 101^2 01^2 01^2 01^2$ $(01)^2 (10)^2 1 (10)^2 1^2 01^2$ $(01)^2 (10)^2 1^2 01^2 01^2 01^2$ $(01)^2 101^2 (01)^2 101^2 01^2$ $(01)^2 101^2 01^2 01^2 01^2 01^2$

6. Analysis of the sequences

The complexity of a finite sequence may be interpreted as the extent to which a sequence resembles a random one [10]. In this section, we will examine the complexity of the sequences generated by our Essential Sequences algorithm (EssentialSeq), by means of the theory of LZ algorithms, proposed by Abraham Lempel and Jacob Ziv.

Among the many variants of the LZ algorithms, we rely on the 1976 version (LZ76) introduced in [10]. The algorithm examines the complexity of finite sequences, based on the number of steps used in its production process. In particular, it is proposed to examine the complexity of finite sequences from the point of view of a 'learning process', that scans a finite sequence from left to right and adds a new word to its memory every time a new substring is found. The size of the vocabulary and the rate of finding new substring are the key factors for determining the complexity of the sequence. Additional details of the complexity calculation can be found in [10].

The figures below allow us to analyze and compare the complexity of random and periodic sequences, and the ones generated by the EssentialSeq algorithm. Two types of complexities are used to evaluate a string: exhaustive, that can be considered a lower limit of the complexity measurement proposed by Lempel and Ziv, and primitive, that may be an upper limit. The LZ-

Table 3: Concatenations for Example 5.2

rotation interval	Farey Neighbours	Concatenations of order $k = 7$
$[0.5, 0.555]$	$1/2$ $5/9$	$(01)^{10}1$ $(01)^9(10)^41^2$ $(01)^8(10)^51^2$ $(01)^8(10)^41(10)^41^2$ $(01)^7(10)^61^2$ $(01)^7(10)^51(10)^41^2$ $(01)^7(10)^41(10)^51^2$ $(01)^7(10)^41(10)^41(10)^41^2$ $(01)^6(10)^61(10)^41^2$ $(01)^6(10)^51(10)^51^2$ $(01)^6(10)^51(10)^41(10)^41^2$ $(01)^6(10)^41(10)^51(10)^41^2$ $(01)^6(10)^41(10)^41(10)^51^2$ $(01)^6(10)^41(10)^41(10)^41(10)^41^2$ $(01)^5(10)^51(10)^51(10)^41^2$ $(01)^5(10)^51(10)^41(10)^41(10)^41^2$ $(01)^5(10)^41(10)^51(10)^41(10)^41^2$ $(01)^5(10)^41(10)^41(10)^41(10)^41^2$

complexity has been calculated using the MATLAB code proposed in 2012 by Quang Thai ([14]) and referred here to as LZ76-algorithm.

In Figure 7 we compare the LZ-Complexity of three types of finite sequences: random, periodic and essential concatenations. To produce essential concatenations we start with the two basic itineraries, A and B , and then concatenate them n times following essential sequence patterns (see algorithm 11). Next, for a fixed n , we calculate the average LZ-Complexity of all essential concatenations. This value is represented on the y -axis. Finally we compare it with the average complexities of random sequences with the same length as essential concatenations and periodic sequences being concatenation of n times of A .

In Figure 8 we see the distribution of the values of the LZ-Complexities of random(red) and essential concatenations(blue) sequences. Let us note that we obtain not only different averages (as in Figure 7) but the distribution of essential sequence is much less dispersed around the average value.

As it could be expected we see that:

- LZ-Complexity of random sequences (primitive and exhaustive) is much higher than complexity of essential concatenations and periodic sequences.
- Complexity of essential sequences is close to complexity of periodic se-

Table 4: Concatenations for Example 5.3

rotation interval	Farey Neighbours	Concatenations of order $k = 6$
$[0.4, 0.6]$	$\frac{2}{5}$ $\frac{1}{2}$	$(01)^7 1$ $(01)^6 (10)^2 1^2$ $(01)^5 (10)^3 1^2$ $(01)^5 (10)^2 1 (10)^2 1^2$ $(01)^4 (10)^3 1 (10)^2 1^2$ $(01)^4 (10)^2 1 (10)^3 1^2$ $(01)^4 (10)^2 1 (10)^2 1 (10)^2 1^2$ $(01)^3 (10)^3 1 (10)^2 1 (10)^2 1^2$ $(01)^3 (10)^2 1 (10)^2 1 (10)^2 1 (10)^2 1^2$

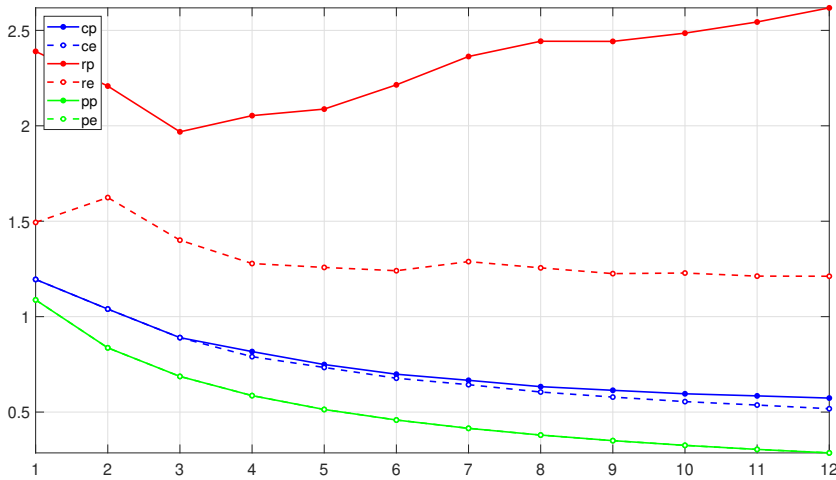


Figure 7: Average complexity (vertical axis) of random (rp,re), periodic (pp,pe) and EssentialSeq(cp,ce) sequences using LZ76-algorithm with primitive ($_p$) and exhaustive ($_e$) complexities. The horizontal axis corresponds to the number of sequences examined.

quences, however the first one is a little bit higher.

- Only primitive LZ-Complexity of random sequences increases with the length of sequences, all other LZ-Complexities are decreasing or become constant.

7. Discussion

Let us briefly summarize the presented results. We propose a series of algorithms that allow, starting with a Lorenz-like map, to calculate its rotation number and rotation interval, compute the itinerary of a periodic orbit based

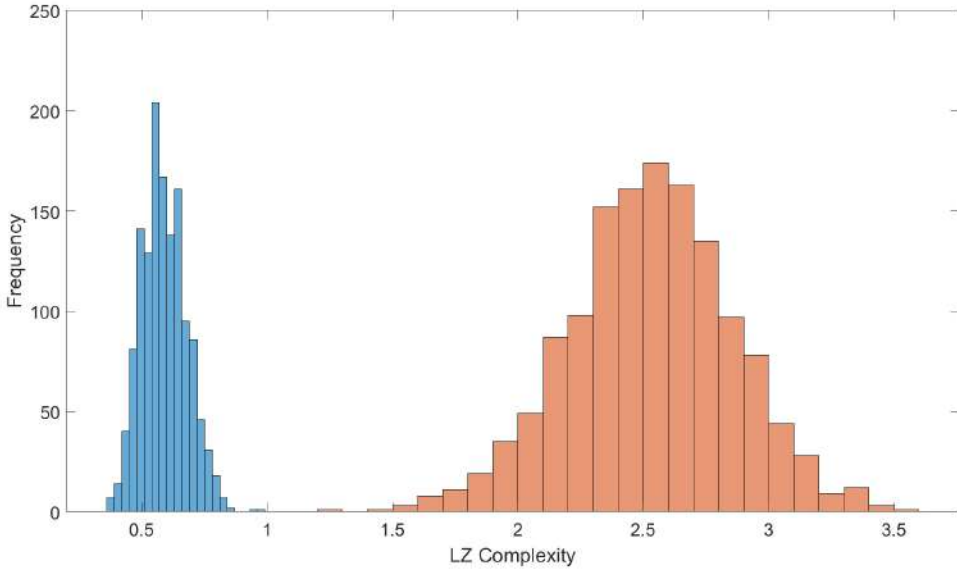


Figure 8: Histogram of average of LZ Complexities for sequences generated by EssentialSeq (blue) and Random sequences (red). The complexity was calculated using *primitive* version of LZ76-algorithm.

on Proposition 3.1; approximate the limits of its rotation interval by two Farey neighbours, and finally to generate concatenation of itineraries of finite union of periodic orbits. Additionally we present some examples of Lorenz-like maps, linear and non-linear, and the output of our algorithms.

Lastly, in order to asses the complexity of the sequences generated by FupoConcat, we perform an analysis and comparison, in terms of LZ-complexity, of our sequences with periodic and random ones and conclude that our sequences have, on average, better LZ-complexity values.

Possible extension of this work could include investigation of longer concatenations of periodic orbit itineraries which however might be a computational challenge (because of the exponential growth of calculations in both obtaining the itineraries and their LZ-complexity).

Note also that here we calculate itineraries of periodic orbits on algebraic level, i.e. by rotation numbers and concatenations but we can also extend our computer programs to calculate (numerically) itineraries of general orbits (i.e. their starting finite parts) and then compare LZ complexity of itineraries of such non-periodic orbits with complexity of random sequences. In fact, our preliminary investigation shows that LZ complexity of itineraries of non-periodic orbits of the maps investigated in the current work is only a bit lower than this if random binary sequences of corresponding length.

REFERENCES

- [1] L. Alsedà, J. Llibre, M. Misiurewicz and C. Tresser, Periods and entropy for Lorenz-like maps *Ann. Inst. Fourier (Grenoble)* 39, 1989, 929–952. Cited on pp. 245 and 248.
- [2] P. Bartłomiejczyk, F. Llovera-Trujillo and J. Signerska-Rynkowska, Spike patterns and chaos in a map-based neuron model, *Int. J. Appl. Math. Comput. Sci.* 33, 2023, 395–408. Cited on pp. 245 and 246.
- [3] P. Bartłomiejczyk, F. Llovera-Trujillo and J. Signerska-Rynkowska, Analysis of dynamics of a map-based neuron model via Lorenz maps, *Chaos*, 34, 2024, 043110. Cited on pp. 245 and 246.
- [4] P. Bartłomiejczyk, F. Llovera Trujillo and J. Signerska-Rynkowska, *FUPOLibrary*, <https://www.mathworks.com/matlabcentral/fileexchange/135937-fupolibrary>, MATLAB Central File Exchange, 2023. Retrieved September 27, 2023. Cited on pp. 253 and 261.
- [5] P. Bartłomiejczyk, F. Llovera Trujillo and J. Signerska-Rynkowska, *FUPOLibrary*, <https://github.com/bartlomiejczyk/FUPOLibrary>, GitHub repository, 2023. Retrieved September 27, 2023. Cited on pp. 253 and 261.
- [6] Y. Choi, Attractors from one dimensional Lorenz-like maps, *Discrete Contin. Dyn. Syst.*, 11 (2004), 715–730. Cited on p. 245.
- [7] M. Courbage, V. I. Nekorkin and L. V. Vdovin, Chaotic oscillations in a map-based model of neural activity, *Chaos* 17, 043109, 2007. Cited on p. 245.
- [8] W. Geller and M. Misiurewicz, Farey-Lorenz permutations for interval maps, *Int. J. Bifurcation Chaos*, 28 (2018), 1850021. Cited on pp. 245, 248, and 251.
- [9] R. L. Graham, D. E. Knuth and O. Patashnik, *Concrete mathematics. Second Edition*, Addison-Wesley Publishing Company, Inc, 1994. Cited on pp. 248 and 249.
- [10] A. Lempel and J. Ziv, On the Complexity of Finite Sequences, *IEEE Trans. Inf. Theory* 22 (1976), 75–81. Cited on p. 264.
- [11] P. Oprocha, P. Potorski and P. Raith, Mixing properties in expanding Lorenz maps, *Adv. Math.* 343 (2019), 712–755. Cited on p. 245.

- [12] F. Rhodes and Ch. L. Thompson, Rotation numbers for monotone functions on the circle, *London Math. Soc.* 34 (1986), 360–368. Cited on p. 247.
- [13] J. E. Rubin, J. Signerska-Rynkowska, J. D. Touboul and A. Vidal, Wild oscillations in a nonlinear neuron model with resets: (II) Mixed-mode oscillations, *Discrete Contin. Dyn. Syst. - B* 22 (2017), 4003–4039. Cited on p. 245.
- [14] Q. Thai, calc_lz_complexity, https://www.mathworks.com/matlabcentral/fileexchange/38211-calc_lz_complexity, MATLAB Central File Exchange. Retrieved February 27, 2024. Cited on p. 265.

Obliczanie tras okresowych dla odwzorowań Lorenza.

Frank Fernando Llovera Trujillo


Streszczenie Istnienie i struktura orbit okresowych stanowią istotną część badań układów dynamicznych. Obliczenia analityczne są jednak możliwe tylko w nielicznych przypadkach, a numeryczna identyfikacja orbit okresowych jest wykonalna jedynie wtedy, gdy są one atraktorami dla dużego zbioru warunków początkowych. Stanowi to szczególne wyzwanie, zwłaszcza w układach chaotycznych. W niniejszej pracy, opierając się na teoretycznych wynikach W. Gellera i M. Misiurewicz (2018), przedstawiamy procedurę umożliwiającą określenie trajektorii zdecydowanej większości orbit okresowych odwzorowań typu Lorenz. Podajemy także konkretne algorytmy wraz z gotowymi do użycia narzędziami obliczeniowymi, dostępnymi w otwartych repozytoriach. Ponieważ odwzorowania Lorenza występują jako podukłady wielu złożonych modeli i są powszechne w różnych zastosowaniach, nasze wyniki otwierają nowe możliwości badania ich okresowej struktury.

2010 *Klasyfikacja tematyczna AMS (2020)*: Primary: 37E05, 37-04; Secondary: 37E45, 37E15.

Słowa kluczowe: Lorenz-like maps, periodic orbits, itineraries, rotation interval, Farey-Lorenz permutations, random binary sequences..



Frank Fernando Llovera Trujillo received his Masters degree in Mathematics and Physics from University of L'Aquila (Italy) and Gdansk University of Technology (Poland) in 2019. He has been a Phd student of Mathematics at Gdansk University of Technology since 2020. His scientific interests include dynamical systems, chaos and its applications, neuronal networks and data science.

FRANK FERNANDO LLOVERA TRUJILLO 
GDAŃSK UNIVERSITY OF TECHNOLOGY, DOCTORAL SCHOOL
GABRIELA NARUTOWICZA 11/12
80-233 GDAŃSK, POLAND
E-MAIL: frank.llovera.trujillo@pg.edu.pl

COMMUNICATED BY: Łukasz Płociniczak

(Received: 30th of November 2024; revised: 31st of December 2024)